MODELING OF GAS RELEASE FROM AN UNDERGROUND PIPELINE

A Thesis

by

OLA H SROUR

Submitted to the Office of Graduate and Professional Studies of
Texas A&M University
in partial fulfillment of the requirements for the degree of

MASTER OF SCIENCE

Chair of Committee,	Konstantinos Kakosimos
Co-Chair of Committee,	Luc Vechot
Committee Member,	Thomas Seers
Head of Department,	Arul Jayaraman

July 2020

Major Subject: Chemical Engineering

ABSTRACT

The underground gas releases from buried pipelines can cause serious damage to the environment, properties, and population. This work aims at modelling the underground gas releases using a computational fluid dynamics numerical tool to allow the user to obtain a desired property (velocity, release rate, etc.) and visualize the behavior of a release. This was done through performing a sensitivity analysis on five crucial parameters that affect the results significantly, namely, the meshing size, soil particle diameter, turbulence model and the granular viscosity characterizing the soil. The resulting model was validated and used to delineate the boundaries between the different regimes corresponding to various release forces. The regimes are the resulting outcomes of the methane's flow which vary according to its release force ranging from migration through the soil, to uplift visible on the ground, till a crater formation. The pipeline burial depth was changed to investigate the effect of the change of burial height on the regime. The result was presented on a nomograph that allows to identify the regime corresponding to a given inlet force and pipeline burial depth, for an upward release orientation. The effect of the release orientation on the outcome was investigated for given pressures.

DEDICATION

I dedicate this work to everyone who believed in me and stood by my side starting with my family who was there since day one; passing through every one who became family by choice throughout my academic journey. Among these people are my husband Mohammad Lameh and my best friend Wafa Imran who I am honored to dedicate this work to.

ACKNOWLEDGEMENTS

I would like to thank my committee chair, Dr. Konstantinos, my committee co-chair, Dr. Luc, and my committee member, Dr. Thomas, for their guidance and support throughout the course of this research. Moreover, I would like to thank the Mary Kay O'Connor Process Safety Center (MKOPSC) at Qatar, who offered me continuous support. I am proud being a part of this center for two years.

I would also like to thank the research computing team for the continuous assistance and help needed concerning the RAAD supercomputer.

Thanks also to my friends and colleagues; the department faculty and staff for making my time at Texas A&M University a great experience. The list of friends and faculty staff is unlimited. However, I would like to dedicate a big thanks to my best friend, Wafa Imran, who was there for me since day one, till the moment I am writing these words.

Finally, thanks to my mother, father, brothers and sister in law for their encouragement. I would not have been able to do it without their continuous support. The special thanks is to my colleague, friend and family member, my husband Mohammad, for his patience, help, support, care, and love. No words can describe my appreciation for the long nights and constant back-up that I received from him throughout this journey.

CONTRIBUTORS AND FUNDING SOURCES

Contributors

This work was supported by a thesis committee consisting of Dr. Konstantinos Kakosimos, Dr. Luc Vechot of the Chemical Engineering Department and Dr. Thomas Seers of the Petroleum Engineering Department. All of the work conducted for the thesis was completed by the student independently.

Funding Sources

The graduate student was supported by a fellowship from Texas A&M University at Qatar and Mary Kay O'Connor Process Safety Center at Qatar.

TABLE OF CONTENTS

Page

LIST OF FIGURES

Page

LIST OF TABLES

Page

1 INTRODUCTION

Buried pipelines are essential transmitters of natural gas, which worldwide consumption is expected to increase from 120 trillion cubic feet (Tcf) in 2012 to 203 Tcf in 2040 according to the *International Energy Outlook 2016* (IEO2016) Reference case[1]. However, these pipelines are prone to unforeseen leaks due to the operational and surrounding conditions that alter the state of the pipeline. The leaks can range from small with low flow discharges (e.g. flange leaks or corrosion) to big with high flow discharges (e.g. pipeline rupture due to mechanical failure, accumulation of natural gas after a small leak, weld cracks or excessive corrosion)[2]. Disastrous incidents happened and cost the environment, site, workers and neighbors. One major incident happened in Belgium, Ghislenghien, on the 30th of July 2004, and was reported to be the worst disaster in half a century. The incident occurred when a gas leak happened in a 1m diameter underground gas pipeline. The leak was accompanied with a loud noise, shake and cavity on the ground. The intensity of the leak increased with time until an explosion occurred. This was followed by a gas cloud that ignited and produced a fireball, whose flare height attained around 200m away from the source and kept burning for 20 minutes. The crater formed was of 10m diameter and 4m depth. The incident resulted in 24 deaths, 132 injuries, the destruction of industrial and personal properties as well as agricultural fields over a radius of 200m, as shown in Figure 1. The economic losses were estimated to be 100 million euros[3].

Figure 1: The incident site during and after the disaster in Ghislenghien, Belgium, July 2004 (reprinted from Aria, 2009[3])

1.1 Problem Description

During a release, the natural gas faces the soil as an obstacle, that it should overcome[4]. The release outcome is dependent on the release parameters that are numerous. Out of these parameters, the literature have dealt with the properties of the soil (nature, water content, compaction layers), the hole characteristics (dimensions, orientation), the pipeline conditions (initial pressure, volumetric flow rate) and the pipeline features (diameter, depth)[5]. The outcomes can be distinguished between underground and above ground phenomena, where there are regimes observed above-ground as a result of the phenomena happening under-ground. The first outcome is a simple movement of the gas in the soil (e.g. diffusion, which is mixing the substance through the air[6]) with no visible observation on ground. This regime is entitled migration and can be accompanied with small cracks at the extreme case[5]. The second outcome is a fluidization phenomenon underground and a certain degree of uplift above-ground[4,5]. The visible phenomena from above ground will be an uplift, that according to the intensity will be either low or strong[5]. The low uplift is accompanied with the generation of cracks, whereas the strong uplift tend to be accompanied with a crater[5]. This category of fluidization will be accordingly divided into two regimes: low and strong uplift. The last outcome is a crater formation (a visible gap on the ground, through which the gas leakage will

behave as a free jet)[4,5]. During a crater, the soil is displaced underground and on-ground. A high release force can produce a full-bore rupture, and the leaked gas can cause toxic, explosion and fire threats on the environment, properties, and population.

1.2 Problem Statement

The underground gas release from buried pipelines is accordingly a remarkable frustration that can be catastrophic. For mitigating the risks associated with it, a thorough understanding of the process is needed in order to be able to reproduce it. Accordingly, work has been conducted in this vast field to reproduce the situation mathematically, numerically or experimentally. Some mathematical work attempted to quantify at steady/unsteady state the amount of gas leakage[7–10]. Other numerical work using Computational Fluid Dynamics (CFD) attempted to simulate some cases for dispersion (above-ground) and some others for underground, to evaluate the properties (pressure, temperature, velocity etc.) and leakage flow rate out of a hole[11–13]. In this area, some work generated correlations to link these various properties[14,15]. In the experimental field, there is existing work that identified the diffusion of some gases from underground. However, almost none of the existing work aimed at evaluating the different possible regimes (outcomes) associated with a certain release input the way introduced here; except recent experimental work that aimed to visualize the outcome associated with a release at the hole[4,5]. This experimental work gave rise to this side of the phenomenon and it is summarized in Section 2.6, below.

The conduction of an experiment is significant for visualization and certification of the phenomena that happen during a release. However, this can not be afforded prior to each installation due to the large time and resources demanded; which makes the amount of information that can be extracted from it to be limited. The technological developments have allowed simulating models that can describe the behavior of such systems feasible. With the increased computational power,

computers are able to solve equations and problems with high complexity similar to the ones describing the gas flow through the soil. With significantly lower costs than the experimental approach, developing a model that can simulate the behavior of the gas release is of great importance to further understand the process and predict its consequences.

For that purpose, this work aims at adding value to the studies already performed on the gas release from buried pipelines through establishing a 3D CFD model that describes the consequences of an underground gas release. The model allows the user to identify the regimes associated with various release forces, at various leak characteristics (leak orientation, burial depth). It is able to describe any property and/or behavior resulting from a release after inputting a certain scenario, described through a given burial depth, inlet pressure and release orientation. This is done through testing various release pressures up to 80bars for an upward release orientation and a pipeline burial depth of 100cm, and determining the outcome regimes and the release rate for each case. To represent the data, two plots are generated. One plot allows to identify the release rate associated with the various inlet pressures for a height of 100cm and an upward release orientation. Another plot allows the determination of the regime associated with a release force, and permits a fine delineation of the boundaries between the different regimes (migration, low uplift, strong uplift and crater), by combining the results obtained from this model along with the outcome of the experiment[5].

Moreover, to test the applicability of the model to various input parameters (in addition to the release pressure), the outcome regime is obtained when varying the pipeline burial depth at three given pressures. The outcome from the burial depth study is added to the generated plot along with additional experimental points. This completes the nomograph allowing the identification of the regime associated with a certain release pressure and pipeline burial depth for an upward release

orientation. Infinite combinations can be added to complete the nomograph that can serve as basis for regime identification. Finally, the outcome is tested when varying the leak orientation (upward, downward, to the left and to the right) for two pressures to identify its effect on the regime.

2 LITERATURE REVIEW

2.1 Mathematical Modelling and Verification

In this section, some mathematical models established to characterize the leakage from pipelines are presented, with the associated validation using their own/other's experimental work.

2.1.1 Buried Pipelines

Wakoh and Hirano[9] studied the diffusion process of a leaking flammable gas into the soil by suggesting a convection-diffusion equation to calculate the concentration distribution at different times and locations around the release point. The flammable gas studied was liquefied petroleum gas comprised of 95% propane. Diffusion happens when the substance is mixed with air while convection happens when the substance moves by the movement of air[6]. The equation was derived by taking into consideration the effect of both diffusion and convection on the movement of the substance[6]. The equation relates the concentration of the substance to the volumetric leakage flow rate (assumed constant), diffusion coefficient, porosity, time and space as shown in Equation 1. Wakoh and Hirano[9] built their own experimental data to validate their generated concentration model. The diffusion coefficient used (5×10^{-5} $m^2.s^{-1}$) – and found to perform a good match between experimental and theoretical results – was very high compared to the commonly used molecular diffusion coefficients. It was not found through a thorough literature, but by data fitting. This could be attributed to the higher flow rates used, in addition to the convection and diffusion working in the same direction, at the same time.

$$\rho = \frac{\left(\frac{3Qt}{4\pi\varepsilon}\right)^{1/3}}{x} erfc\left(\frac{x-\left(\frac{3Qt}{4\pi\varepsilon}\right)^{1/3}}{2(Dt)^{1/2}}\right) \quad (1)$$

Another diffusion model for simulating underground hydrogen leakage was presented by Parvini and Gharagouzlou[16]. The near-field submodel (leakage of hydrogen through the soil pores) was

used as an input for the far-field submodel (dispersion into either an open or closed space). For the near-field modeling, the equations used were Darcy's law, the continuity equation and the component transfer equations in porous medium that represent the differential equations for concentrations variation with time. The outcomes from this submodel were the distribution of the hydrogen concentration at different points in the soil (and the flux). The validation of near-field submodel was done by using the experimental data obtained by Okamoto et al.[8]. The far-field model studied the possibility of fire, explosions and toxicity and their expected effect on the domain, in the case of the minimum possible leakage of hydrogen. The results showed that there was a possibility of a flash fire only in the case of open air. However, there was a chance of both fire and explosion in the case of the confined space.

Okamoto et al.[8] performed full-scale leakage tests for hydrogen from buried pipelines. They monitored the change of hydrogen concentration with space and time. Given that hydrogen is lighter than air, it was able to diffuse upwards into the soil. It was found that it requires around 50 hours for the leakage rate into the ground to equalize the dispersion rate into the atmosphere. It was also shown that the region over which the hydrogen concentration was relatively high (10 vol% and higher) extended to ± 300cm around the leak, which was considered safe to not attain any nearby buildings or sites. Moreover, the area over which the gas concentration was 0.008 vol% or higher was present at a distance of ± 250cm above the leak point, what allows to install a gas detector for preventative detection of a leak just before any aggravation. Okamoto et al.[8] also built a mathematical model based on Darcy and Fick's laws, that was tested and gave valid results.

According to Hibi et al.[7], the movement of the chemical substances in the vapor phase in soil is much more complicated than in the water phase. This is due to the fact that is characterized by Knudsen diffusion, difference in molecular weights of the multi substances, and multi-component

gas model in addition to the diffusion, advection and dispersion that occur in both phases[17,18]. Fick's law was used to model the diffusion of materials in a binary-gas system in the soil by Sleep and Sykes[19] and Kneafsey and Hunt[20] previously. However, Fick's law is unable to model the transport of chemical substances in multi-component gas system. For that purpose, Hoeg at al.[21] used Blanc's law[22], derived from Stefan-Maxwell Equation[23], to model the movement of chemical substances in a multi-component gas system where the gases – except the traced gases present in small concentrations – are fix. For studying the transportation of the chemical substances in a multi-component gas phase present in the soil, for any range of concentrations, the Stefan-Maxwell equation and the dusty gas model are used[7]. Accordingly, Hibi et al.[7] used the dusty gas model to characterize the diffusion of multi-component gas systems within soil. This was done by deriving the compound diffusion represented by Equation 3 and the compound velocity represented by Equation 4 which were used to formulate the advection-diffusion equation (Equation 2) through the finite element method.

$$N_i^T = -D_i^* \nabla C_i + V_{gi}^* C_i \tag{2}$$

$$D_i^* = \theta_g \tau D_{cij} \tag{3}$$

$$V_{gi}^* = -\frac{\theta_g \tau M_i g D_{cij}}{RT} - \left\{\frac{\theta_g \tau D_{cij}}{CRT} \sum_{j=1, j\neq i}^{v} \frac{D_j}{D_{ij}} + \frac{K_g k_s}{\mu_g}\right\} \nabla\left(P_g + \rho_g g z\right) - \frac{D_{cij}}{C} \sum_{j=1, j\neq i}^{v} \frac{1}{D_{ij}} \left(\sum_{k=1, k\neq i, k\neq j}^{v} \frac{D_j}{D_k} N_k^D\right) \tag{4}$$

They did their own experimental model, shown in Figure 2, using a column where they injected the traced gas (methane or carbon dioxide) to the soil already having air (nitrogen and oxygen). Pressure regulators and samplers were present to take samples to the gas chromatography to read the concentrations of the traced gas. They compared between the obtained molar fractions from their model (dusty gas model-DG), Fick's law and the experimental data gathered from the

column, using a binary gas system being air-traced gas. Comparisons were also done between the results obtained from the experiments, Blanc's law and DG model assuming three components being nitrogen-oxygen-traced gas, in addition to the results obtained from DG model assuming a binary gas system (air-traced gas).

There was a very good agreement between DG and the experimental results, except for some samples due to the extraction error during sampling. However, some differences were detected between Fick's law and DG and were associated to Knudsen diffusion, only included in the DG. The results got by Blanc's model were inaccurate except for the oxygen variation because of its capacity at simulating dilute quantities only, certifying that Blanc's model is for limited range of concentrations, on the contrary of DG which was successful at predicting the obtained molar fractions for a wide range of MW and viscosities. It was also concluded that the binary gas system was successful as much as the three components system. In addition, in case the permeability is lower than that used in this study (2.09×10^{-11} m^2), the Knudsen diffusion will be lower than 15×10^{-4} m^2/s, and the compound velocity can be simplified. Simulations using the simplified compound velocity were tried and gave consistent results with the original compound velocity, since the value in the study can perform well with both the original and the simplified equations, being the boundary value between them. Accordingly, the simplified version can be used for low permeabilities (as silt or clay) and low Knudsen diffusion coefficient, so that the latter becomes dominant in the compound diffusion (this was not tested yet).

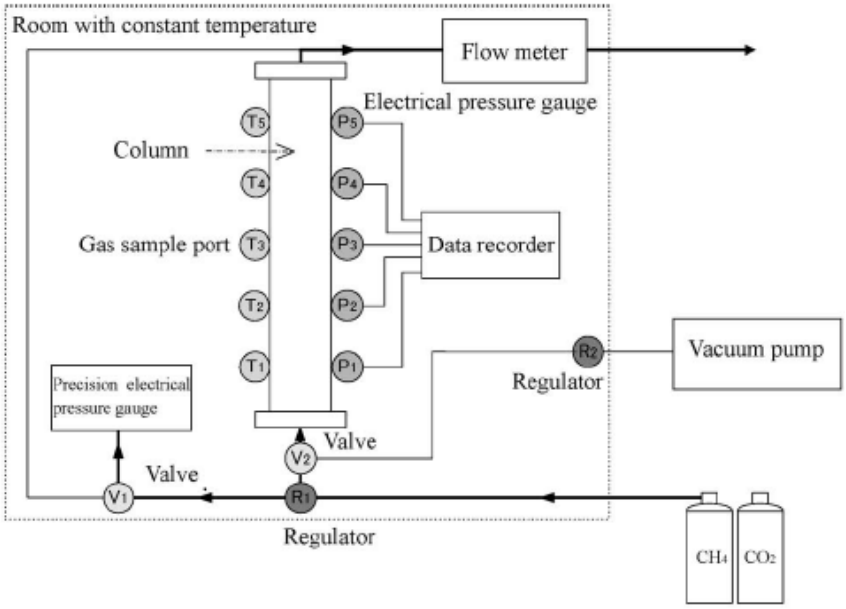

Figure 2: Experimental Setup reprinted from Hibi et al, 2009[7]

2.1.2 Surface Pipelines

Lu et al.[10] presented theoretically equations for calculating the leakage flow rate at steady state and unsteady state conditions, for different cases of models depending on the ratio of the hole diameter to the damaged pipeline diameter, for medium-pressure urban natural gas pipelines. Different parameters were studied at different positions in the case of steady flows, and at different times in the case of unsteady flows. The unsteady model gave better accuracy and ability to compute the effect of several parameters along the release. For that purpose, it was applied to various accident scenarios to investigate the effect of different initial pressure and hole size on the needed time to reach steady state, that was obtained to be less than 10 minutes. In addition, it was used to compute the leakage rate and the leakage amount over time.

2.2 Fluidization based work

In this section, some of the work done on internal fluidization of soils subject to a localized flow is presented.

Alsaydalani et al.[24] setup experiments to test the internal fluidization in granular soils. They reported the most significant points gathered from the available literature on the behavior of granular soils subject to a localized flow[25–27]. Out of the available work, it can be deduced that:
1- At low flow rates, only diffusion of the gas through the soil will be observed.

2- For high packing density (one minus the porosity), above 50%, the particles of the bed affect the flow at the orifice[28].

3- High flow rates result in complexities that the Darcy's law cannot express. These complexities are mainly the result of the fluid-matrix interactions that arise when inertial forces are no longer negligible compared to viscous forces (the limit of Darcy's applicability is a Reynolds number of around 5 for packed beds)[29].

4- Fluidization is first induced near the orifice, and depending on the release pressure, it will be induced in the upper layers. Ergun equation can be used to estimate the pressure at which fluidization occurs[30].

5- A fluidization zone is then created, surrounded by a mobile layer of static particles[31].

6- At high flow rates, the whole bed is fluidized[26].

Alsaydalani et al.[24] continued the investigation through injecting water into the soil present in a Plexiglas-lined tank through a small orifice from which the flow into the tank was upward. They confirmed the available findings on the topic - stated above - and added the investigated effects of

some parameters on the fluidization. They found that the properties of the granular material (particle size, sphericity, permeability), height of the bed and flow rate affect the forces applied on the granular bed and accordingly play a role in the determination of the onset of fluidization (where fluidization starts). The findings can be summarized by the following:

1- The more we get down towards the opening of the orifice, the more is the excess pressure.

2- The pressure upstream needed for initiating fluidization increases with increasing bed height, decreasing orifice opening, increasing particle size and increasing sphericity.

3- As the flow rate increases, the fluidized region propagates progressively in the upward direction.

Textural/pedogenic properties such as angularity, total organic carbon, and clay content can also have an effect; however they were not studied in this work.

2.3 CFD based work

In this section, some work that involved using computational fluid dynamics software for studying the release/dispersion from a leaking pipeline is presented.

2.3.1 Buried Pipelines

The work done by Ebrahimi-Moghadam et al. (2018)[14] was an enhancement of an earlier work done by Ebrahimi-Moghadam et al. (2016)[15], from a 2-dimensional to a 3-dimensional analysis of natural gas leakage from both above and under - ground pipelines in the urban gas distribution zone. They performed a CFD based model using ANSYS software, for evaluating the amount of pipeline leakage, on the basis of a steady, compressible and turbulent flow. In both papers, the used turbulence model was the standard k-ε model, and the natural gas was assumed as pure methane and modelled as an ideal gas (proved to be accurate by several, such as Lu et al.[10] and

Luo et al.[32]). The geometries used for the analysis of the buried pipeline focused at analyzing the area around the hole zone by looking at the pipeline and the soil without modelling the dispersion process, as shown in Figure 3. For the case of the buried pipeline using a 3D model[14], the results showed that the main pressure variation occurs above the hole where the methane penetrates to the soil by means of the pressure difference. The velocity contours showed that the highest velocity is achieved at the hole location (83m/s) with the highest Mach number of 0.13 <<1, meaning that a subsonic flow is expected in the whole region, while the two-dimensional simulation indicated the presence of a sonic flow at the hole location[15]. This showed that the 3D simulations give more adequate results for the case of buried pipelines. Both papers also studied the change in the volumetric flow rate at the hole with the variation of three parameters: pipe diameter (for nominal diameters of 11.46cm, 16.36cm and 20.46cm), hole diameter (from 0.5cm to 8cm), and inlet pressure (3-5 bar) to come up with correlations relating these parameters. After fitting the results, the final outcome was a correlation for the volumetric flow rates (valid for the pressure range between 3 and 5 bar), where the flow is proportional to the inlet pressure, the square of the hole diameter, and the fourth power of the ratio between the hole and pipe diameters[14].

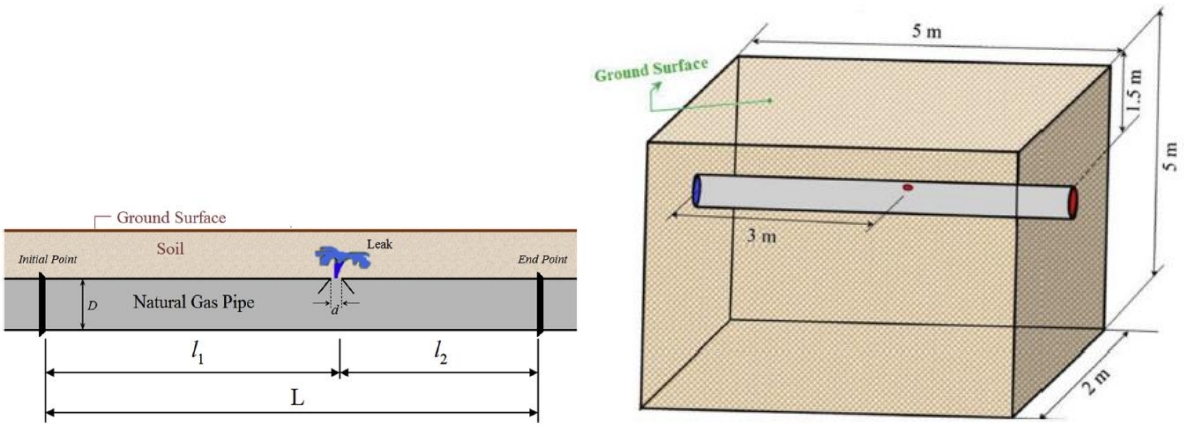

Figure 3: Scheme representation for the buried pipeline case for the 2D case (left) and 3D case (right) (reprinted from Ebrahimi-Moghadam et al. 2018[14] and 2016[15])

Nouri-Borujerdi and Ziaei-Rad[13] studied the gas flow in a high-pressure buried pipeline, subject to friction and heat transfer, along which a small pressure loss occurs during the transportation of gas between two given stations. The flow was studied on the basis of a one-dimensional compressible steady-state condition. The derived governing equations (equations of state, equations for properties and equations for mass, momentum and heat transfers) were solved through a Fortran code. The study evaluated the effects of the friction and heat transfer on several outcomes such as Mach number, temperature, pressure and mass flow rate. The simulation was validated by using one experimental and another numerical cases from previous studies. The results showed that the choked flow rate increases with decreasing the temperature of the gas inside the pipe, or when the heat transfer to the pipe is reduced.

Wilkening and Baraldi[12] focused on the safety implications of the dispersion of gases to the atmosphere in case of accidental releases from buried pipelines. Different scenarios were investigated using CFD – ACE software for accidental hydrogen and methane leakage from pipelines. The buried pipeline was included in the geometry to compute the release rate. The densities were computed through ideal gas law. The LES (Large Eddy Simulation) turbulence model was used because it was able to give similar results to k-ε model in less time. Small time-steps were used due to the critical high-speed flow (sonic) condition in the release zone because of the high-pressure difference between the pipeline and the environment (10 bars). Four cases in a 2D frame were investigated, where results for both gases were obtained, each in two different scenarios (with/without wind) in the presence of blocks representing buildings. A 3D simulation was conducted for one case for comparison purposes. It was found that after a release starts, an expanding jet forms over the hole. After a while, the flow becomes controlled through buoyancy and wind rather than by the impulse of the jet. Especially in the case of methane release, the

configuration with wind could be more serious than without wind, since some flammable mixture might accumulate in larger recirculation zones behind buildings, causing a real threat by imposing ignition risk. It was also found that speed and buoyancy effects leave the hydrogen further from the ground. The 2D simulation underestimated the effect of friction on the jet propagation, however some important results could be extracted out of the 2D simulations (due to the suitable run time they take) although the 3D was more accurate.

2.3.2 Surface Pipelines

Mouloudi and Esfahani[11] simulated a one dimensional transient compressible flow in a damaged gas pipeline through introducing dimensionless parameters into the equations and the conditions. The equations were solved by using a finite difference method, in order to compute the amount/rate of the gas dissipated from the leaking pipeline. Two approaches were used in the study: the hole model when the relative hole diameter (ratio of hole to pipeline diameters) is less than 15% and the full rupture model otherwise. For the hole model, the mass flow rate was found to be dependent on the relative hole diameter only, and independent of friction term and pressure (for pressures between 4 and 69 bars). Whereas for the full rupture model, it was found to be dependent on the relative hole diameter and the friction term.

2.4 Crater - Domino Effect

In this section, some work that dealt with the domino effect risk associated with a crater formation upon an underground release is presented.

Gasunie, Batelle and Advantica are existing empirical models for characterizing the crater formation regime's dimensions[33]. The Gasunie model was developed by the Delft Hydraulics Laboratory and sponsored by a transmission pipeline company in The Netherlands[34]. The Batelle model was developed according to studies done in the Batelle Institute in attempts to improve

Gasunie model[34]. The Advantica model was developed by several gas transmission pipelines operators with the technical coordination of GL Noble Denton[35]. The work conducted by Acton et al.[35] attempted to provide guidelines on the minimum separation distances between underground parallel pipelines, specifically transporting natural gas. The determination of a safe distance for preventing a domino effect from happening is obtained through considering several parameters that lead to the puncture/rupture of a pipeline lying in the proximity of an already failed one. These parameters are the pressure and/or heat load on a pipeline after a neighboring pipeline rupture/puncture, and the exposure of a pipeline to a ground crater formed around the neighboring pipeline. The main criterion used is that a pipeline must lie outside the crater formed by the failed pipeline. Following this concept, effective distances were computed for three types of soil (sandy, clay and mixed) for different pipeline diameters, for a range of operating pressures (20-150 bar), at a burial depth of 120cm[35].

Silva et al.[33] relied on the method of computing the crater width in order to estimate the separating distances for minimizing the risk of a domino effect. For that purpose, they used the Advantica model's results (values for effective distances) to generate an explicit formula for the crater width computation on the basis of their inferred conclusion from Acton et al.[35] that the maximum crater width is twice the effective distance. They also constructed a new model (the Accident-based model) that is based on historical accidents from forty-eight real accidents that were gathered and reported. The four models were tested for 17 cases and it was concluded that the best empirical models for computing the crater width were Batelle and Accident-based models because they account for significant parameters like the pipeline operating pressure, the specific heat ratio of the gas and the soil density[33]. Following the same strategy, the crater dimensions were the basis of assessing the separation distance between underground pipelines for Amaya-Gómez et al.[2]. Beside

the already mentioned models, this paper work attempted to create a more accurate probabilistic-based model for the estimation of the crater dimensions. The model consisted of predicting the ratio of crater width to crater depth through a multivariate regression approach based on 57 accidents, then the dimensions were obtained with the use of a regression prediction interval and the width-depth joint probability function according to three suggested scenarios: less severe, most likely and worst. The computed dimensions allowed the determination of any possibility to a domino effect when taking different scenarios. The approach was applied on a real accident where a domino effect happened. When the crater was assumed to be symmetrical, the neighboring pipeline to the ruptured one lied outside the crater domain. However, when the crater was taken as asymmetrical, the neighboring pipeline lied in the crater zone and a domino effect was expected, as was the real case. Other existing guidelines are present to specify the safe distances for an effective separation between the underground lying pipelines. One approach is based on pipeline diameters, where for each range of pipeline diameters, the suggested effective distance is different (a distance of 1000cm for a pipeline diameter smaller than 20.32cm, a distance of 1300cm for a pipeline with a diameter between 25.4cm and 45.72cm, etc.)[36]. Another approach evaluates several parameters, out of them the possibility of a jet fire and its effect. This approach was applied by Ramírez-Camacho et al.[37], where they evaluated the effects of several parameters on the probability of a domino effect occurrence: hole location, jet direction and its corresponding solid angle, diameter of the source pipe, diameter of the target pipe and the distance between the pipes. The effects of the parameters were analyzed and were linked to the diameters of both pipelines and the distance between them. The developed mathematical model to evaluate the probability of a domino effect showed that the probability is proportional to the diameter of the target pipe, and inversely proportional to the diameter of the source pipe and the separating distance between both

pipes[37]. The crater width computation for identifying the necessary separating distance between underground pipelines remains a powerful and the simplest way[33].

2.5 Release Orientation

In this section, some work that studied the effect of the change in the release orientation on the resulting release from a buried pipeline is presented.

Yan et al.[38] conducted experimental work for testing the diffusion of methane in soil for an underground gas pipe leak. Low release rates (5×10^{-5} – 40×10^{-5} m^3/s) were used for a leaking pipe of diameter 20cm, buried 90cm below the surface, having a hole of diameter 0.5cm, the flow from which goes in the upward direction. Gas sensors were installed in various locations inside the soil in order to measure the change in concentration with time and space. The schematic of the experiment is shown in Figure 4.

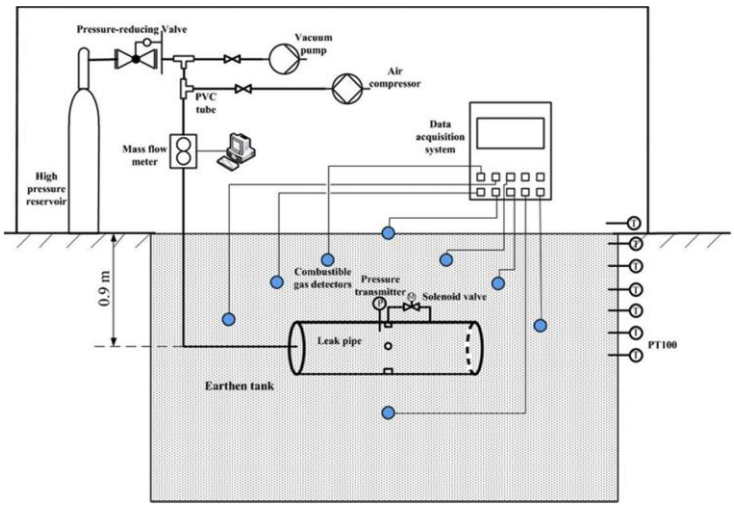

Figure 4: Schematic for the experimental setup reprinted from Yan et al, 2015[38]

In an attempt to investigate the effect of the leak direction on the results, four different leak points were used at the highest flow rate of 40×10^{-5} m^3/s. The directions were horizontal (left and right) and vertical (upwards and downwards). In the region below the pipe, the leak direction did not affect the concentration distribution, except when the flow was upwards. In that case, the concentration was found to be smaller compared to the other directions. In the region above the pipe, the leak direction affected the results. At the ground surface, the variation of the concentrations with time and their corresponding values were significantly impacted by the direction. After 4 hours of simulation, the concentration of methane at the ground surface - point (0,0,0) - was 0.95 vol% for an upward flow, 0.35 vol% for a downward flow, 0.8 vol% for a flow to the left and 0.5 vol% for a flow to the right. In another region above the pipe, below the ground surface, the left and right flow directions had a higher impact on the results than the upward and downward directions that had a minimal influence[38].

Vianello & Maschio[39] discussed the consequences of an underground pipe failure transporting natural gas. They considered the cases of bore rupture (hole diameter = pipe diameter), and medium to large hole effects. Small hole incidents were neglected as the consequences of such incidents are negligible. Concerning medium and large hole cases, the consequences varied according to the location of the hole and the direction of the leak. Hence, the pipe cross section was divided into 4 quadrants as shown in Figure 5.

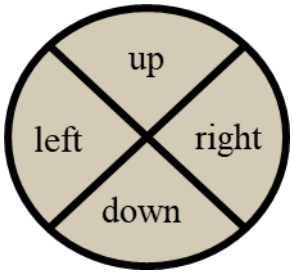

Figure 5: Four possible regions of the release orientation out of a leaking underground pipeline

The consequences from a hole formation in region 4 were neglected because of the corresponding low flow rate. The leak from a hole in region 1 (vertical) was modelled as a vertically upward flow with the same velocity as that in the pipeline, while the leak from a hole in regions 2 and 3 (horizontal) was modelled as an upward flow with an angle 45^{o} and a velocity of 70m/s. It was found that both vertical and horizontal leaks had similar consequences related to vapor cloud explosion and flash fire, while the vertical leakage resulted in lower jet fire thermal radiation.

2.6 Experimental Investigation

In this section, recent small/large scale experimental work identifying the various consequences associated with a leaking buried pipeline is presented.

A Joint Industrial Program (JIP) named 'CRATER' was launched in 2013 for the sake of enhancing the knowledge about the consequences of leakages from buried pipelines by conducting large scale, nearly-real experiments[4]. The different scenarios that were tested were obtained by varying release parameters such as: the type of the released gas, its initial pressure, the diameter of the hole, the nature of the soil and the release orientation. The used pipe was of 40cm diameter, 300cm long and buried at a depth of 100cm below the ground surface. Both sides of the pipeline were closed and a smaller pipeline was inserted into the pipeline to continuously feed the input gas

in order to maintain the desired pressure constant inside the pipeline. The experimental setup dimensions can be seen in Figure 6.

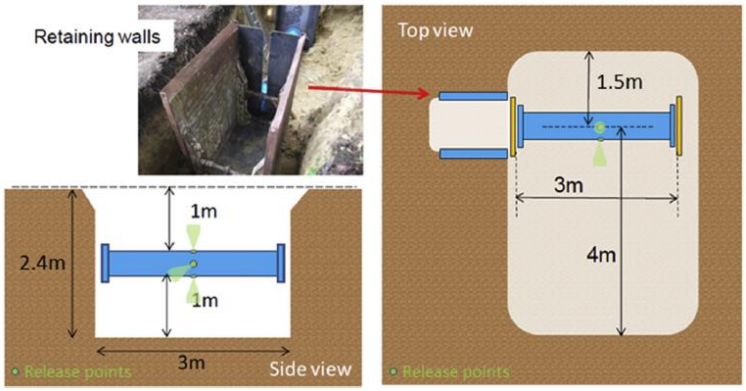

Figure 6: Position and dimensions of the experimental setup reprinted from Houssin-Agbomson et al.[4]

In the paper presented by Houssin-Agbomson et al.[4], the reported results were for a part of the investigations including: methane and hydrogen as released gases, initial pressure from 17 to 78 bars, 1.2cm hole diameter, sandy and clayed soils, and upward, downward and horizontal release orientations. There were three possible outcomes on the soil expected from the 11 reported trials: crater formation, uplift of the soil and mixed situation. The crater is formed when the soil will be expelled, where a gap will be formed on the ground surface and the gas is released as a free jet, as shown in Figure 7.

Figure 7: Crater formation reprinted from Houssin-Agbomson et al.[4]

The uplift happens when the evacuation of the gas is not strong enough to form a crater, but will uplift the soil, and the gas finds a way to be released through the crown found at surface, as shown in Figure 8.

Figure 8: Uplift of the soil reprinted from Houssin-Agbomson et al.[4]

The mixed situation is an intermediate event, where at first a similar situation to the uplift of the soil occurs, but then the gas will find a single point, where it will continue its release. These two phenomena are successively shown in Figure 9.

Figure 9: Mixed situation comprised of crown release (left) and unique point release (right) reprinted from Houssin-Agbomson et al.[4]

The results showed that, for an upward vertical release, using sandy soil, the nature of the released gas will not change the outcome. The outcome was a crater formation for an initial pressure starting between 36 and 47 bar, an uplift of the soil for an initial pressure between 18 and 36 bar, and a mixed situation in between. The higher the pressure, the higher a crater formation is probable. When changing the release orientation of the hole, with methane being the gas released, downward and horizontal orientation gave less impact for the same initial pressure than the upward orientation. The reason behind this is that for a pressure of 56 bar, the upward orientation resulted in a crater, however the result was only an uplift in the other two cases. Moreover, the results for the same conditions but with clay instead of sand, gave lighter effects (uplift instead of crater) when tested with high pressures, for both gases in an upward direction. This is due the fact that clayed soil is more elastic and cohesive than sandy soil.

The JIP named ‘crater’ focused on nearly-real scale experiments, and therefore there was a limited number of conclusions. Accordingly, GRTgaz in collaboration with INSA Rouen-Normandie school continued the work by performing 101 laboratory scale tests to study the outcomes of a release from a buried pipeline[5]. Out of the variety of parameters that can affect the release, they studied the effects of the initial gas pressure, the leak diameter, the pipeline depth, the water content (W) and the nature of the soil (sandy and clayed soils). Three main outcomes were available: the migration of the gas through the soil with no visible outcome on the ground, uplift of the soil expressed by small cracks with variable size accompanied by a minor elevation of the ground, and a crater characterized by a hole from which the release will act as a free jet. The visible results are presented in Figure 10.

Figure 10: Uplift examples in sandy soil (left) and clayey soil (middle), and crater example (right) (reprinted from Bonnaud et al., 2018[5])

However, several observations were done during the study. The time factor seemed to have significant effects on the results. When starting with a gas migration, the outcome can be an uplift; and when starting with an uplift, the final outcome can be a crater. This is due the fact that the gas dries the region around the release and expands the available cracks and cavities in the cases of migration and uplift. The cavities are different for different types of soil since the clay is more

cohesive than sand and the drying phenomena affects the sand more than clay. According to these observations, the possible release outcomes were the following: gas migration, uplift occurrence after some seconds, uplift, uplift accompanied by a crater after some time and crater. These were grouped into four categories according to a coefficient that is 0% for pure gas migration and 100% for pure crater formation. The groups were: gas migration for the interval [0,17], low uplift for [17,50], strong uplift for [50,85] and crater for [85,100]. After gathering the data obtained from the old and current studies, Bonnaud et al.[5] presented an empirical model to predict the outcome of a leak from a buried pipeline through a graph presenting the coefficient % versus the release force (obtained by multiplying the initial pressure by the surface of the hole that were both studied), at different heights of soil for both sandy and clayey soils. It should be noted that the water content for sandy soil was of minor effect for a water content higher than 5% and accordingly the graph was independent of the water content. Figure 11 shows the delineation of the boundaries between the different possible outcomes of the release.

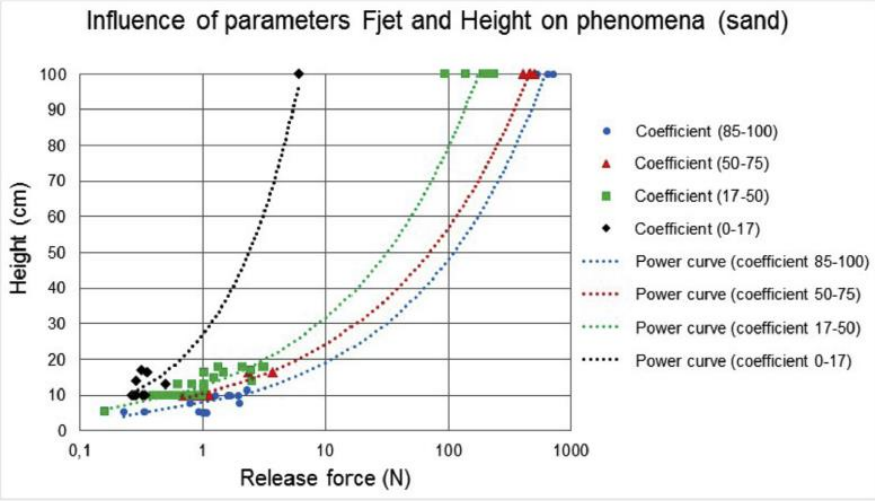

Figure 11: Identification of the different groups for the various combinations of height and release force from both studies for sandy soil and a water content > 5% (reprinted from Bonnaud et al., 2018[5])

Figure 12 shows the empirical model that allows the identification of the expected consequence out of a release for a given height, water content and release force for sandy and clayey soils.

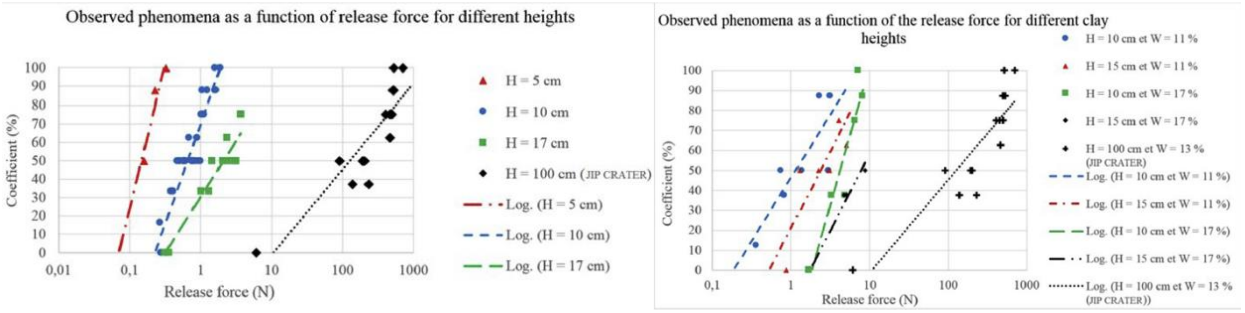

Figure 12: The expected outcome as function of the release force at different heights for sand (W>5%) [left] and for clay (various W) [right] (reprinted from Bonnaud et al., 2018[5])

2.7 Joule-Thomson Cooling Effect

In this section, some of the work done on the contribution of the Joule-Thomson Cooling to the aggravation of the release outcome from a buried pipeline is presented.

Bonnaud et al.[5] (who did experimental investigations for gas leakage from a buried pipeline) made a significant observation at the hole, where a remarkable pressure difference occurs, leading to a drop in temperature, causing a freezing phenomenon at the hole. This remark could not be fully explained due to the limited amount of corresponding observations. However earlier work studied this phenomenon in more details, entitled Joule-Thomson Cooling, which happens after a drop in temperature due to the gas expansion upon release. Ai and Liu[40] performed simulation and experimental investigation of the temperature drop upon leak of argon, and showed that the temperature can drop down by around 60°C by simulation, and it reached -48°C in the experimental

setup. They showed that the stress intensity factor is much greater than the fracture toughness of the steel. The accompanying corresponding low temperature, however, being a good conductor with high density, makes the steel walls act as a buffer against the localized cooling effect. The danger of full bore rupture due to the cooling effect is eminent in a cold environment and when the leak takes enough time to cool down the pipe[40].

2.8 Computational Fluid Dynamics

In this section, the concept of computational fluid dynamics is approached, along with the significant models that are input.

Modelling the behavior of an underground gas release involves the study of the motion of the gas through the soil up to the atmosphere. The field of the investigation of the interactive motion of large number of particles (molecules or atoms) is called Fluid Dynamics. Computational Fluid Dynamics (CFD) is the field of studying such motions through solving a wide set of equations to reveal some important properties and quantities of the fluid (like temperature, pressure, velocity…), and their spatial and time frame variations. CFD applications date back to 1970s, and its development was following the development of computers and their computational power. CFD started as an approach to treat problems in product design, control and operations, without the need to perform expensive (time and money wise) experimental work. Large scale applications of CFD, that involve environmental problems for example, have been made possible thanks to the achievements in large capacity computers and in complex solving techniques[41,42]. The main equations used in the description of the flow are derivatives of mass, energy, and momentum balances. Other equations and models are used to determine fluid properties that are affected by the motion (like equations of state, viscosity models, thermal conductivity models, Newton's law for viscous stress, Fourier's law for conduction…). The set of these equations is

called the complete Navier-Stokes System, and by applying the respective boundary and initial conditions, the system is solved to obtain the aforementioned outcomes. The solution is obtained through discretizing the system's geometry into meshes, which will allow transforming the differential equations into algebraic equations by assuming conserved properties in each mesh[42].

2.8.1 Turbulence models[43]

The literature contributing to modelling gas releases from buried pipelines shows that turbulence flow behavior should be considered to describe the flow regime of the leaked gas. Turbulence is a complex fluid motion that is hard to be modelled due to its randomness. Consequently, the available models for turbulent flows have limitations that need to be identified in order to choose a suitable model for a given application.

A recent review done by Argyropoulos and Markatos[43] tackled the existing turbulence models, with the challenges and successes of each one among the different domains. Their focus was on the models for single phase flow, however, two of the presented models were suggested for multiphase applications. These models are the k-ε and k-ω models which are subsets of the Reynold Averaged Navier Stokes (RANS) equations. The RANS equations are semi-empirical models simulated through solving Navier Stokes equation with other correlations to determine the Reynold's stresses.

2.8.1.1 Mathematical Modeling

Consider a Newtonian fluid having a turbulent flow, which is a continuum, described by Navier-Stokes equation. For the fluctuations present in the fluid properties, Reynold's decomposition is defined as follows:

$$\phi = \bar{\phi} + \phi'$$

Where ϕ is an instantaneous quantity representation, $\bar{\phi}$ is the average quantity whereas ϕ' is the fluctuation in the quantity. Thereby, there exists not a single quantity but multiple, owing to fluctuations.

For a limiting case where an incompressible fluid exists with a single phase for an average time, the continuity equation and Navier-Stokes equation become as follows respectively:

$$\frac{\partial \bar{u}_i}{\partial x} = 0$$

$$\frac{\partial \bar{u}_i}{\partial t} + \frac{\partial (\overline{u_\iota u_j})}{\partial x_j} = -\frac{1}{\rho}\frac{\partial \bar{p}}{\partial x_i} + v\frac{\partial^2 \bar{u}_i}{\partial x_i x_j} - \frac{\partial (\overline{u_\iota' u_j'})}{\partial x_j}$$

This equation is called Reynolds-Averaged Navier–Stokes (RANS) equation, where $\bar{u}_i$ is the average velocity, u_i' is the fluctuating velocity, $\rho \; and \; v$ are the fluid density and kinematic viscosity respectively, and the Reynold's tensor stress is represented by:

$$\tau_{ij} = \overline{u_\iota' u_j'}$$

This is a symmetric tensor with 6 independent components. Thus, given the above equations, it can be observed that the unknown quantities exceed the knowns ones due to the presence of the fluctuations that arise due to turbulence. Having six stresses, three velocity components and pressure as unknowns for the given continuity and Navier Stokes equation, additional equations are required to solve the problem. This is done through characterizing the Reynold's stresses by using the Boussinesq eddy-viscosity approximation. Here, Reynold's stresses can be taken as packets of fluids which basing on the Kinetic Theory of Gases have collisions and exchange momentum. Thus, they are represented by the following:

$$\tau_{ij} = \overline{u_i' u_j'} = \frac{2}{3}\kappa\delta_{ij} - v_t\left(\frac{\partial \bar{u}_i}{\partial x_j} + \frac{\partial \bar{u}_j}{\partial x_i}\right)$$

$$k = \frac{1}{2}\overline{u_i' u_i'} = \frac{1}{2}\left(\overline{u_1'^2} + \overline{u_2'^2} + \overline{u_3'^2}\right)$$

Here, k represents the turbulence kinetic energy, δ_{ij} is the Kronecker delta, and v_t is the turbulence kinematic viscosity. It is important to note that unlike the molecular kinematic viscosity, the turbulence kinematic viscosity, v_t, varies at each point over the entire flow region. Thus, the Navier Stoke's equation becomes:

$$\frac{\partial \bar{u}_i}{\partial t} + \frac{\partial(\overline{u_i u_j})}{\partial x_j} = -\frac{1}{\rho}\frac{\partial \bar{p}}{\partial x_i} + \frac{\partial}{\partial x_j}\left[(v + v_t)\frac{\partial \bar{u}_i}{\partial x_j}\right]$$

Where the isotropic part equals to $\bar{p} = \bar{p} + \frac{2}{3}k$.

The unknown quantity v_t needs to be described to fully characterize the momentum. By doing the dimensional analysis, it is seen that the unknown quantity v_t is proportional to the characteristic velocity V_t and characteristic length L_t. There are methods to compute these quantities, that are the zero-equation, one-equation and two-equation models. The zero-equation model describes the quantities V_t and L_t as algebraic expressions, whereas the one-equation model, describes the V_t as the square root of the turbulence kinetic energy and L_t as the algebraic term. Hence,

$$v_t = C_{v1} L (k)^{\frac{1}{2}}$$

C_{v1} being the dimensionless quantity. Lastly, the two-equation models utilize differential equations for both quantities and then recalculate v_t by either model ($k - \varepsilon$ or $k - \omega$):

$$v_t = \begin{cases} C_\mu f_\mu \dfrac{k^2}{\varepsilon} & (k-\varepsilon\ model) \\ \alpha^* \dfrac{k}{\omega} & (k-\omega\ model) \end{cases}$$

Here, C_μ and α^* are constants, f_μ is the dampening function, ω is the dissipation per unit turbulence kinetic energy and ε is the rate of turbulence energy dissipation.

Further work in this area have aimed at nonlinearity of the strain-rate and have resulted into nonlinear eddy viscosity models. However, for this work, the linear-eddy viscosity model (RANS) using two-equation models are used.

2.8.1.2 Two Equation Models

The two-equation models are named so owing to the requirement of two transport equations in addition to the Navier-Stokes equation. The first one is to solve the turbulence kinetic energy (k) and the second one can be: the dissipation rate of turbulence kinetic energy (ε), the specific dissipation rate (ω), the length scale (l), the product of k ~ l, the time scale τ, the product of k and τ and others. However, the most widely used equations in the literature are $k-\varepsilon$ and $k-\omega$ models. The $k-\varepsilon$ model involves solving two equations to determine the turbulence kinetic energy (k) and its dissipation rate (ε). The $k-\omega$ model also involves two equations, one of them is solved to determine k, while the other is used to determine the specific dissipation rate (ω).

2.8.1.2.1 $\boldsymbol{k-\varepsilon}$ Model

It is one of the most commonly used models derived by Launder and Sharma. It is presented as follows:

i- The kinematic eddy viscosity:

$$v_t = C_\mu \frac{k^2}{\varepsilon}$$

ii- Turbulence kinetic energy:

$$\frac{\partial k}{\partial t} + \bar{u}_j \frac{\partial k}{\partial x_j} = \frac{\partial}{\partial x_j}\left[\frac{(v + v_t)}{\sigma_k}\frac{\partial k}{\partial x_j}\right] - \varepsilon + \tau_{ij}\frac{\partial \bar{u}_i}{\partial x_j}$$

iii- Turbulence dissipation rate:

$$\frac{\partial \varepsilon}{\partial t} + \bar{u}_j \frac{\partial \varepsilon}{\partial x_i} = \frac{\partial}{\partial x_j}\left[\frac{(v + v_t)}{\sigma_\varepsilon}\frac{\partial \varepsilon}{\partial x_j}\right] + C_{\varepsilon 1}\tau_{ij}\frac{\partial \bar{u}_i}{\partial x_j} - C_{\varepsilon 2}\frac{\varepsilon^2}{k}$$

Where, Prandtl numbers for k and ε equal to $\sigma_k = 1.0$, $\sigma_\varepsilon = 1.3, C_\mu = 0.09$, $C_{\varepsilon 1} = 1.44$ and $C_{\varepsilon 2} = 1.92$.

The k-ε is the most mature model with an abundant literature for a wide range of applications. It is the most used and tested two equation models[41,44], however, it gives major errors when predicting flows with adverse pressure gradients and extra strains. Thus, inaccurate results are predicted for separated flows and acts poorly in characterizing the viscous sublayer.

2.8.1.2.2 Modified $k - \varepsilon$ Models

Several modifications have been proposed; however, the most important ones include the Realizable $k - \varepsilon$ Model and the ReNormalization Group (RNG) $k - \varepsilon$ Model. These models have recently been used for turbulent flows past a rotating cylinder, dispersion of pollutants in case of large tank fires and street canyon flows.

2.8.1.2.2.1 Realizable $k - \varepsilon$ Model

This model is based on the satisfaction of realizability constraints on normal Reynold's stresses and Schwartz inequality for turbulent shear stresses. Further, C_μ is computed by eddy-viscosity equation. The constants are $\sigma_k = 1.0$, $\sigma_\varepsilon = 1.2$, $C_{\varepsilon 1} = 1.44\ and\ C_{\varepsilon 2} = 1.9$. By these

modifications, the limitations for separated flows, jets, mixing layers, channels and boundary layers are substantially improved.

2.8.1.2.2.2 RNG $k-\varepsilon$ Model

RNG $k-\varepsilon$ model focused on improving the recirculation length in separating flows. It gives a better prediction for separated flows but fails in predicting flows with acceleration. This was done by improving the $C_{\varepsilon 2}$ coefficient that was changed to:

$$C_{\varepsilon 2} = C_{\varepsilon 2} + \frac{C_\mu \eta^3 (1 - \eta/\eta_0)}{1 + \beta_1 \eta^3}$$

$$\eta = \frac{Sk}{\varepsilon}, S = \sqrt{2S_{ij}S_{ij}}, S = \frac{1}{2}\left(\frac{\partial \bar{u}_i}{\partial x_j} + \frac{\partial \bar{u}_j}{\partial x_i}\right)$$

Where, S is the mean strain rate and S_{ij} is the deformation vector. The constants for this model are $\sigma_k = 0.72, \sigma_\varepsilon = 0.72, C_\mu = 0.085, C_{\varepsilon 1} = 1.42, C_{\varepsilon 2} = 1.68, \beta = 0.012\ and\ \eta_o = 4.38.$

2.8.1.2.3 $k-\omega$ Model

This model was presented by Kolmogorov in 1942, after which many modifications have been proceeded. Hence the latest version presented by Wilcox in 2006 is presented by:

i. The kinematic eddy viscosity:

$$v_t = \frac{k}{\tilde{\omega}}, \tilde{\omega} = max\left\{\omega, C_{lim}\sqrt{\frac{2S_{ij}S_{ij}}{\beta^*}}\right\}, C_{lim} = \frac{7}{8}$$

ii. Turbulence kinetic energy:

$$\frac{\partial k}{\partial t} + \bar{u}_j \frac{\partial k}{\partial x_j} = \frac{\partial}{\partial x_j}\left[\left(V + \sigma^* \frac{k}{\omega}\right)\frac{\partial k}{\partial x_j}\right] - \beta^* k\omega + \tau_{ij}\frac{\partial \bar{u}_i}{\partial x_j}$$

iii. Specific dissipation rate:

$$\frac{\partial \omega}{\partial t} + \bar{u}_j \frac{\partial \omega}{\partial x_j} = \frac{\partial}{\partial x_j}\left[\left(V + \sigma \frac{k}{\omega}\right)\frac{\partial \omega}{\partial x_j}\right] - \beta\omega^2 + \frac{\sigma_d}{\omega}\frac{\partial k}{\partial x_j}\frac{\partial \omega}{\partial x_j} + a\frac{\omega}{k}\tau_{ij}\frac{\partial \bar{u}_i}{\partial x_j}$$

iv. Auxiliary equations and closure coefficients:

$$a = 0.52, \beta = \beta_a f_\beta, \beta_0 = 0.0708, \beta^* = 0.09, \sigma = 0.5, \sigma^* = 0.6$$

$$\sigma_d = \begin{cases} 0, & \frac{\partial k}{\partial x_j}\frac{\partial \omega}{\partial x_j} \le 0 \\ \sigma_{d0}, & \frac{\partial k}{\partial x_j}\frac{\partial \omega}{\partial x_j} > 0, \end{cases} \quad f_\beta = \frac{1 + 85\chi_\omega}{1 + 100\chi_\omega}, \quad \chi_\omega = \left|\frac{\Omega_{ij}\Omega_{jk}S_{ki}}{(\beta^*\omega)^3}\right|, \quad \Omega_{ij} = \frac{1}{2}\left(\frac{\partial \bar{u}_i}{\partial x_j} - \frac{\partial \bar{u}_j}{\partial x_i}\right)$$

where $C_{lim}$is the stress-limiter strength, f_b the vortex-stretching function, χ_ω the dimensionless vortex-stretching parameter and ω_{ij} the mean-rotation tensor.

The $k-\omega$ model is widely used as well, and it has advantages over $k-\varepsilon$ model in achieving higher accuracy for boundary layers with adverse pressure gradients, viscous sub-layers, free shear flows and separated flows. The drawbacks of this model are related to its inability to predict flows with free stream boundaries (like jets)[41,43,44].

2.8.1.2.4 Recent two-equation models

i. Shear Stress Transport Model (SST)

It combines the advantages of both the $k-\varepsilon$ and $k-\omega$ models and has been applied for many applications including aerodynamic flows and turbomachinery. This model acts very well in describing boundary layers under adverse pressure gradients.

ii. Two-time Scale Model

These are multi-scale models which use separate transport energy equations for energy transport across the spectrum. Its mathematical modeling is shown by the following:

$$v_t = \left(C_\mu \frac{k k_p}{\varepsilon_p} \right)$$

$$\frac{D k_p}{D t} = \frac{\partial}{\partial x_j} \left((v + v_t) \frac{\partial k_p}{\partial x_j} \right) + P_k - \varepsilon_p$$

$$\frac{D k_T}{D t} = \frac{\partial}{\partial x_j} \left((v + v_t) \frac{\partial k_T}{\partial x_j} \right) + \varepsilon_p - \varepsilon_T$$

$$\frac{D \varepsilon_p}{D t} = \frac{\partial}{\partial x_j} \left((v + v_t) \frac{\partial \varepsilon_p}{\partial x_j} \right) + C_{P1} \frac{\varepsilon_P}{k_P} P_k - C_{P2} \frac{\epsilon_P^2}{k_P} + C'_{P1} k_P \frac{\partial \bar{u}_i}{\partial x_m} \frac{\partial \bar{u}_i}{\partial x_j} \varepsilon_{lmk} \varepsilon_{ijk}$$

$$\frac{D \varepsilon_T}{D t} = \frac{\partial}{\partial x_j} \left((v + v_t) \frac{\partial \varepsilon_T}{\partial x_j} \right) + C_{T1} \frac{\varepsilon_P \varepsilon_T}{k_T} - C_{T2} \frac{\epsilon_2^T}{k_T}$$

These equations are derived from mean Reynold's Stress equations. The coefficients used include $C_\mu = 0.09, C_{P1} = 2.2, C'_{P1} = -0.11, C_{P2} = 1.8 - 0.3 \frac{\frac{k_P}{k_T} - 1}{\frac{k_P}{k_T} + 1}, C_{T1} = 1.08 \frac{\varepsilon_P}{\varepsilon_T}, C_{T2} = 1.15$ and $P_k = -\overline{u_i u_j} \frac{\partial \bar{u}_i}{\partial x_j}$

Here, k_p and k_I are turbulence kinetic energy and dissipation ranges. P_k is the rate at which turbulence energy is produced from the mean motion, ε is the rate at which turbulence energy is dissipated, ε_p is the rate at which energy is transferred out of the production range whereas ε_T is the rate at which energy is transferred into the dissipation range from the inertia range.

The above derived $k-\varepsilon$ model performs better than the standard single-scaled $k-\varepsilon$ model for plane and round jets. It also handles the complex-flows that involve reattaching and separating flows. This due to the replacement of ε_p to P_k in the dissipation rate ε equation.

2.8.1.2.5 Low Reynold's Number Modifications

The previously mentioned models predict well accurately for high Reynold Numbers, however fail for laminar flow regime or flows near the wall, where the Reynold Number is pretty low and viscous forces are significant. Hence, models that work in such regimes are called Low Reynold Number (LRN) Models. Amongst the many present, the following equations are presented by Bredberg for the $k-\omega$ model:

$$\frac{\partial k}{\partial t}+\frac{\partial}{\partial x_j}(\bar{u}_j k)=\frac{\partial}{\partial x_j}\left(\left(v+\frac{v_t}{\sigma_k}\right)\frac{\partial k}{\partial x_j}\right)+P_k-C_k k\omega$$

$$\frac{\partial \omega}{\partial t}+\frac{\partial}{\partial x_j}(\bar{u}_j \omega)=\frac{\partial}{\partial x_j}\left(\left(v+\frac{v_t}{\sigma_\omega}\right)\frac{\partial \omega}{\partial x_j}\right)+C_\omega\left(\frac{v}{k}+\frac{v_t}{k}\right)\frac{\partial k}{\partial x_j}\frac{\partial \omega}{\partial x_j}+C_{\omega 1}\frac{\omega}{k}P_k-C_{\omega 2}\omega^2$$

where the turbulence kinetic viscosity is presented by:

$$v_t=C_\mu f_\mu \frac{k}{\omega}$$

and the damp function is given by:

$$f_\mu=0.09+\left(0.91+\frac{1}{Re_t^3}\right)\left[1-exp\left\{-\left(\frac{Re_t}{25}\right)^{2.75}\right\}\right]$$

the constants for the given model are $C_\mu=1, C_k=0.09, C_\omega=1.1, C_{\omega 1}=0.49, C_{\omega 2}=0.071, \sigma_k=1\ and\ \sigma_\omega=1.8$

This model shows significant improvements over the Wilcox $k-\omega$ model for the cases that involve channel flow, backward facing step flow and rib-roughened channel flow.

2.8.2 Multiphase Flow Models

The multiphase modelling in CFD provides a powerful tool to reflect the fluid behavior within a solid bed[45]. Generally, there are two approaches that serve such aim: Eulerian-Eulerian treatment and Eulerian-Lagrangian treatment[41]. The Eulerian-Eulerian approach, also known as Two-Phase Model, treats both the fluid and the solid as continua. Each of the phases has its controlled volume (obtained from the volume fraction); and the transport of heat, mass, and momentum are treated in proportion to these volumes. The granular properties are reserved from the granular theory equations[46]. In the Eulerian-Lagrangian approach, only the fluid is taken as a continuum. The solid phase is discrete, and the model equations are applied for each particle, resulting in more computational demand. The Eulerian-Lagrangian model is more accurate as it takes into consideration the different interactions between the particle, and between them and the boundary, however, it is not recommended for the majority of applications[41] since the Eulerian-Eulerian is more practical.

The Eulerian-Eulerian approach solves the principal conservation equations in proportion to every phase volume fraction. The continuity equation solved in ANSYS Fluent is represented by Equation 5[47]:

$$\frac{1}{\rho_{rq}}\left(\frac{\partial}{\partial t}\left(\alpha_q\rho_q\right)+\nabla.\left(\alpha_q\rho_q\vec{v}_q\right)\right)=\sum_{p=1}^{n}(\dot{m}_{pq}-\dot{m}_{qp}) \quad (5)$$

Where ρ_{rq} is the volume averaged density of phase q, α_q is the volume fraction of phase q, ρ_q is the physical density of phase q, $\vec{v}_q$ is the velocity of phase q, $\dot{m}_{pq}$ equates to the mass transfer from phase p to phase q and similarly $\dot{m}_{qp}$ equates to the mass transfer from phase q to phase p.

The momentum equations solved in ANSYS Fluent are of the form presented by Equation 6[47]:

$$\frac{\partial}{\partial t}\left(\alpha_q \rho_q \vec{v}_q\right) + \nabla.\left(\alpha_q \rho_q \vec{v}_q \vec{v}_q\right) = -\alpha_q \nabla \mathrm{p} + \nabla.\bar{\bar{\tau}}_q + \alpha_q \rho_q \vec{g} + \sum_{p=1}^{n}(K_{pq}(\vec{v}_p - \vec{v}_q) + (\dot{m}_{pq}\vec{v}_{pq} - \dot{m}_{qp}\vec{v}_{qp}) + (\vec{F}_q + \vec{F}_{lift,q} + \vec{F}_{vm,q}) \quad (6)$$

Where $\bar{\bar{\tau}}_q$ is the stress-strain tensor for phase q, K_{pq} is the interphase momentum exchange coefficient, $\vec{F}_{lift,q}$ is the lift force acting on a secondary phase p in a primary phase q and similarly $\vec{F}_{vm,q}$ is the virtual mass force acting on the phase.

2.8.3 Soil[41,46,48,49]

One the main challenges for a predictive CFD model is the representation of the soil. For that purpose, the Eulerian-Eulerian model used to characterize the soil must be understood thoroughly. The secondary phase - solid (here soil) is a granular material, constituted of a large number of particles, which behaves as a dispersed phase in the carrier fluid that supports this flowing phase. There are solid-solid, fluid-fluid and solid-fluid interactions. The Eulerian-Eulerian model treats both the fluid (primary phase) and the solid (secondary phase) as continua and each of the phases has its controlled volume.

The granular properties of the solid are reserved from the granular theory equations. They model the flow of the granular phase by accounting for the following forms of granular dissipation:

a. In a dilute region of the flow, the particles randomly fluctuate and the viscous dissipation is kinetic.
b. In a more concentrated region, some particles start colliding and the viscous dissipation is now kinetic + collisional.
c. At very high concentrations, the particles collide more and the sliding becomes frictional, the dissipation is different and is frictional.

These forms are illustrated in Figure 13.

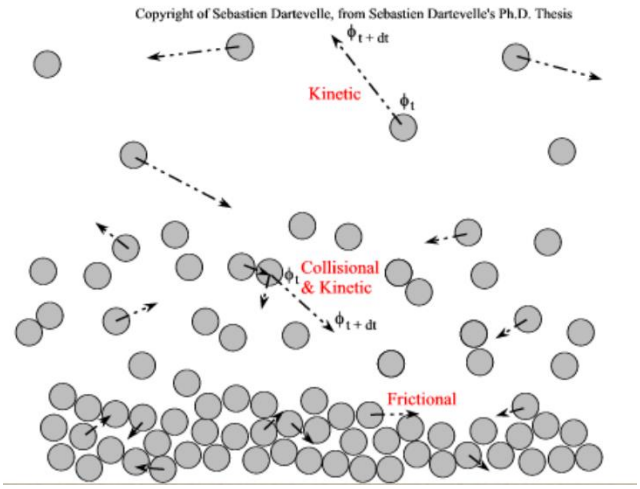

Figure 13: The main forms of the dissipation in a granular flow (reprinted from Dartevelle, 2003[48])

The momentum transfer will be different according to the kind of dissipation and the granular regime. This is manifested in the momentum equation of the solid phase, which is a function of the fluid pressure, solids stress tensor and interaction terms, as shown in Figure 14 and in Equation 6 from the last section. The solids stress tensor is the origin of the granular characteristics of the

solid phase. It is a function of the strain rate, solids pressure and bulk and shear viscosities. The shear viscosity is a function of kinetic, collisional and frictional viscosities.

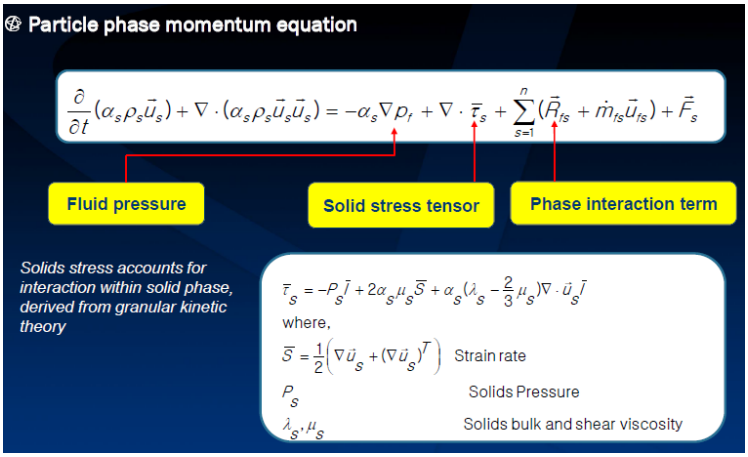

Figure 14: Momentum equation of the solid phase (reprinted from Gyo-Soon from CD-adapco Group[50])

The pressure and the viscosities are function of the radial distribution function and the granular temperature. The radial distribution function is a correction term that modifies the probability of collision close to packing limit, which is the solid volume fraction at maximum packing. The granular temperature is associated with the random fluctuating particle velocity and is calculated by solving its transport differential equation.

These granular properties are modeled according to different models, that are available in the CFD software.

3 METHODOLOGY

The goal of this research is to provide a model to simulate an underground leakage of methane from a buried pipeline. Such model enables the identification of the different possible outcomes (regimes) resulting from an input release situation. After establishing the model, the main input parameter we are aiming to study is methane inlet pressure, to delineate the boundaries between the different regimes and to obtain the mass release rate at the ground. To prove the applicability of the model, the burial depth of the pipeline and the release orientation are varied for given pressures. To achieve the goal, **five** stages are followed:

Stage 1:

Conduct of a literature review on the topic, specifically: the mathematical, numerical and experimental models that attempted to model an underground release, the various possible regimes, the characterization of the soil in CFD software, the different factors that affect the release, and the possible outcomes that can be calculated and deduced from the model. This stage was accomplished and summarized in Chapter 2.

Stage 2:

Buildup of the 3D model on the CFD software ANSYS Fluent. The modeling is comprised of: constructing the geometry, followed by performing the meshing and finalized by setting up the models that characterize the problem in hand. These are constructed according to the experimental work found in literature from Stage 1[4]. At stage 2, attempts will be made to discover the significant parameters to the problem, that will allow to visualize the different outcome regimes. This will also allow to identify the parameters that should not be considered, as they will not be relevant to

the case studied. This stage will result in a model, including the necessary parameters, however not the optimum ones. This stage is summarized in Chapter 4.

Stage 3:

Finalize the model through conducting a sensitivity analysis to find the optimum parameters for the ones proved to characterize the model in Stage 2. The parameters will be changed one at a time by fixing the others. The parameters of interest are the meshing refinement degree, soil particle diameter, turbulence model, granular viscosity and frictional viscosity of the soil. The optimum parameter is one that is in accordance with the experimental work used for the validation[4]. In case more than one model is in accordance with the experiment, the more advanced model is chosen because its computations are based on less assumptions i.e. more accurate. At the same time, the model should give the desired outcome in an acceptable solution time and a precision level.

Stage 4:

Conduct a case study to identify the different possible regimes/outcomes according to the inlet pressure for an upward release orientation and a soil burial depth of 100cm. After validating the applicability of the model in Stage 3, and fixing all the optimum parameters found, the inlet force (or pressure) applied on the hole is varied to obtain the outcome regime and the mass release rate. To represent the data, two plots are generated. One plot allows to identify the mass release rate at the ground associated with the various inlet pressures for a burial depth of 100cm and an upward release orientation. Another plot combines the outcome of the model along with the outcome of the experiment[5], allowing the delineation of boundaries between the possible regimes, according to the inlet force at a burial depth of 100cm.

Stage 5:

Test the applicability of the model to various input parameters, by identifying the outcome regime when varying the soil burial depth at three given pressures. The outcome from the burial depth study is added to the generated nomograph along with additional experimental points. Accordingly, the overall outcome of this study is a nomograph permitting the detection of the regime associated with a certain release pressure and burial pipeline depth for an upward release orientation. Infinite combinations can be added to complete the nomograph that can serve as basis for regime identification. This nomograph is for a single release orientation. This could be replicated for various release orientations if this parameter has an effect on the outcome. To test this, the outcome regime is obtained when varying the leak orientation (upward, downward, to the left, to the right) for two given pressures.

4 CFD MODEL BUILDUP

For constructing the model, the steps followed on ANSYS Fluent Software are: construction of the geometry, performance of the meshing, setting up the models, and generation of the results.

4.1 Geometry

The geometry is set in accordance with the experimental setup of Houssin-Agbomson et al.[4], mentioned in the literature part (experimental investigation), as shown in Figure 15.

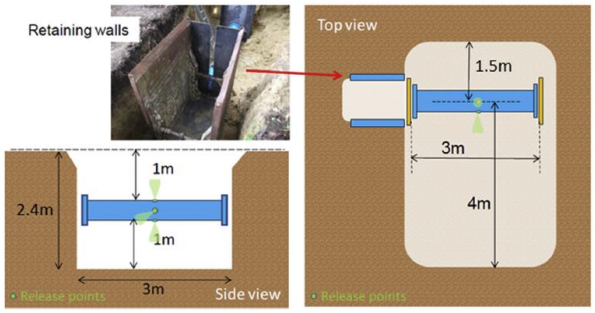

Figure 15: The geometry of the experimental setup used for the validation of the developed CFD model (reprinted from Houssin-Agbomson et al., 2018[4])

The model is constructed as a 3D model. The lower part (soil) is a 3D rectangular shape of dimensions 550cm×240cm×300cm in which a pipeline of 40cm diameter with a hole of 1.2cm is buried at a depth of 100cm. The upper part (atmosphere) is modeled with the same dimensions as the soil, with the height of 500cm. The resulting geometry is shown in Figure 16.

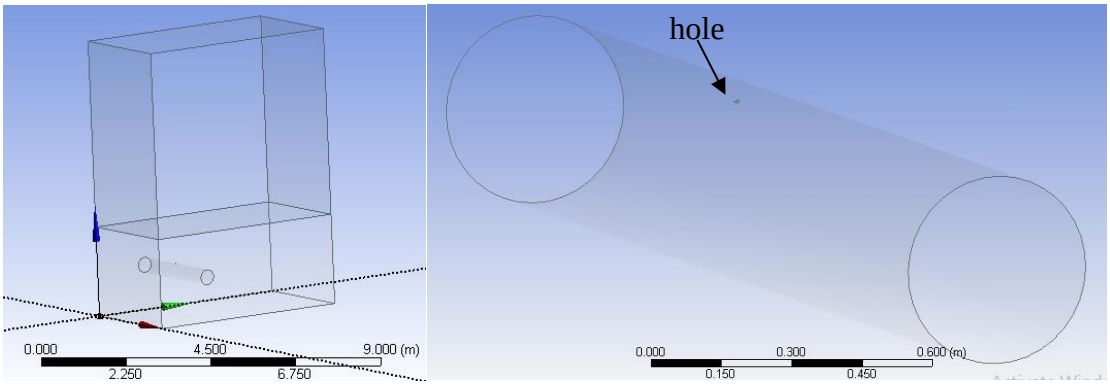

Figure 16: The geometry developed in ANSYS Fluent

In addition, at this step, the different parts of the geometry are identified so that the necessary boundary condition is set at a later stage. The different parts are shown in Table 1.

Table 1: Names of the selected parts of the geometry

Bodies	**Faces**	**Walls**	**Atmospheric pressure outlets**
Atmosphere	Inlet (inlet of the pipe)	Walls of the soil Wall of the pipe	The different faces of the atmosphere
Soil	Outlet (outlet of the pipe)		
Fluidinpipe (comprised of the gas in the pipeline)	Interface 1 and 2 (faces of the hole intersecting with the soil and the gas, respectively)		

4.2 Meshing

Meshing is the stage of the division of the geometry into nodes in which the principal physical conservation equations will be solved. The finer the mesh, the more precise the result is, but the more the computational time needed. Accordingly, the aim is to refine in a way to obtain an acceptable precision within a reasonable time frame. Various meshes were performed along the project to find the optimum mesh. At this stage - stage of model buildup - the parameters of interest are discovered, and the meshing is discovered to be one of them as it affects the results.

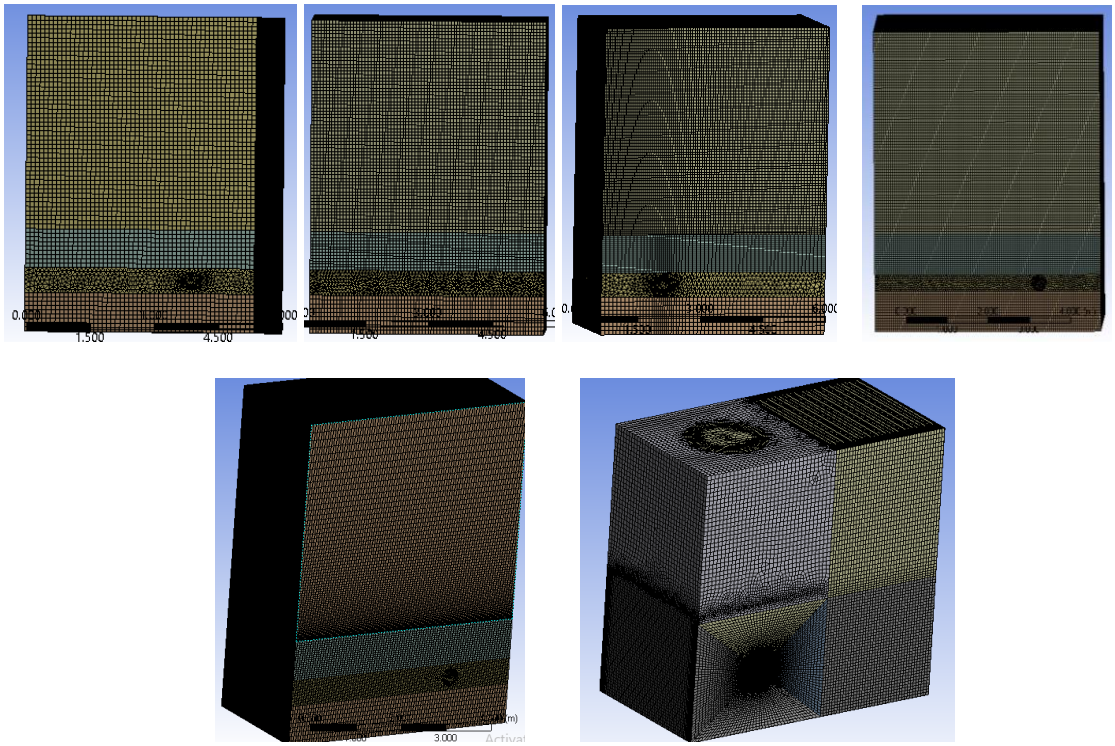

Figure 17: Different meshes performed along the project

The meshes of the first raw of Figure 17 have number of elements of 260,000 – 870,000 and 1 million, respectively from left to right. For the second raw, the number of elements is 2 million, 3

million and 4 million elements respectively from left to right. These refinements are performed to check how far can the refinement go while giving results within a reasonable amount of time. At this stage no sensitivity analysis is done, to choose the best mesh, because this is the work performed in Chapter 5. Rather, this stage is done to reveal that the mesh affects the results, and that it's preferable to keep the number of elements less than 4 million as the computation becomes prohibitive, even using a supercomputer.

4.3 Fluent Setup

The model is set to be transient since the interest of the project is to study the evolution with time, with a gravitational constant of -9.81 m/s^2 in the y-direction. The four main aspects to characterize are: the **multiphase system**, the **turbulent behavior**, the **boundary conditions** and the **software solver characteristics**.

4.3.1 The multiphase system

Due to the presence of soil, air and methane, there is a multiphase system having several phases interacting. The multiphase flow will be modelled through the Eulerian-Eulerian approach, treating the soil, methane and air as a continuum; each phase represented through its volume fraction. This approach requires much less computational power than the Eulerian-Lagrangian method and it is recommended in literature for CFD simulations with such big domains of soil.

The materials are first specified as air, soil and methane. Then, air is specified as primary phase, soil as secondary granular phase (being a solid), and methane as another secondary non-granular phase. The soil is characterized according to the granular theory (mentioned in the Soil section) that distinguishes the soil and characterizes it as a solid. This is done by following these steps in ANSYS Fluent:

The soil is first defined as a material by setting its **density**. Then, the soil material is chosen as a secondary granular phase that requires the following granular properties: **Particle diameter**, **Granular viscosity**, **Granular bulk viscosity**, **Frictional viscosity**, **Granular temperature**, **Solids Pressure**, **Radial distribution**, **Elasticity modulus** and **Packing limit** where:

- **Granular viscosity**: includes the kinetic and collisional terms of the shear viscosity.
- **Granular bulk viscosity:** accounts for the resistance of the granular particles to compression and expansion.
- **Frictional viscosity:** additional viscosity to the granular viscosity term that will sum up to give the solids shear viscosity.
- **Elasticity modulus:** a measure of a substance's deformation upon stress application. It is the slope of the stress-strain curve of the material in the elastic deformation region.
- **Packing limit:** solids volume fraction when all particles are touching each other: when they are packed in the greatest possible density.
- **Radial distribution:** function that modifies the probability of collision close to packing limit.
- **Granular temperature:** associated with the random fluctuating particle velocity.

For the experimental work followed, two types of soil are used: clayey (CL) and sandy (SP-SM) soils according to the **USCS: Unified Soil Classification System**[4]. This classification gives general guidelines about the soil **density** (needed for the material), **particle diameter** (one of the granular properties) and **porosity** (needed for initial conditions). The remaining granular properties are characterized according to the granular theory models available in the software. The chosen model will be mentioned according to the performed case.

4.3.1.1 Density and Porosity[51,52]

To get the density and porosity of the corresponding soils, the following definitions are used.

- Specific gravity G_s: $Gs = density\ of\ solid\ particles\ /\ density\ of\ water$

  Typically: 2.65-2.85. For sand: 2.65 and for clay: 2.7

- Void ratio e: $e = \frac{Vvoids}{Vsolids}$
- Porosity n: $n = \frac{Vvoids}{Vtotal}$
  - e and n are related by: $e = \frac{n}{(1-n)}$ and $n = \frac{e}{1+e}$
- Water content w: $w = \frac{M_{water}}{M_{solids}}$ can be higher than 1
- Saturation S: $S = \frac{Vwater}{Vvoids} = \frac{Vwater}{Vwater+Vair}$ can be maximum 1
  - S and w are related by this equation: G_s*w = S*e
- Density (kg/m^3):

1. For a dry density – all voids filled by only air (no water): $\rho_{dry} = \frac{1000*G_S}{1+e}$
2. For a fully saturated density – all voids filled by only water: $\rho_{saturated} = \frac{1000*(G_S+e)}{1+e}$
3. For something in between – not fully saturated – where there is both air and water: $\rho = \frac{1000*(G_S+e*S)}{1+e}$

For the clayey and sandy soils used in our case, the USCS guidelines are the following:

For clay CL: ρ = 1520-1920 kg/m^3 for a w = 12-24%

For sand SP-SM: ρ = 1600-2000 kg/m^3 for a w = 11-21 %

Application Examples to get density and porosity:

If middle values of the given ranges above are taken, the density and porosity can be calculated for each of the soils.

1. **Clayey soil CL:** ρ = 1720 kg/m^3 and w = 18% for S = 70%
   - $\rho_{dry} = \frac{\rho}{1+w} = \frac{1720}{1+0.18} = 1458$ kg/m^3
   - $\rho_{dry} = \frac{1000*2.7}{1+e} = 1458$ → e = 0.85 → **n = 0.46**
   - $\rho_{saturated} = \frac{1000*(2.7+0.85)}{1+0.85} = 1919$ kg/m^3 (if S = 1)
   - If S = 0.7 → $\rho = \frac{1000*(2.7+0.85*0.7)}{1+0.85}$ → **ρ = 1781 kg/m^3**
2. **Sandy soil SP-SM:** ρ = 1800 kg/m^3 and w = 16% for S = 70%
   - $\rho_{dry} = 1552$ kg/m^3
   - e = 0.71 → **n = 0.42**
   - $\rho_{saturated} = 1965$ kg/m^3
   - **ρ = 1840 kg/m^3**

4.3.1.2 Particle Diameter[51,52]

Based on **USCS**, the particle diameter range for each of the soils is presented by the following.

1. **Clayey soil CL**

To classify as CL, the soil should have %fines > 50%

Thus, CL has:

>50% has particles <0.0075cm

<50% has particles >0.0075cm

2. Sandy soil SP-SM

To classify as SP-SM, the soil should have

1- %sand > %gravel

2- %fines = 5-12%

Particle diameter: Gravel: 0.475 → 7.5cm

Sand: 0.0075 → 0.475cm

Fines (silt and clay): <0.0075cm

Thus, SP-SM has:

>40% of the particles between 0.0075 and 0.475cm

<12% of the particles between 0 and 0.0075cm

Remaining is >0.475cm

In this work, soil is studied as sand. Out of the obtained ranges for the density, porosity and particle diameter, the density is fixed at 1800 kg/m^3, the porosity is taken to be 40% and the particle diameter is modeled as a constant value (closest possible to the average of the values in the range). The aim is to achieve the expected outcome to validate the study using the experimental work[4]. To do that, the values obtained from USCS are used as guidelines that can be changed according to the outcome, as the software treats the soil differently, and since the values belong to ranges and not given values.

4.3.2 The turbulent behavior

Having a turbulent flow, a turbulence model should be specified. The standard k-ε model is a well-known model that is successful in various applications. It is used as a base model and it will be varied according to the need along the project. Updated k-ε and others two-parameter models will be tried. At this stage, the aim is to check whether the turbulence model should be considered as affecting or not.

4.3.3 The boundary conditions

The boundary conditions are related to the names specified during the geometry construction step. The boundary conditions are various: inlet pressure-velocity-mass flow rate, walls (no-slip condition), interfaces (to make any part homogeneous inside the geometry), symmetry (2 or more sides behave the same), etc. For our case the force of the gas can be input through an inlet pressure, or mass flow rate. The inlet can be the inlet of the pipeline or at the hole. The various boundary condition combinations for inputting methane are tried to find the most suitable one for this work. In all cases, the atmosphere has an ambient pressure at the external boundaries, acting as imaginary ends of the atmosphere (because we are interested in the part of the atmosphere where the leak will extend only). The soil has walls on the sides, as the experiment includes a pipeline closed from both sides.

4.3.4 The software solver characteristics

The software solver characteristics are the parameters the solver uses to make the simulation converge and/or more accurate. They are: **methods**, **controls** and **simulation time specifications**.

4.3.4.1 Methods

The way the derivatives in the conservation equations are obtained and approximated affects the accuracy of the model. This will lead to a converging and/or precise solution. Accordingly, the methods for solving should be specified in this part. The scheme used for the pressure-velocity coupling is the SIMPLE method. The schemes used for the spatial discretization of all the properties (momentum, volume fraction, k, ε…) are varied to optimize accuracy and computational time. If the computational time is fairly acceptable, the second order upwind and/or QUICK are used. The transient formulation is solved using the First Order Implicit scheme.

4.3.4.2 Controls

The controls are represented by the correction (relaxation) factors that are multiplied by the solution at every iteration to adjust it before entering the next iteration. This is used to make the solution converge better and give a quicker solution. The relaxation controls are varied according to the refinement, time step size and the geometry itself. Low relaxation factors are used due to the hard-computational demand.

4.3.4.3 Simulation time specifications

This includes the time step size, number of time steps that will give rise to the real time desired to simulate, and the maximum number of iterations that are set before proceeding into the next time step. The time step size is highly related to the mesh size because the Courant Number Cr: $Cr = \frac{u \times \Delta t}{\Delta x}$ (u the velocity of the flowing gas, Δt is the time step size, Δx is the mesh size) should stay small (close to 1), otherwise the simulation diverges. While having a refined mesh, the time step size should be automatically small for minimizing the Cr.

4.4 Results

The geometry, meshing and model setup steps mentioned are the general guidelines applicable for every simulation, to which properties, models and specifications are input to run every case. The simulation presented in this section are the ones followed to discover what models and properties to input after fixing the geometry and meshing to 1million elements. In a first attempt, the goal is to test if the model is properly working and generating a leak across the geometry. For that purpose, the first case does not include any soil, but only air and methane. Air is included everywhere along the geometry except at the only place methane is present: the hole. Methane is going out of the hole through setting the boundary condition at the hole as a pressure inlet of 50 bars. Since the aim of the work is to maintain a constant pressure at the hole with time[4], the pipeline can be kept or removed as long as the pressure is constant at the hole. This is why, the pipeline is removed to easily input a boundary condition at the hole, since the aim is to test whether the model is working or not. The standard k-ε model is used to model the turbulence in the system.

Figure 18a shows the volume fraction distribution of methane along the plane of the release after 5 seconds of simulation. Methane is spreading above the hole till the end of the atmospheric boundary, as is the case of a crater in the presence of a high pressure. The quantity of methane diminishes gradually the more the distance is away from the hole. Figure 18b shows the velocity contour of methane, showing a high velocity of 250 m/s at the hole that progressively diminishes while going up.

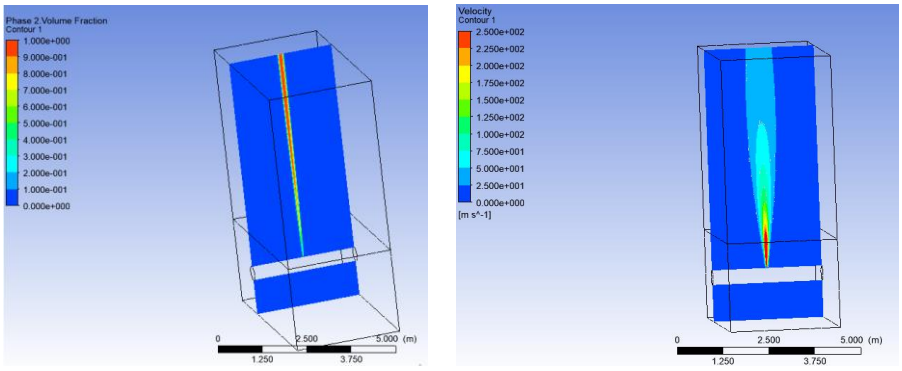

(a) (b)

Figure 18: Case 1 Methane Volume Fraction after 5s (a) and Methane Velocity after 5s (b)

Next, soil is added with a density of 1800 kg/m^3, porosity of 0.4, and default granular properties. By this it means that the particle diameter is 0.001cm, the granular viscosity has a constant value of 10^{-5} kg/m.s, no granular bulk viscosity or frictional viscosity are included, the packing is assumed spherical and so the packing limit is 0.63, the rest of the properties are modelled through default models that are not studied in this work. The same conditions mentioned above still hold. However, the case diverged immediately as it could not converge with the pressure input at the hole, in the presence of soil. This condition requires a lot of computation and iteration to calculate the velocity and the mass flow rate. It should be noted that inputting a velocity could solve the problem, however velocity is a property that is not usually known or specified. In order to achieve the desired pressure, the mass flow rate is input as an inlet boundary condition at the hole of 0.01 kg/s, with all the conditions mentioned above. The distribution of the volume fraction of soil obtained after 0.01 s and 0.23 s is shown in Figure 19.

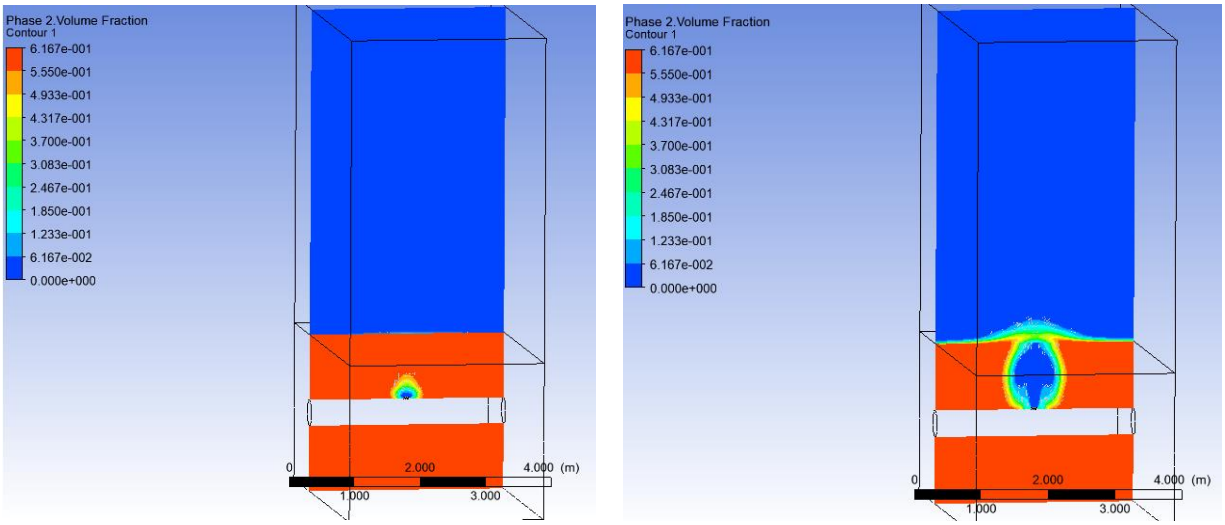

(a) (b)

Figure 19: Soil volume fraction at t=0.01s (a) and at t=0.23s (b)

The mass flow rate condition did not diverge; however, at t=0.01s, the pressure at the hole is 26.7bar, whereas at t=0.23s, the pressure at the hole is 0.12bar. This means that fixing the mass flow rate as a boundary condition does not allow the fixation of a certain pressure; rather it changes with time. The aim of this project is to input a constant pressure inside the pipeline along time; this is why the mass flow rate boundary condition is not a suitable choice.

To solve this issue, the hole is considered as an interface boundary condition. This option means that the hole is a common continuous part between the pipeline and the soil, at which the software itself will compute the properties, whereas the boundary condition is now specified at the pipeline entrance and exit. The boundary conditions are pressure inlet from both side of the pipeline, which allow to maintain a constant pressure in the pipeline and at the hole, along the time of the simulation. The other boundary conditions, multiphase modeling, and turbulence model are still used as before. This leads to a converging solution. Three different pressures are tried to simulate this case: 10, 36 and 47 bar. This is done because the different pressures are expected to generate

different regimes. The corresponding volume fraction of methane and soil are shown along the plane passing through the hole in Figure 20.

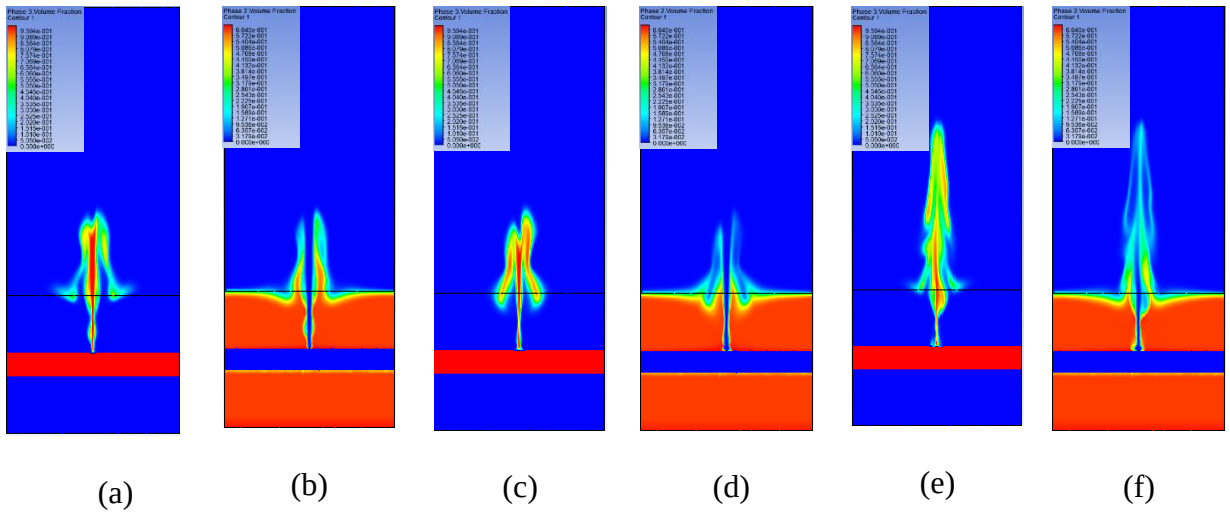

(a) (b) (c) (d) (e) (f)

Figure 20: Volume fraction of methane at pressure of 10 bars (a) 36 bars (c) 47 bars (e) and volume fraction of soil at 10 bars (b) 36 bars (d) and 47 bars (f)

According to the pressures, 10 bars should not trigger a crater. It should result in an uplift and cracks, whereas Figure 20a shows that the volume fraction of methane is unity at the interface between soil and atmosphere, meaning that the soil is being fully displaced by methane. The result shows that the model is over-estimating the outcome. As the granular properties are by default i.e. no full characterization of the soil is yet done, this is not surprising. This is why, granular properties are input. The granular viscosity is modelled through gidaspow model (instead of a constant value), the granular bulk viscosity is modelled through Lun et al. model (instead of no bulk viscosity), the frictional viscosity is modelled through Shaeffer (instead of being excluded) and the packing limit is kept 0.63. The case is conducted at only the lowest pressure of 10 bars because there it is expected to visualize low uplift.

Out of this run, the methane volume fraction at time of 5s is extracted and shown in Figure 21. To evaluate the success of this run, it is compared to the previous results with default properties, shown in Figure 20a. As can be seen from the plots, the granular properties made the soil resist the movement of methane, as the methane leaking area is smaller now, however the methane is still fully displacing the soil. This means that the expected regime is not visualized yet.

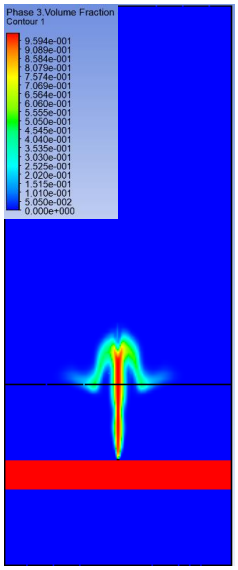

Figure 21: Methane volume fraction at 10bars after characterizing granular properties

To solve this, a variety of parameters can be investigated: turbulence model, particle diameter, phase interactions modelling, and others. At this stage, it is unknown which parameter will affect the outcome. This is why, various tests are conducted starting from the 10bars case. The first one is the decrease of pressure from 10 to 1bar. The aim from this test is to verify if any pressure will trigger diffusion ever, to understand whether the problem arises from a certain pressure, or this regime is not visualized at all with the current modelling. The result is almost identical in terms of

outcome, where methane is displacing the soil almost completely; and no diffusion or uplift are visualized. This is why, other parameters are now changed as well starting from 1bar, as the diffusion will be visualized at this low pressure first rather than 10bars. The tests performed and the outcomes obtained are summarized in Table 2.

Table 2: Trials performed to visualize uplift starting from the case of 1bar

Case description	**Original case**	**Turbulence model change**	**Particle diameter change**	**Include phase interaction**
Turbulence model	Standard k-ε	Realizable k-ε	Standard k-ε	Standard k-ε
Particle diameter (cm)	0.001	0.001	0.01	0.001
Mass transfer Modelling	Not modelled	Not modelled	Not modelled	Include mass transfer between methane diffusing from the gaseous mixture (air and methane) to the solid mixture (soil and air)

Table 2: Continued

Outcome	Soil fully displaced	Soil fully displaced	Strong uplift where the soil is not fully displaced	Diffusion visualization at all pressures with inaccurate results

As shown from Table 2, the turbulence model change was not the solution. It should be noted that this means that the realizable k-ε is not the solution at the low pressures, not that the turbulence model generally does not affect the regime or that it is not a crucial parameter. As for the inclusion of the phase interaction, there are several options to model the interactions between the phases. This allows the characterization of all the phases, among which the soil, which is significant for this study. This is done through specifying the drag, mass transfer, lift, etc. Among the different options, the mass transfer is modelled, through activating the species model. The species model allows the definition of mixtures defined from species, usually used when a species is present in small amounts with another dominant. Here, two phases are defined: the gaseous phase (methane and air) and the solid phase (soil, methane and air). This is done to characterize the mass transfer, from the methane species present in the gaseous phase to the methane phase present in the solid phase. Initially, methane is only present in the gaseous phase. Mass transfer is included as methane will diffuse and become present in the solid phase. Although this allowed the visualization of the diffusion at low pressure, through a lower methane volume fraction along the release than usual, but the results were not accurate as the pipeline does not fully contain methane. This is due to the soil entering to the pipeline although it is specified as wall. In addition to this problem, this diffusion was also visualized at high pressure so it was not highly dependent on the pressure. The

investigation in this domain was not fruitful in showing good results, although this might be an important parameter, but it is not that relevant to this project. It is more relevant to test the particle diameter, as the particle diameter present in the experimental work[4,5] is bigger than 0.001cm.

This is why, the mesh is adjusted in a way to allow for the particle diameter to be increased. This is because the smallest mesh size should be bigger than the particle diameter to avoid numerical problems. It should be noted that since the hole diameter is 1.2cm, then the mesh size has a limitation for increase, which is around 0.23cm, allowing to input a particle diameter of 0.01cm. Trying this particle diameter made the methane leak without displacing all the soil and forming a crater, as shown in Figure 22a.

The particle diameter parameter is the first to make this visualization possible, and accordingly this is a critical parameter, that should be further investigated. It should be noted that the particle diameter made this visualization possible at such a low pressure. However, since the pressure range is broad (up to 80bars), that does not mean that the particle diameter will be the most affecting parameter for all pressures. In addition, if the turbulence model is changed after changing the particle diameter, it might have a big effect. It is not comprehensive whether it affects generally or not. Accordingly, the only conclusion that can be drawn is that among the tried parameters at 1ow pressure, the particle diameter is the solution for the given pressure.

Knowing that the particle diameter made the model better, now other parameters are changed to discover if they affect the result further. This is why, the standard k-ω turbulence model is tried, while keeping all the others parameters the same, the particle diameter of 0.01cm among them. The result shown in Figure 22b reveals that a different result is obtained, as methane did not even attain the ground with standard k-ω, whereas it surpassed the ground with standard k-ε, in Figure

22a. This shows that the result will be affected by the turbulence model as well, and the regime obtained can be optimized accordingly. In other words, this is an additional parameter that can adjust the model. Additionally, the frictional viscosity is removed, and the result changed, as the leak spreads more in this case than the two other cases. The methane volume fraction is however smaller along the release than in the case of Figure 22a i.e. it is expected to give a lower outcome than the standard k-ε.

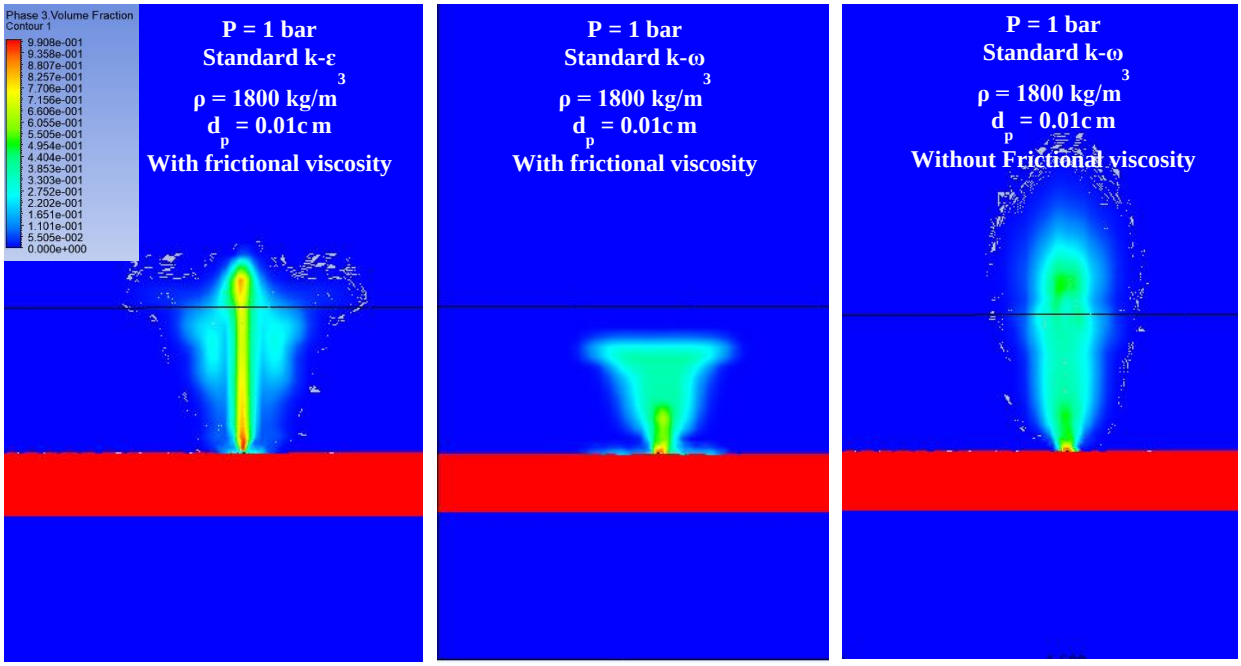

(a) (b) (c)

Figure 22: Effect of frictional viscosity and turbulence model on the result outcome

From this section, it can be concluded that the turbulence model, the particle diameter, the frictional and granular viscosity (as they complete each other and both characterize the viscosity of the soil) are parameters that affect the results. There are others, but these are the crucial ones

chosen to be studied. Since a lot of combinations exist to test them, a sensitivity analysis is performed while varying each one at a time and fixing the others, to find the optimum model characterizing the parameter. By optimum it is meant that it is the one that allows best validation with the experimental work[4,5] at the maximum amount of pressures, as it is almost impossible to test all the pressures, and it is insufficient to test only one. It should be noted that no sensitivity analysis can be conducted before a mesh independent study, as the coarsest mesh that gives the most accurate results should be found. This mesh is the one after which, no matter how much refinement is done, the results no longer change in a significant amount with respect to the additional needed computational power. Therefore, the sensitivity analysis is first conducted on the meshing, followed by the particle diameter. For these two, when the results keep varying, that means the best one is not yet found. Whenever the result no longer changes, it means that the best choice (mesh or particle diameter) is achieved. This is because the mesh is a numerical criterion (not defined by the experiment) that is found by this method for any problem. For the particle diameter, it is increased as much as possible with no numerical problems, as it is already defined by the experimental work to be in the range of a millimeter. After that, the turbulence model, frictional viscosity and granular viscosity models are tested. In additional to the previous reasoning, for these three parameters, validation should be aimed. This means that the regime obtained in the experimental work should be visualized at the best accuracy possible so that the model is chosen. It is no longer sufficient to just compare between the different models to choose the best, but the results should be compared with experimental work also.

5 SENSITIVITY ANALYSIS

Out of the model build-up in Chapter 4, it was deduced that there are a lot of parameters that can affect the behaviour of the model; the ones significant to this project are the meshing size, the particle diameter, the turbulence model and the granular viscosity model.

For that purpose, a sensitivity analysis is conducted where one parameter is varied at a time, while the others are maintained constant. Throughout the sensitivity analysis, the density of the soil is fixed at 1800 kg/m^3 and the release orientation is upwards. Each study on a parameter is done on at least two pressures because the chosen model should fit the range of pressure up to 80 bars.

The parameters to be changed are summarized in Table 3. The base case is using particle diameter of 0.01cm, turbulence model of standard k-ω, granular viscosity of Gidaspow and frictional viscosity of Shaeffer. This means that when one parameter is varied, the other parameters will be fixed at the base parameters. Once the optimum parameter is found, it becomes the new basis for the rest of the study.

Table 3: Parameters and models studied in the sensitivity analysis

Parameter / Model	**Trials**				
Meshing	Refinement #0		Refinement #1		Refinement #2
Particle diameter (cm)	0.001		0.005		0.01
Turbulence	Standard k-ε	RNG k-ε	Standard k-ω	BSL k-ω	SST k-ω
Frictional Viscosity	Modeled (Shaeffer)			Neglected	
Granular viscosity	Gidaspow et al. model			Syamlal-Obrien model	

Before proceeding into the sensitivity analysis results, it should be noted that the available experimental work used for validating the results is mostly qualitative. In this sense it is meant that although the resulting regime is known, but there is not a unique way to validate. Therefore, there should be some guidelines set to decide for the regime. These guidelines are quantitative results plotted to visualize properties and quantities generated throughout the leak for each case. The guidelines used are properties such as: the mass flow rate at the ground (interface between soil and atmosphere), the average methane and/or soil volume fraction along a sphere volume located in various places in soil. These volumes are located near the hole (x=1.5, y=1.55, z=1.5), near the atmosphere (x=1.5, y=2.4, z=1.5), between soil and atmosphere (x=1.5, y=1.9, z=1.5), to the left of the soil (x=1.5, y=2.22, z=0.5) and to the right of the soil (x=1.5, y=2.22, z=2.5). These locations are shown in Figure 23.

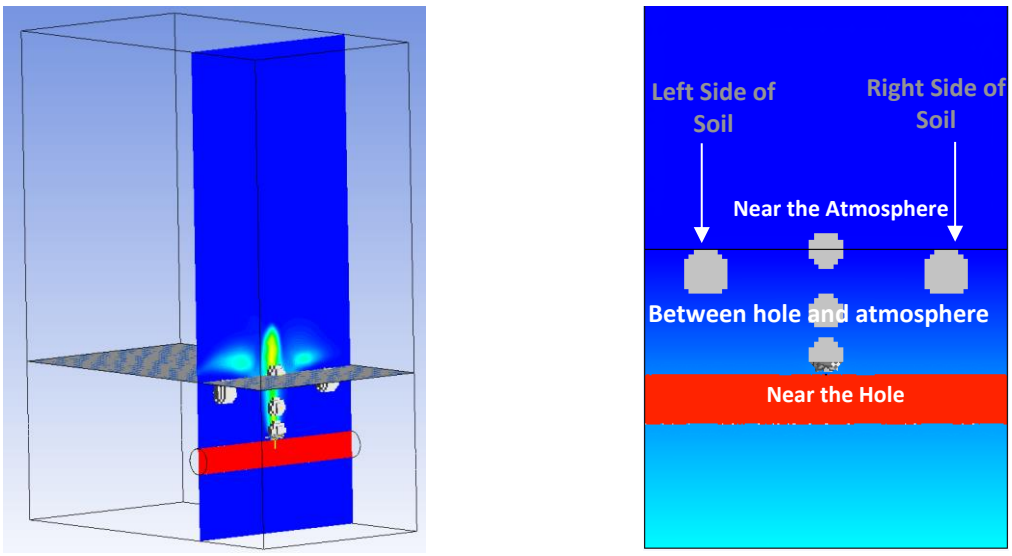

(a) (b)

Figure 23: Locations set for properties computations used for the sensitivity analysis: ground surface for mass flow rate (a) and sphere volumes for volume fraction (b)

These plots will be used according to the case; meaning that for the meshing and the particle diameter, the best option is the one that keeps giving different results; whereas for the turbulence and viscosities models, the best model is also the one that gives the intended regime. Accordingly, the soil volume fraction is valuable in the case of turbulence model to visualize the regime whereas it is not necessary in the meshing step; as the meshing can be decided from any important parameter that keeps changing, whether it is the soil or methane volume fraction. In the meshing choice, the importance is to no longer see any change, because the aim is to find the finest mesh that gives the best results accuracy within an acceptable computational time.

5.1 Meshing

The first parameter that is changed is the mesh size, while the four other parameters are fixed. The different meshes performed are shown in Figure 24. The coarsest mesh is entitled refinement #0 with 870,000 elements, the medium mesh is entitled refinement #1 with 1,400,000 elements and the finest mesh is entitled refinement #2 with 2,300,000 elements. These meshes are run with three different pressures: 1 bar, 15 bar and 40 bars. The mass flow rate at the ground, and the average methane volume fraction at the five spots will be shown in the results of every case.

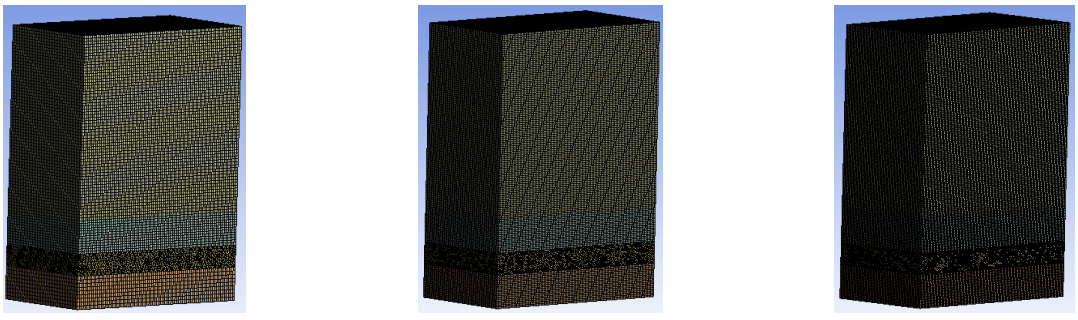

(a) (b) (c)

Figure 24: Meshes performed for sensitivity analysis (a) Refinement #0 (b) Refinement #1 (c) Refinement #1

The first tested pressure is 15 bars, being an intermediate pressure. The results of methane mass flow rate at the ground are shown in Figure 25. The results show that refinement #0 gives a much different result than the other refinements, suggesting that the mesh is affecting the results in the first place, and suggesting that one of the two refinements (1 and 2) should be picked to proceed with the analysis.

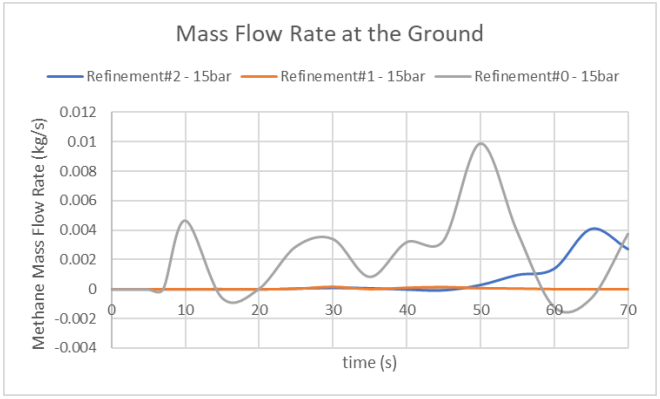

Figure 25: Methane mass flow rate at the ground with time for the different meshes at pressure of 15 bars

The methane average volume fraction results at various locations are shown in Figure 26. The results near the hole and between the hole and atmosphere gave similar results for all the meshes, meaning that no conclusion can be drawn from these plots. The difference was clearer in the location near the atmosphere, to the left and to the right of the soil. These plots show that refinement #0 is giving different results whereas both refinement #1 and refinement #2 are giving similar results, proving the points made in Figure 25. This suggests that refinement #1 should be chosen, as the results are no longer changing, and there is no need to make the computation harder.

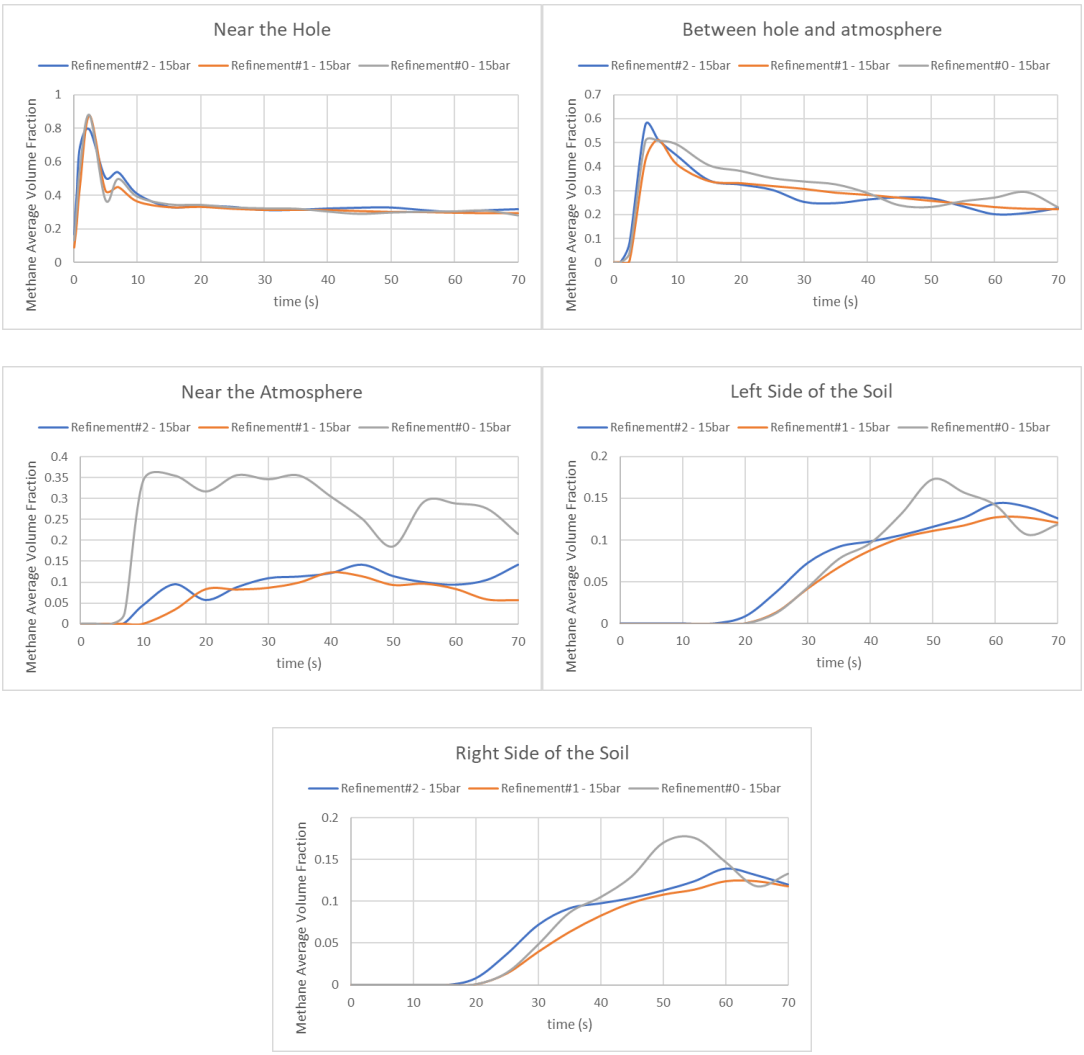

Figure 26: Methane average volume fraction with time for the different meshes at 15 bars

To confirm this, a higher pressure of 40 bars is tested. The mass flow rate at the ground shown in Figure 27 confirms the trend that refinement #1 and #2 are giving close results. To make sure, the average volume fraction of methane is also obtained.

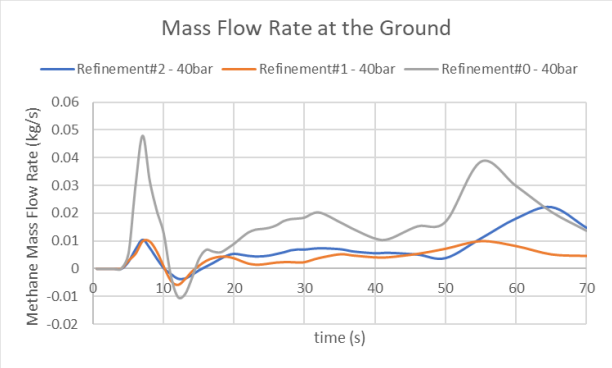

Figure 27: Methane mass flow rate at the ground with time for the different meshes at pressure of 40 bars

The methane average volume fraction results at various locations are shown in Figure 28.

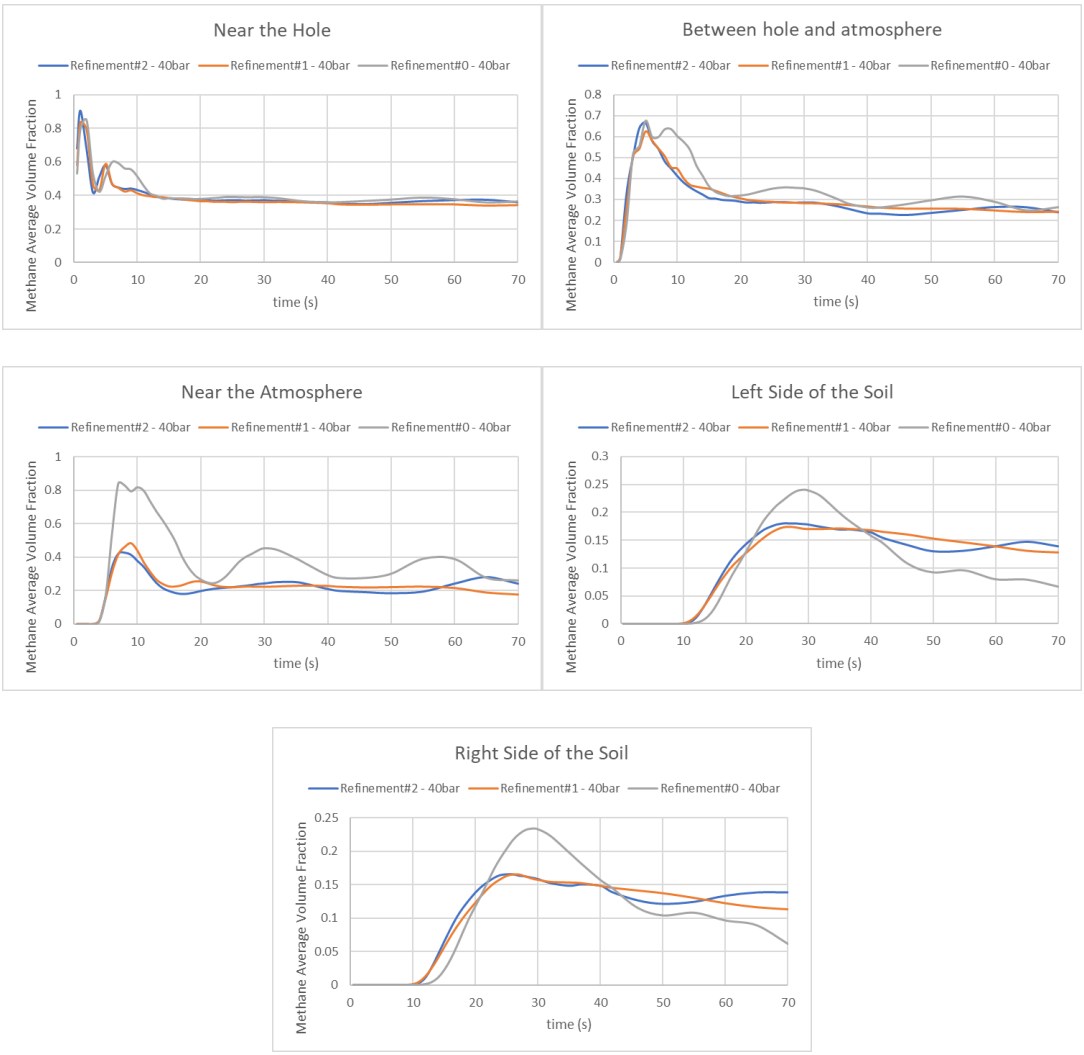

Figure 28: Methane average volume fraction with time for the different meshes at 40 bars

As shown in Figure 28, the trend is confirmed again, and if any difference is detected, it is between refinement #0 and the two others. It can be concluded from what has been presented that the mesh entitled refinement #1 is the best mesh to be used at moderate pressure. However, as the pressure becomes smaller or bigger, the mesh might be more affecting. This can not be known unless tested. This is why, the various meshes are tested at a pressure of 1 bar. The average volume fraction at several locations is shown in the plots of Figure 29. It should be noted that the left and right locations of the soil are not reported because there is no methane at this place in any of the cases, they are both identical to the result obtained Near the Atmosphere.

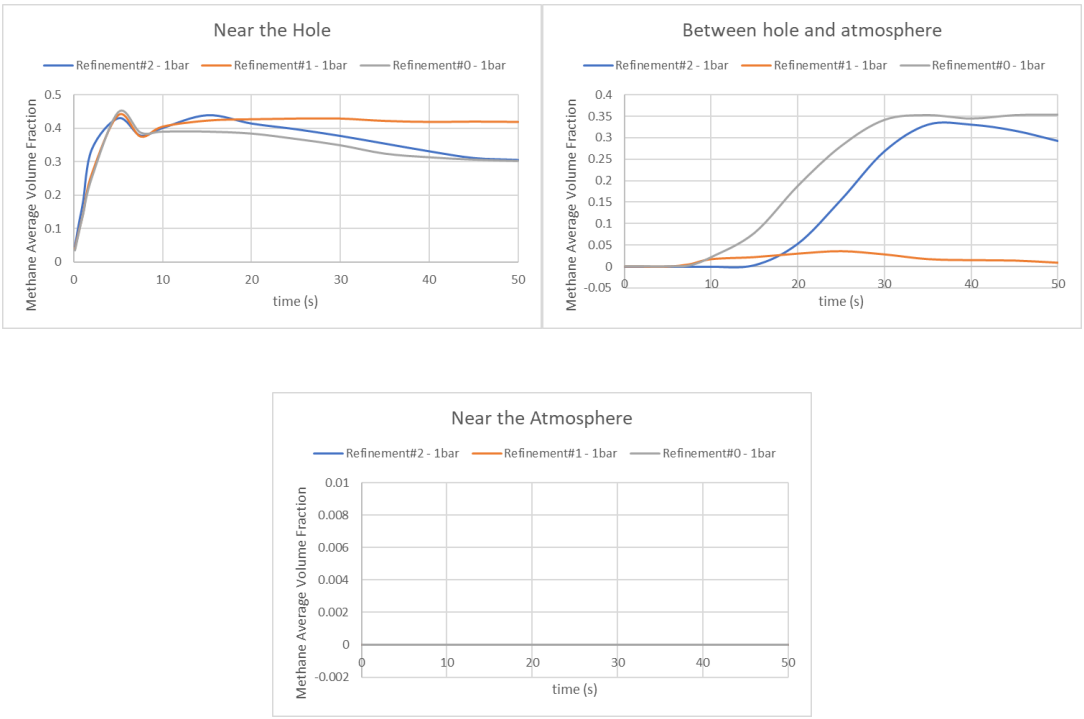

Figure 29: Methane average volume fraction with time for the different meshes at 1 bar

The location near the hole does not give any hint about the best mesh as they seem to be identical. From the location between hole and atmosphere, refinement #1 and #2 seem to give dissimilar results. This suggests that these two refinements will still give different results although the moderate pressures did not suggest that. From the location Near the Atmosphere, no conclusion can be drawn, since the values are all identical approaching zero as the three plots lie on top of each other. It should be noted that also the mass flow rate at the ground is zero in all cases as methane did not reach the ground within 50seconds due to the low pressure. The graph of Figure 30 shows this clearly.

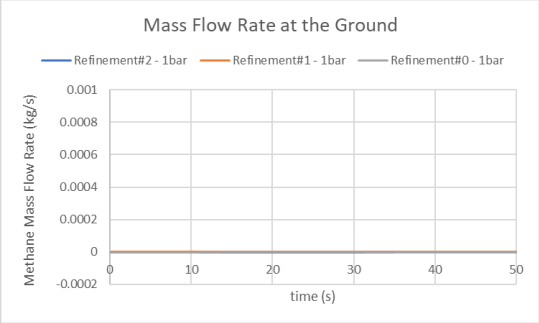

Figure 30: Methane mass flow rate at the ground with time for the different meshes at pressure of 1 bar

From the presented analysis, it is shown that although refinement #1 may be suitable for moderate pressures, but for low pressures the results are still differing. Choosing refinement #2 is more trustworthy and will generate more confident results. It should be noted that another refinement could have been done, however the additional computational power is not necessarily worth the precision obtained; as it was shown that refinement #1 is giving promising results, and so refinement #2 is sufficiently refined to be trusted at the extreme pressures. A refinement #3 with

around 4 million elements was tried but the computational power needed was demanding and it was not feasible to perform all the remaining work with such refined mesh. This is why refinement #2 is chosen to be the mesh for this project.

5.2 Particle diameter

Now that the mesh is fixed, the particle diameter is changed as it was discovered that it affects the soil resistance to the leak and accordingly the regime expected. It should be noted that the particle diameter used in the experiment[4] followed in this project is in the range of a millimeter. Accordingly, it is desired to increase the particle diameter as much as possible. The particle diameters tried are 0.01cm, 0.005cm and 0.001cm at two different pressures of 15 and 40 bars. The mass flow rate at the ground, and the average methane volume fraction at the five spots will be shown in the results of every case.

For the first pressure of 15bars, the results for the methane average volume fraction at the various locations are shown in Figure 31.

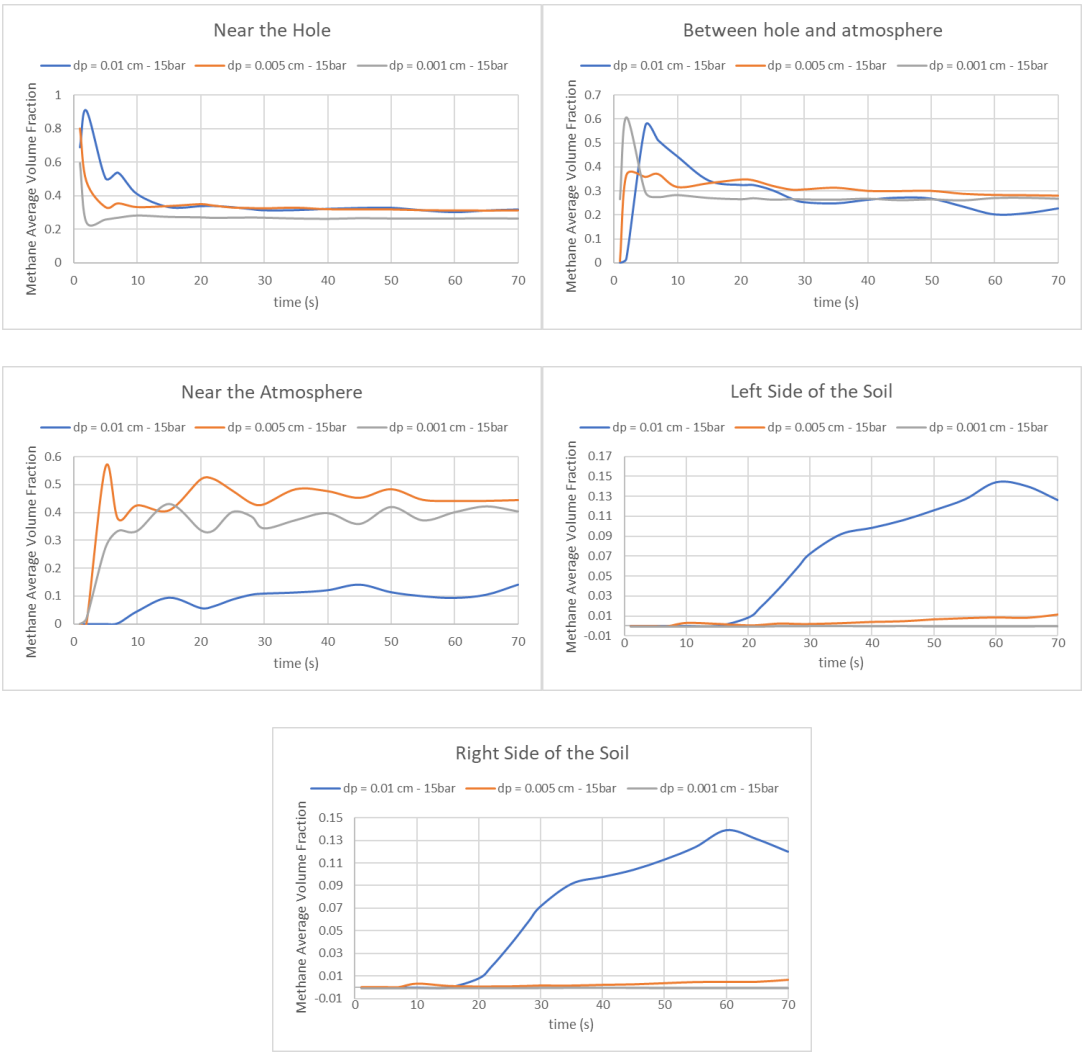

Figure 31: Methane average volume fraction with time for the different particle diameters at 15 bars

The results do not show a great difference between 0.005cm and 0.001cm, but the difference becomes significant at 0.01cm. The plots show that the particle diameter affects the results as the soil resists the movement more. This is shown by the plot Near the Atmosphere, as the methane volume fraction is much smaller near the ground in the case of 0.01cm than the other two smaller particle diameters. That is due to the fact that the soil held methane from going upward, which in turn means that the regime is expected to change. The bigger the particle diameter, the more the

regime is far from a crater. This is why, the big particle diameter allowed the visualization of diffusion for low pressures. To confirm this, the mass flow rate at the ground is plotted and shown in Figure 32. The mass flow rate at the ground is zero in the case of big particle diameter. It should be noted that even though the left and right spots expect more methane, that does not affect the decision of the regime. This means that methane gets scattered toward both sides instead of going upward, confirming the soil resistance to the methane flow. As the goal of this project is to make regimes like diffusion and uplift visible - as crater was visualized easily since the beginning - the particle diameter of 0.01cm is suggested since it allows the soil to resist the flow, making the visualization of low-pressure regimes possible.

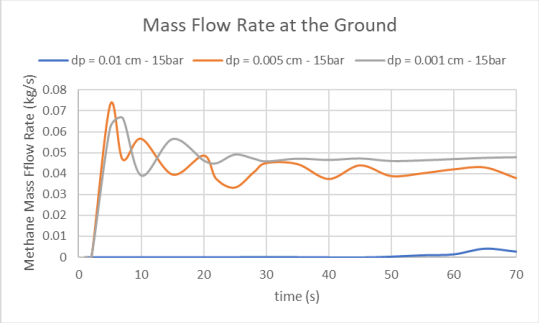

Figure 32: Methane mass flow rate at the ground with time for the different particle diameters at 15 bars

To confirm this, another pressure of 40 bars is used. Methane average volume fraction plots are shown in Figure 33.

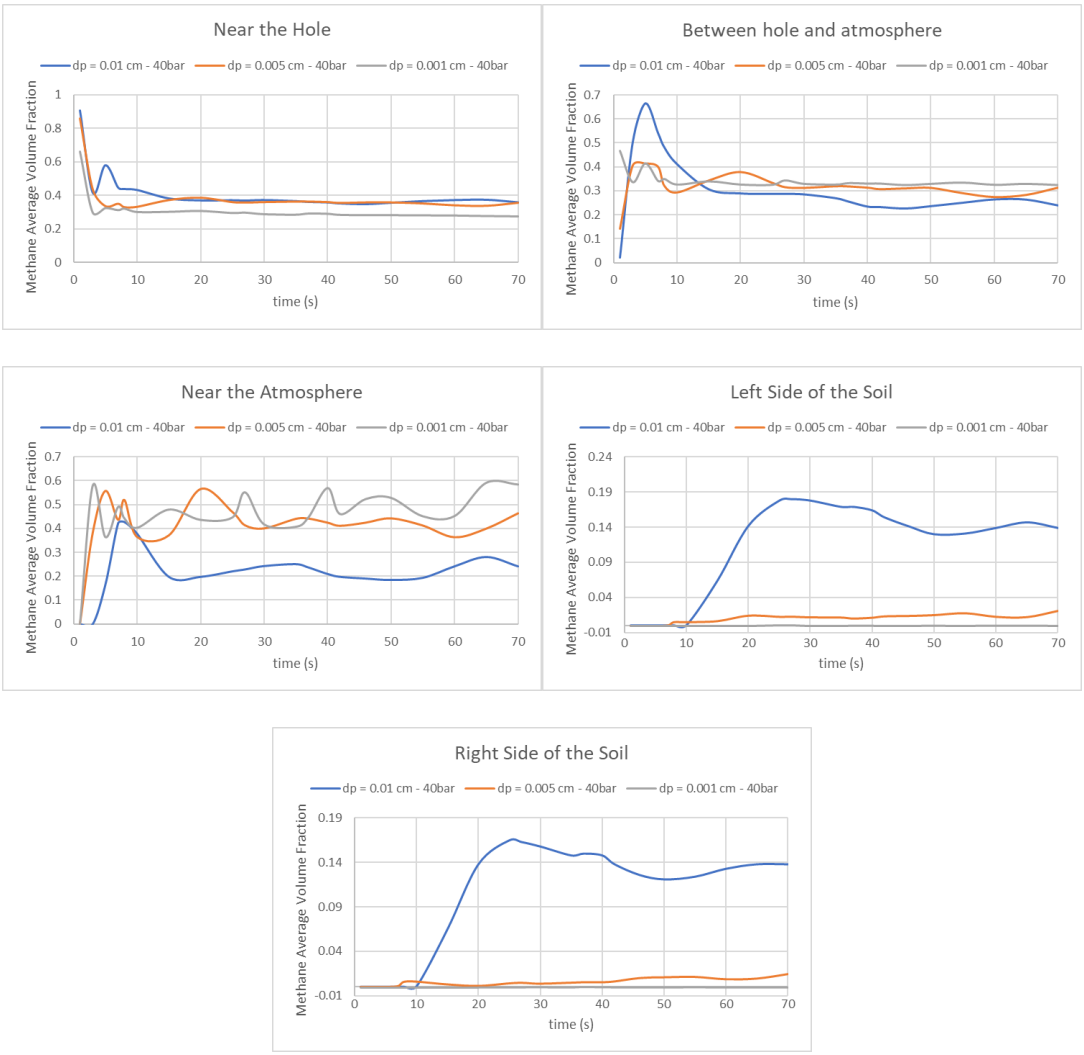

Figure 33: Methane average volume fraction with time for the different particle diameters at 40 bars

The same conclusion can be drawn from the pressure of 40bars. Accordingly, the particle diameter of 0.01cm is fixed for the rest of the project. It should be noted that increasing the particle diameter further was tried but made the case diverge. The smallest mesh size should be greater than the particle diameter. Having a hole of 1.2cm made the smallest meshing size be close to 0.01cm and accordingly the particle diameter cannot be further increased. As the chosen particle diameter can

fulfill the requirement of visualizing the regime, it is good enough to be chosen. The next parameters will be chosen to enhance the regimes visualization further.

5.3 Turbulence model

Now that the mesh and particle diameter are chosen, the turbulence model should be picked. The turbulence model choice is a crucial characterization to the model as it is highly affected by velocity (or pressure). This requires additional effort and tests at various pressures to confirm the applicability of the turbulence model over the entire range of pressure, being up to 80 bars. For that purpose, five turbulence models are tested: standard k-ε, RNG k-ε, standard k-ω, BSL k-ω, SST k-ω for three different pressures of 1, 15 and 66 bars.

In the previous tests for meshing and particle diameter, it was sufficient to test for the difference between the models, meaning that when any difference is noticed, the more computationally demanding is chosen. If this was the case here, any difference detected between k-ε and k-ω will make k-ω the best choice because it is computationally harder and is a more powerful model. However, an additional factor here is the expected regime. As it is shown in the experimental work that with every pressure, an expected regime is attributed, this is what this project is intended to show. Therefore, additional/alternative results to the previously mentioned are generated here, such as the volume fraction of soil, as it allows to present more obviously the regime. To be able to decide from the plots of mass flow rate, methane and soil volume fraction, the different expected regimes according to the pressure should be identified, as shown in Table 4.

The procedure needed for the decision of the regime from the analysis of the plots is mentioned for every case. However, the proper guidelines for this are set when studying the different pressures, as the various regimes are tied to various pressures. To study the pressure effect

however, the model should be finalized, i.e. the turbulence model, the viscosity choice, and the rest of the sensitivity analysis should be completed beforehand. This is why, the regime guidelines are set at this stage but they are systematically mentioned in the first section of Chapter 6, in the pressure case study. For clearly understanding the rest of the sensitivity analysis, this part in the next chapter can be consulted.

Table 4: Regimes associated with different pressures[5]

Pressure (bar)	**Regime**	**End Result**
0.1	Migration	Migration
0.5	Migration	Migration
9	Cracks or uplift	Low uplift – uplift
15	Cracks or uplift	Low uplift – uplift
20	Cracks or uplift	Low uplift – uplift
36	Uplift followed by a crater	Strong uplift – crater
47	Uplift followed by a crater	Strong uplift – crater
54	Uplift followed by a crater	Strong uplift – crater
66	Instantaneous uplift followed by a crater or instantaneous crater	Crater
75	Instantaneous crater	Crater

To verify the outcomes in this part of the study, the methane mass flow rate at the ground and the volume fraction of methane and soil are plotted at two locations from the specified ones in Figure

23b: near the atmosphere and between the hole and atmosphere. The other locations are not crucial for the decision. For the point near the hole, methane is usually present in considerable amounts just above the hole, and decreases with time. This point gave almost identical plots for all the cases and was not significant in the decision making. It should be noted that the volume of the spheres is decreased as the value itself is crucial and should be precisely discovered. Moreover, the location near the atmosphere is updated and is now tangent to the interface between the soil and atmosphere, as this allows better the visualization of the regime. The updated locations are shown in Figure 34.

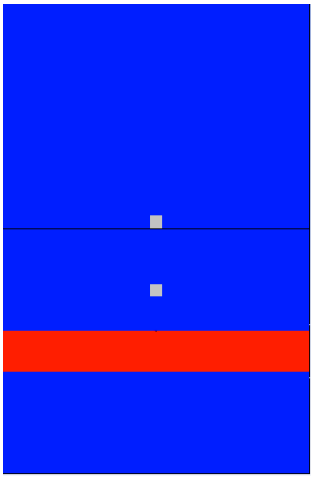

Figure 34: Updated locations of the points between the hole and the atmosphere and near the atmosphere for the computations

The first pressure tested is 1 bar where the expected outcome is in the transition region between migration and slight uplift (close to migration). The average methane volume fraction near the atmosphere and between the hole and atmosphere is plotted and shown in Figure 35. The RNG k-ε model is an enhancement of the standard k-ε model and if the results are different between the two models, the RNG is a better candidate. According to the plots, the RNG k-ε is giving identical

results to the standard k-ε model, meaning that the results are not enhanced and so the additional computational power is not getting an additional precision or better results. This is why, the RNG k-ε can be eliminated directly. In addition, both k-ε models are giving different results from the k-ω models. As known, the k-ω models are more demanding and more powerful. Giving different results suggest that the results with the k-ε are inaccurate, as this model is usually picked to save computational demand in case it gives identical results to k-ω. This can eliminate the standard k-ε option. The standard k-ω is the default model, giving a migration at low pressure, as the volume fraction of methane is very low and approaching zero. From the plot at the location between the hole and the atmosphere, it can be noticed that BSL and SST k-ω are giving results closer to the k-ε than to the standard k-ω. However, no conclusion about them can be drawn yet since none of them is triggering a crater.

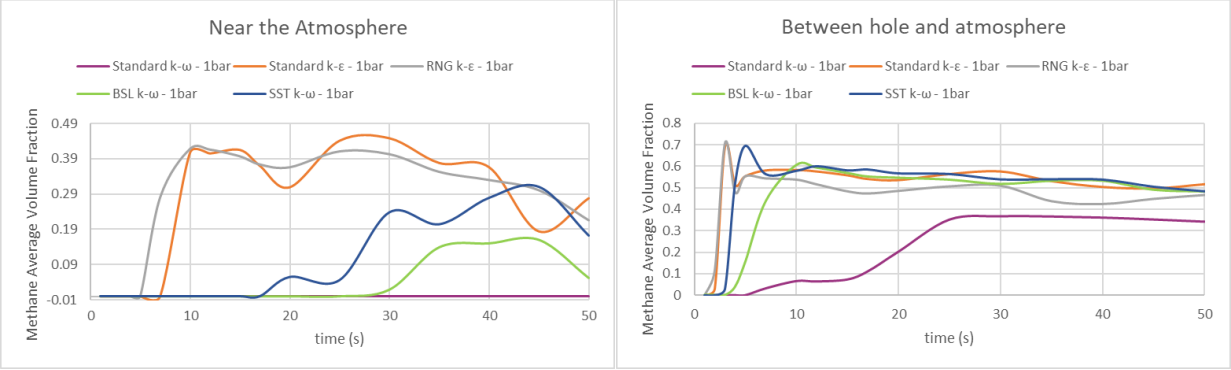

Figure 35: Methane average volume fraction with time for the different turbulence models at 1 bar

To visualize what is happening more, the soil average volume fraction near the atmosphere and between the hole and the atmosphere is plotted and shown in Figure 36. To understand how to read the plots, the following analysis should be done. For the location near the atmosphere, as initially

no soil is present, any value of soil volume fraction greater than zero means that an uplift is starting to occur (otherwise it is a migration). The maximum value of soil reachable there is the packing limit of 63%. It is at this point that the soil is uplifted. Even though this value no longer increases, the uplift height can keep increasing. If the soil volume fraction becomes stable at this value, a low uplift is visible. If a big decrease of soil volume fraction happens after this (achieving near 20% or less), it is an indication that a crater might occur. If the volume fraction stays small (close to zero) then, this is a crater. If the value increases again and stabilizes at high values near the packing limit, this indicates a strong uplift. The location between the hole and atmosphere is also an indication, helpful to complete the result obtained near the atmosphere. Initially, the volume fraction of soil is at the packing limit there. Any decrease in the soil volume fraction means that cracks are visible. The magnitude of the cracks depends on the degree of displacement of soil, dictated by the extent of decrease of the soil volume fraction. For the case of migration, only small cracks can be expected at extreme cases in the beginning, after which the soil volume fraction goes back to the packing limit. In the case of uplifts, the soil volume fraction drops and then go back to values less than or equal to the packing limit, according to the intensity of the uplift (the pressure). For crater, the soil is continuously displaced and so the volume fraction stays very low all the time (less than around 20%). According to these guidelines, the regime is discovered and the model will be approved if it gives the intended regime.

First, the plots of the soil volume fraction in Figure 36 certify that the k-ε models differ from the k-ω. Second, for the location near the atmosphere, the standard k-ω model expects that there is no soil, meaning that there was not any uplift as the soil did not go up, neither methane did. This is confirmed from the location between the hole and the atmosphere as the volume fraction stays 0.6 all the time (initial volume fraction of the soil) since the soil was not displaced. Any methane

available diffused through the air and did not alter the soil volume fraction. As for the k-ε models, the soil was uplifted, as the soil volume fraction reaches around 63% (the packing limit) near the atmosphere. For these two models, there are visible cracks between the hole and atmosphere as the soil is displaced, since the volume fraction drops from its initial value of 63%. The remaining k-ω models are in between.

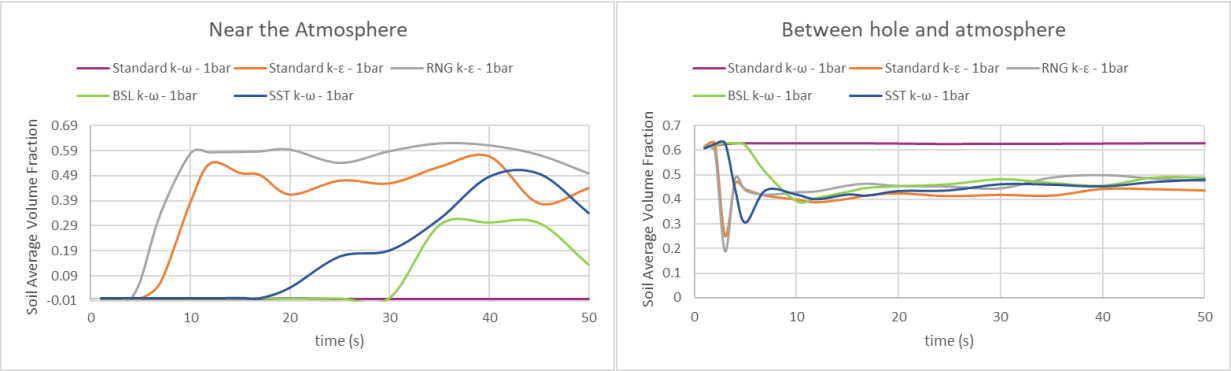

Figure 36: Soil average volume fraction with time for the different turbulence models at 1 bar

Although the different k-ω models are different, however the difference can not decide which one to choose. This is more shown in the mass flow rate of methane at the ground in Figure 37, where the different k-ω models give close results.

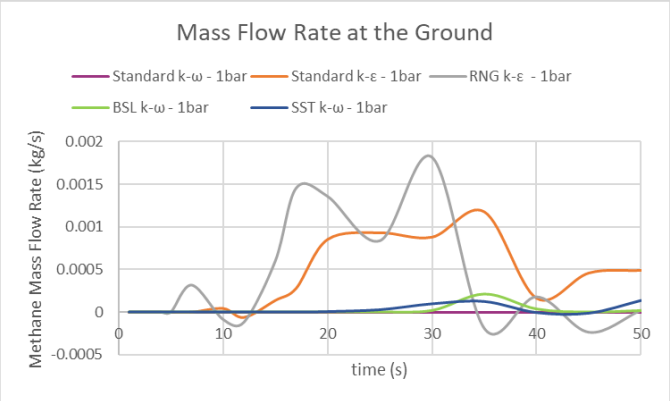

Figure 37: Methane mass flow rate at the ground with time for the different turbulence models at 1 bar

From this analysis, the observed regimes are summarized in Table 5. It can be concluded that none of the models is giving an unexpected regime, as all of them are giving either migration or low uplift, which is expected at 1bar. However, the RNG k-ε model can be eliminated as it is not adding any value to the standard. The standard k-ε and the different k-ω are tested at 15 bars to decide, as no clear decision could be made at 1bar, although it is clear that all the models are over-estimating in comparison with standard k-ω.

Table 5: Outcome regime from the different turbulence models at 1 bar

Pressure 1 bar	
Turbulence model	**Outcome Regime**
standard k-ω	Migration
standard k-ε	Cracks with small uplift
RNG k-ε	Cracks with small uplift

Table 5: Continued

BSL k-ω	Cracks – no uplift
SST k-ω	Cracks – no uplift

At the pressure of 15 bars, the expected outcome is cracks and low uplift. The first plots used to identify the outcomes are the soil and methane average volume fraction between the hole and atmosphere, shown in Figure 38. The plots show that the BSL and SST k-ω models give close results to standard k-ε model whereas the standard k-ω gives different results. For standard k-ω model, the soil volume fraction attains 0.1 and methane volume fractions approaches 0.9 in the beginning because the release is strong. As the time proceeds, the soil volume fraction returns to 63% and the methane volume fraction settles at around 0.3 indicating that there is slight uplift. On the contrary, a strong uplift (even a crater) is expected from the other models as the soil volume fraction is low (around 0.15) and methane volume fraction is high (close to 0.9).

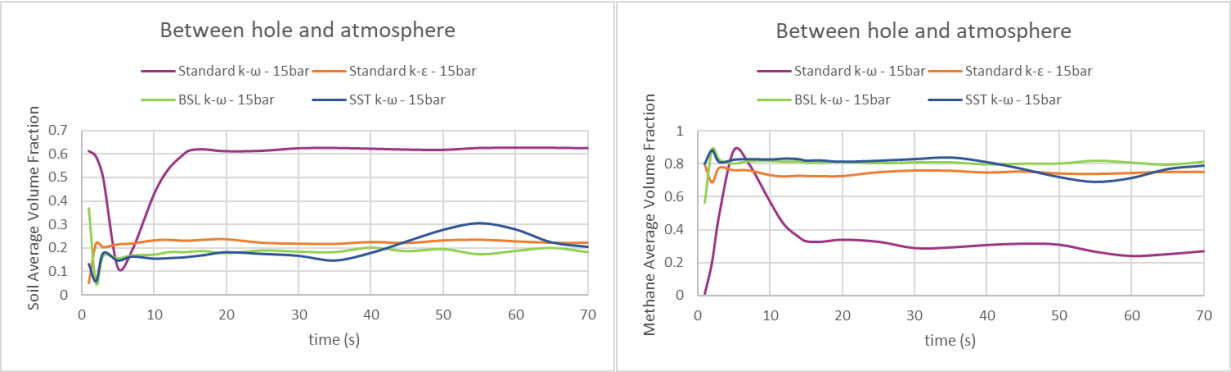

(a) (b)

Figure 38: Average volume fraction with time of soil (a) and methane (b) for the different turbulence models at 15 bars between the hole and atmosphere

To understand this more, the soil and methane average volume fraction near the atmosphere are plotted, as shown in Figure 39. Figure 39a shows that there is at least a slight uplift expected for all models as soil is present upward after the absence of any soil in the atmosphere in the beginning. However, the plots indicate no clear difference between the various models. This is why the methane volume fraction in Figure 39b complements this graph by showing that methane volume fraction approaches 0.3 according to the standard k-ω model whereas the other models expect a volume fraction of around 0.8. This shows that the results obtained in Figure 39a are not identical, because the soil presence in the case of standard k-ω is due to a very slight uplift (volume fraction did not achieve the packing limit and so the uplift is not completely visible), whereas the presence of soil in the case of all the other models is due to a quick uplift followed by a sharp decrease of soil volume fraction. This suggests a strong uplift, near a crater. This indicates that these models are over-estimating as the expected regime is a low uplift.

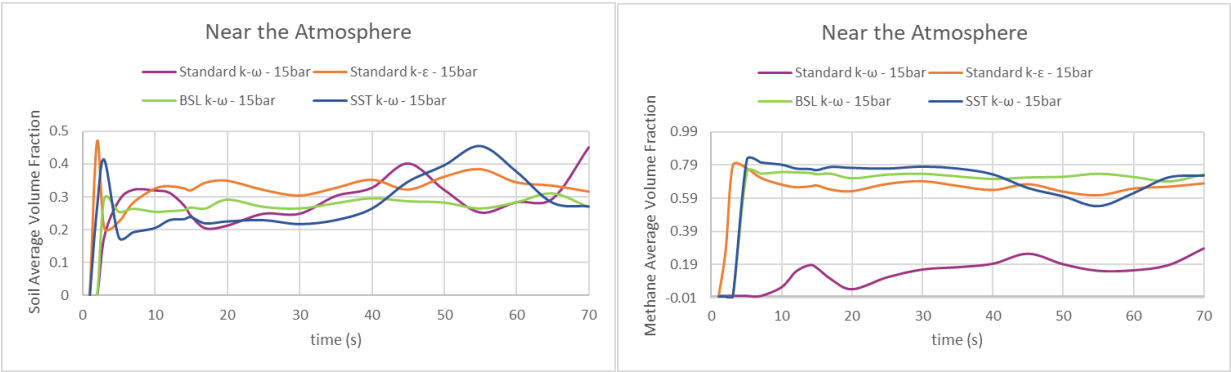

(a) (b)

Figure 39: Average volume fraction with time of soil (a) and methane (b) for the different turbulence models at 15 bars near the atmosphere

This over-estimation is clear also in the mass flow rate at the ground shown in Figure 40. When no significant leak damages (i.e. not more than a low uplift) should be expected at this pressure, all the models except standard k-ω expect otherwise.

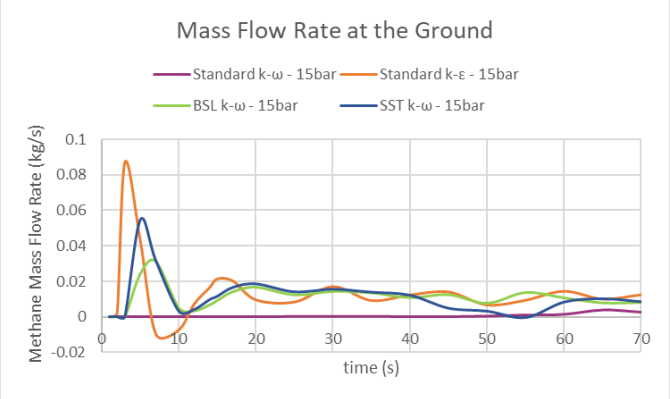

Figure 40: Methane mass flow rate at the ground with time for the different turbulence models at 15 bars

Summarizing the visualized outcomes from the different models, the regimes are shown in Table 6. The closest model giving the expected outcome is the standard k-ω. This eliminates the BSL and SST k-ω models although they are expected to combine advantages from both k-ε and standard k-ω models. These advantages can be useful in different applications than the current study. Accordingly, the results suggest that the standard k-ω model is the best choice, although it may show a little under-estimation. This is why, the pressure of 66 bars is tested with standard and SST

k-ω. This is done as standard k-ω model is giving different results than all of the others and therefore, it is sufficient to test it against one of them.

Table 6: Outcome regime from the different turbulence models at 15 bars

Pressure 15 bars	
Turbulence model	**Outcome Regime**
standard k-ω	Small cracks – very slight uplift
standard k-ε	Extreme cracks, strong uplift
BSL k-ω	Extreme cracks, strong uplift
SST k-ω	Extreme cracks, strong uplift

For the pressure of 66 bars, the expected regime is a strong uplift followed by a crater. The SST k-ω seems to give a crater, and this is expected as it was close to giving a crater at 15 bars even. This can be seen from the volume fraction of both methane approaching unity and soil approaching zero between the hole and atmosphere in Figure 41. From another side, the results are misleading for the standard k-ω as the behavior was not ordinary. Throughout its path, methane flow changed locations. To be able to compare, the same location for SST and standard model should be used. However, for standard k-ω, the path it followed was not stable and this is shown by the delay initially between the two models until they give the same result. Whereas SST k-ω estimates one behavior, the standard k-ω shows a shift in the regime again where it shows a steep decrease in the methane volume fraction and an increase in the soil volume fraction. This shows that the soil retook its place and the result is indicating that the soil is coming back producing no more than an uplift.

Although the location between the hole and atmosphere can indicate the regime, but sometimes it is not sufficient as the regime is visible near the atmosphere, what makes plotting it there necessary.

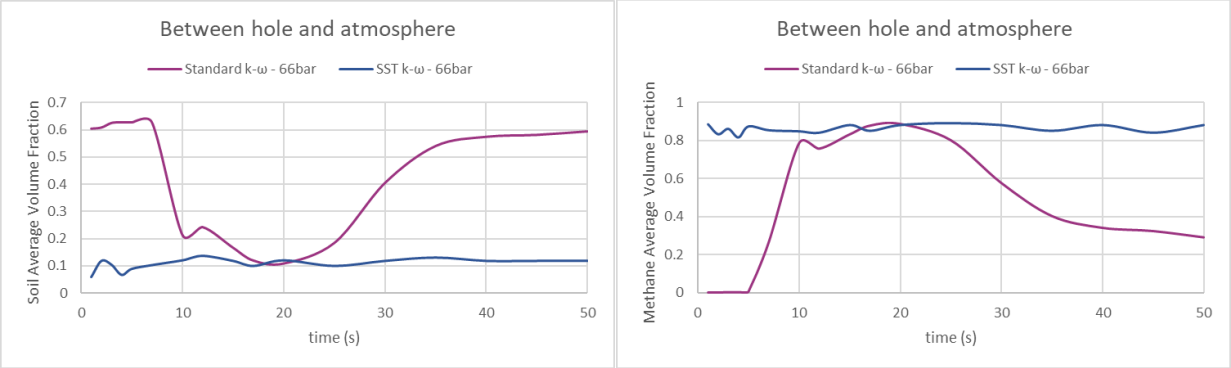

(a) (b)

Figure 41: Average volume fraction with time of soil (a) and methane (b) for the different turbulence models at 66 bars between the hole and atmosphere

The volume fraction of soil and methane near the atmosphere are plotted and shown in Figure 42. The delay in attaining the atmosphere by standard k-ω is shown in Figure 42b. The strong uplift followed by a crater is clear for the SST k-ω whereas for standard k-ω, there are fluctuations. The volume fraction is almost zero initially due to the delay, then there is an uplift causing the soil volume fraction to increase because it is spread. This is followed by a decrease in the soil volume fraction revealing a crater. Finally, the soil spreads again and goes back to the packing limit indicating that this is not a crater, but rather a strong uplift.

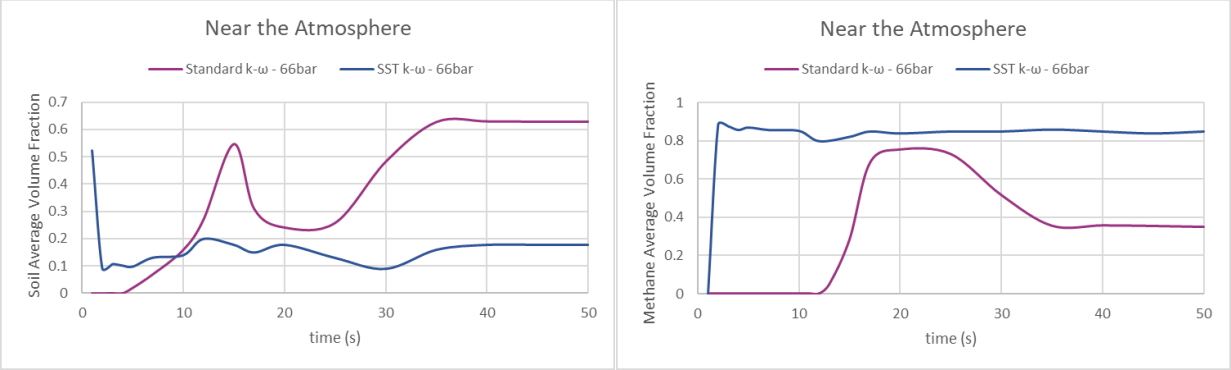

(a) (b)

Figure 42: Average volume fraction with time of soil (a) and methane (b) for the different turbulence models at 66 bars near the atmosphere

At 66 bars, an instantaneous strong uplift is expected and this is shown by both models but with a delay for standard k-ω. Also, the crater regime is not shown by standard k-ω model. This outcome is expected because whereas standard k-ω is a little bit under-estimating, the SST k-ω is over-estimating at all pressures. In addition, the standard k-ω model has some weaknesses when it comes to free streams[43]. This means that the SST can be more powerful at high pressures. The model can be constructed through splitting it over several pressure ranges, where the standard k-ω is used for migration and uplifts visualization, and the SST k-ω is used for crater visualization. This can be justified as the turbulence model depends highly on the pressure, and the pressure range used is wide. However, since the sensitivity analysis is not completed yet, the viscosities should be investigated first because it is probable to solve the problem with the viscosity. This is why, the standard k-ω is picked as the turbulence model for this system because it allowed the visualization of regimes that were not achievable with other models. In the previous chapter, the main problem was that crater was always available and the migration was not visible. This was only solved by standard k-ω and this is why it is the best option.

5.4 Frictional viscosity

Now that the mesh, particle diameter and turbulence model are fixed, the frictional viscosity relevance to the system is identified. This is done by excluding the frictional viscosity that was included in all previous trials. The analysis is performed using three different pressures of 1, 15 and 66 bars. The same plots as the turbulence models are used: soil and methane volume fraction near the atmosphere and between the hole and the atmosphere in addition to the methane mass flow rate at the ground. Among these plots, only the relevant ones that show the outcome will be used as the others might not be helpful to visualize the intended outcome. The main aim of this study is to find out whether the outcome differ in case of presence or absence of frictional viscosity model because the aim is to correct the under-estimation of standard k-ω model.

The first pressure tested is 1 bar. The soil and methane average volume fraction between the hole and atmosphere are shown in Figure 43. Soil volume fraction shows that including or excluding the frictional viscosity leads to the same regime as this can be clearly visualized from this plot. Although the same regime of migration is expected because the soil volume fraction is zero, but the amount/fraction of methane leaking (especially near the atmosphere) is expected to be much more without frictional viscosity. Both amounts are small enough for not triggering any uplift, this is why the soil volume fraction is zero. The model without frictional viscosity predicts an outcome near low uplift, whereas the model with frictional viscosity expects completely a migration where methane does not attain the atmosphere even. As this pressure is in the transition region between migration and low uplift, both models predicted correctly. However, excluding the frictional viscosity is an assumption, that is not justified unless it is giving better results in terms of regime, which is not the case.

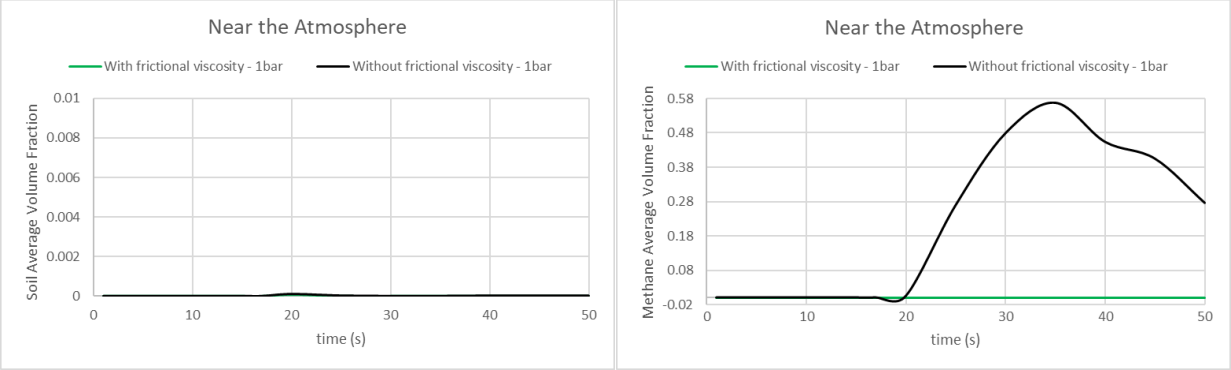

(a) (b)

Figure 43: Average volume fraction with time of soil (a) and methane (b) for the different frictional viscosity trials at 1 bar near the atmosphere

Another pressure of 15 bars is tried. The volume fraction of soil and methane between the hole and atmosphere are shown in Figure 44. The results are almost identical giving no indication about whether the frictional viscosity should be included or not. Before 10 seconds, both models predict cracks, in accordance with what is expected, indicating a low uplift.

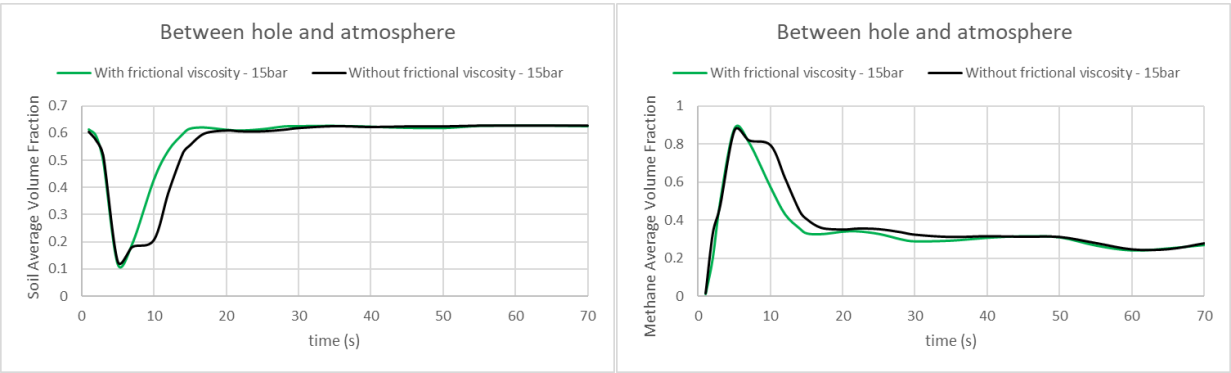

(a) (b)

Figure 44: Average volume fraction with time of soil (a) and methane (b) for the different frictional viscosity trials at 15 bars between the hole and atmosphere

Almost the same thing appears for the point near the atmosphere, in Figure 45, although there is slightly more difference in the results in terms of values, however not in terms of regimes. Excluding frictional viscosity at 1bar over-estimated the amount of methane near the atmosphere in comparison with when the frictional viscosity was included (Figure 43b), whereas for the pressure of 15bar excluding frictional viscosity slightly under-estimated the outcome in comparison with when it was included. For both pressures, both trials are giving acceptable regimes, but no clear trend to decide whether to include or exclude the frictional viscosity.

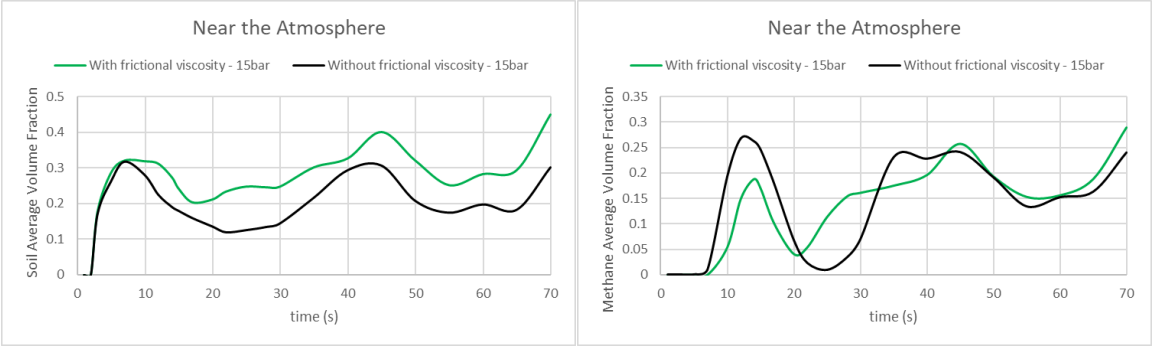

(a) (b)

Figure 45: Average volume fraction with time of soil (a) and methane (b) for the different frictional viscosity trials at 15 bars near the atmosphere

Since 15 bars did not give a clear indication, the 66 bars case is tested, where this pressure should trigger a strong uplift followed by a crater. The results near the atmosphere for soil and methane volume fraction are shown in Figure 46. Without frictional viscosity, there is an instantaneous uplift followed by a crater, followed by an uplift again. This is a typical strong uplift regime. For the case with frictional viscosity, there is a slightly inconsistent behavior. There is a late response, as shown in Figure 46b, after which an approximate strong uplift occurs as the soil volume fraction

increases, then decreases, then increases again. The results show that excluding frictional viscosity is slightly better for this pressure although both of them do not fulfill the required regime.

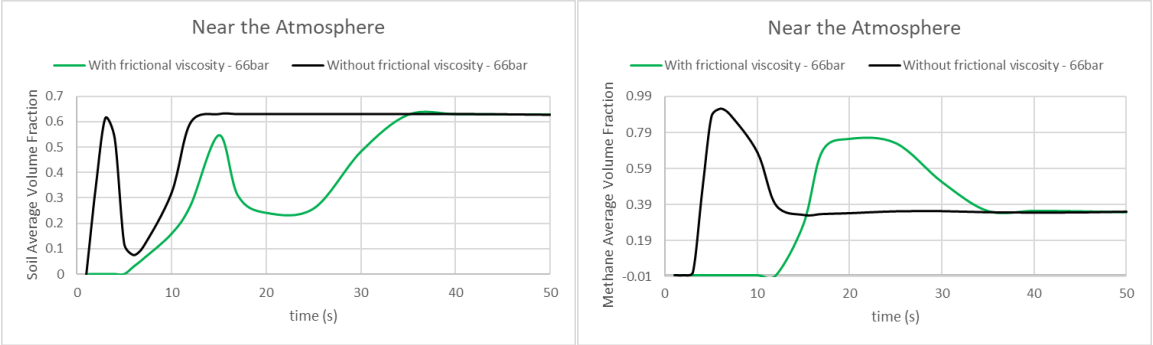

(a) (b)

Figure 46: Average volume fraction with time of soil (a) and methane (b) for the different frictional viscosity trials at 66 bars near the atmosphere

While taking the decision on whether to exclude or include the frictional viscosity, it should be noticed that modelling the frictional viscosity is an additional computation and by including it, there is an account for supplementary phenomenon that can possibly take place. In addition, the outcome has not been always stable. The trends for 1 and 15 bars are slightly opposing each other. Although it is an option to exclude the frictional viscosity, as the results are slightly better without it, but there is the granular viscosity that is not tested yet. The granular viscosity might be a chance to enhance the results and still not drop any parameter.

In this work, the frictional viscosity is kept as the assumption of removing it does not add a lot to the study in terms of regimes (which is of importance for the study), and the granular viscosity is

tested. It should be noted that excluding the frictional viscosity is a sound option too since the granular viscosity is going to be tested next.

5.5 Granular viscosity

Now that the mesh, particle diameter, turbulence model and frictional viscosity are fixed, the granular viscosity effect on the results is identified. This is done through using both available models in ANSYS Fluent: Gidaspow model and Syamlal-O'Brien model at four different pressures: 1, 15, 40 and 66bars. This is done at four pressures because it is the last part of the sensitivity analysis and should adjust the model as it was not enhanced by the frictional viscosity removal.

The first tried pressure is 1bar. The plots of the soil and methane volume fraction between the hole and atmosphere in Figure 47 show that the two granular viscosity models give almost identical results of migration at 1bar, as desired.

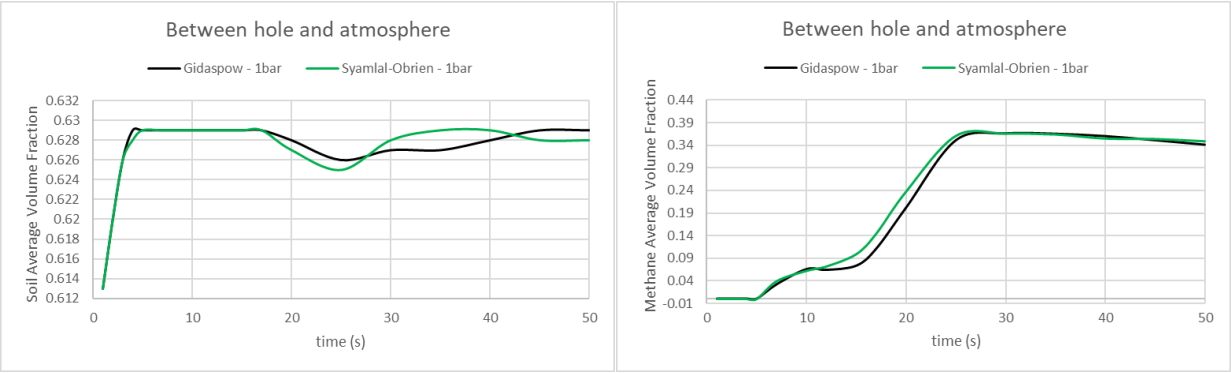

(a) (b)

Figure 47: Average volume fraction with time of soil (a) and methane (b) for the different granular viscosity models at 1 bar between the hole and atmosphere

The plots near the atmosphere in Figure 48 show identical results, where neither methane nor soil is present because no uplift happens, and methane does not even reach the top. The outcome is migration from both models, and no decision can be made about the better granular viscosity model at this stage.

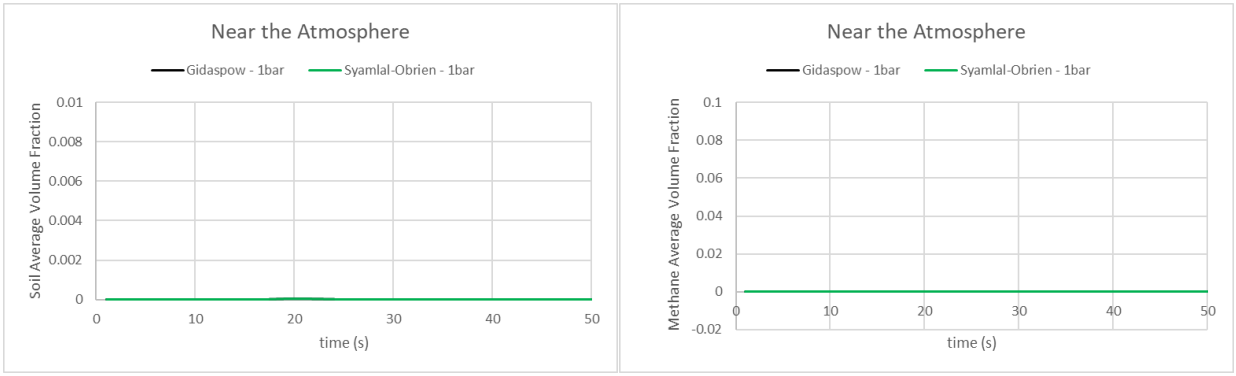

(a) (b)

Figure 48: Average volume fraction with time of soil (a) and methane (b) for the different granular viscosity models at 1 bar near the atmosphere

It should be noted that it would have been normal if methane reached the top and it would still be migration because the uplift happens when soil starts being displaced not when methane is not there. However, in this case, the low pressure was not enough to make methane attain the atmosphere in 50seconds as it is clear from Figure 49.

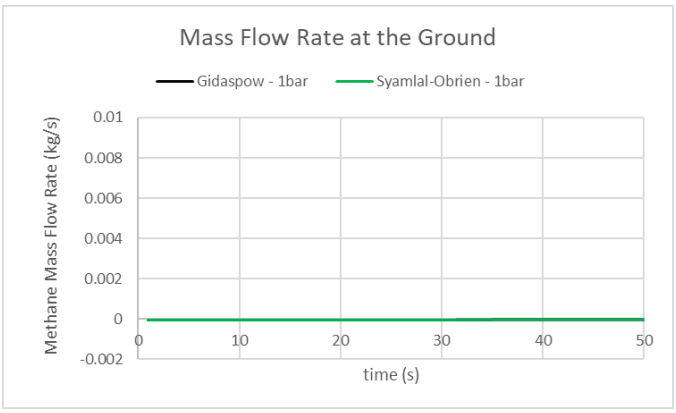

Figure 49: Methane mass flow rate at the ground with time for the different granular viscosity models at 1 bar

For the 15bars case, the plots of the volume fractions between the hole and atmosphere in Figure 50 indicate the presence of cracks and accordingly that an uplift is expected. The results are almost identical, but the low uplift is slightly clearer for the Syamlal model as the soil volume fraction takes a little more to reach the packing limit.

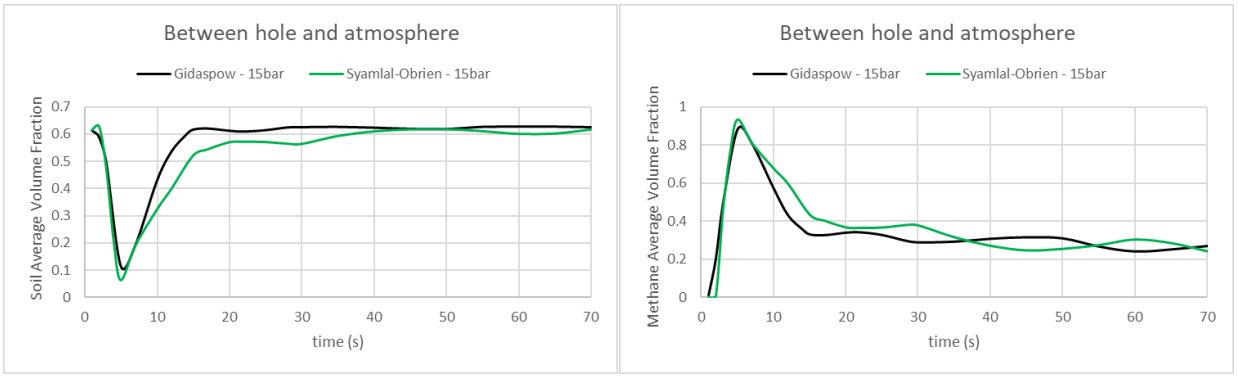

(a) (b)

Figure 50: Average volume fraction with time of soil (a) and methane (b) for the different granular viscosity models at 15 bars between the hole and atmosphere

To visualize more what is happening, the volume fractions are drawn near the atmosphere, as shown in Figure 51. The results show that there is soil that was displaced into the atmosphere as the soil volume fraction is positive and this shows an uplift estimated from both models. Syamlal-Obrien model estimates higher volume fraction of soil and methane near the atmosphere. The difference is not significant between both models and both of them are giving acceptable results in terms of regimes. However, Syamlal-Obrien predicts better as the volume fraction of soil is closer to the packing limit, and so the slight under-estimation of the turbulence model is adjusted.

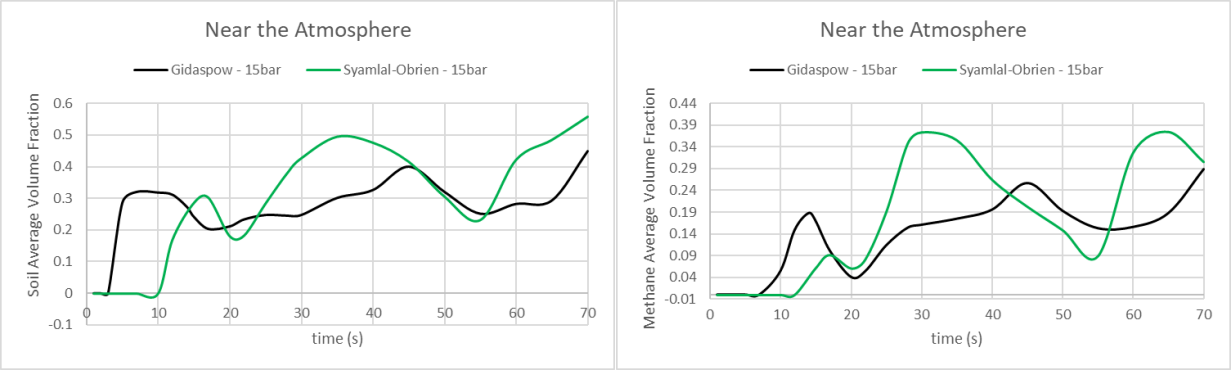

(a) (b)

Figure 51: Average volume fraction with time of soil (a) and methane (b) for the different granular viscosity models at 15 bars near the atmosphere

As both models are giving acceptable results till now, more pressures should be investigated. This is why the pressure of 40 bars is now included in the investigation. The soil and methane volume fraction near the atmosphere are shown in Figure 52. At 40bars, a strong uplift is expected. For a strong uplift, the soil volume fraction should show an uplift initially, followed by a decrease showing a crater, followed by an increase to the packing limit. The first uplift is shown by both

models as the peak of the soil volume fraction reaches near 60% but the crater following the uplift is shown by Syamlal model more clearly than Gidaspow model. This can be confirmed from the methane volume fraction that achieves 90% for Syamlal and 75% for Gidaspow. Following this, the soil volume fraction goes back to the packing limit according to both models. Accordingly, both models predict a strong uplift, but Syamlal model better predicted it.

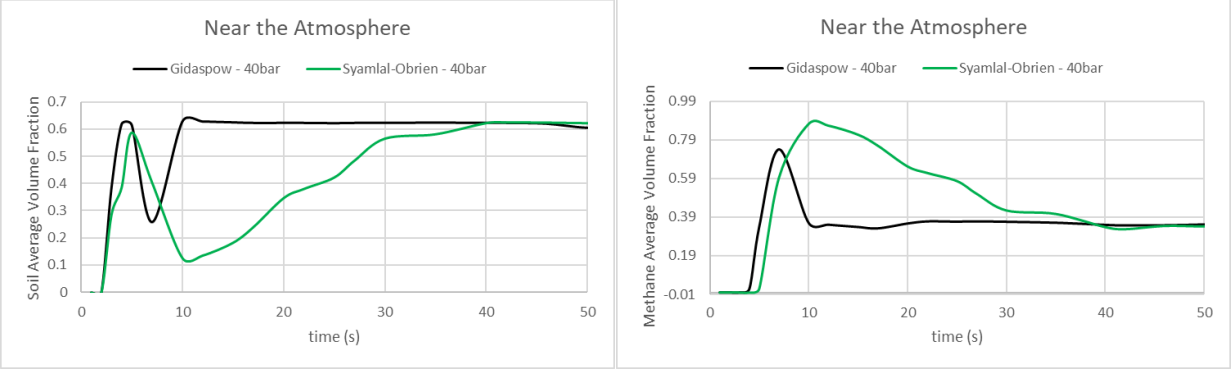

(a) (b)

Figure 52: Average volume fraction with time of soil (a) and methane (b) for the different granular viscosity models at 40 bars near the atmosphere

One missing thing is to confirm whether the expected regime is obtained with Syamlal model at 66 bars as this was a problem with the turbulence model where no correct outcome was obtained with Gidaspow. To confirm this, the methane and soil volume fraction near the atmosphere are plotted at 66bars as shown in Figure 53. Syamlal model gives a strong instantaneous uplift followed by a crater. When the outcome is a strong uplift, the soil volume fraction first increases, then decreases (crater), then goes back to the packing limit after the crater (the drop in soil volume fraction). For the case of a crater (extreme crater), the soil volume fraction is expected to increase,

then decrease and stay almost zero. For the pressure of 66bars, the outcome is in between. The regime is crater, but it is not extreme. This is why, the expected result should be first an increase in the soil volume fraction (uplift), followed by a decrease (crater) that should not go back to the packing limit (as it is not a strong uplift) but can increase slightly. This is exactly the outcome given by Syamlal model in Figure 53a. Gidaspow model outcome was explained several times before, as this was a strong uplift since after the decrease of soil volume fraction, it went back to the packing limit. This confirms that Symlal is fitting for all pressures and accordingly it will be chosen for modelling the granular viscosity.

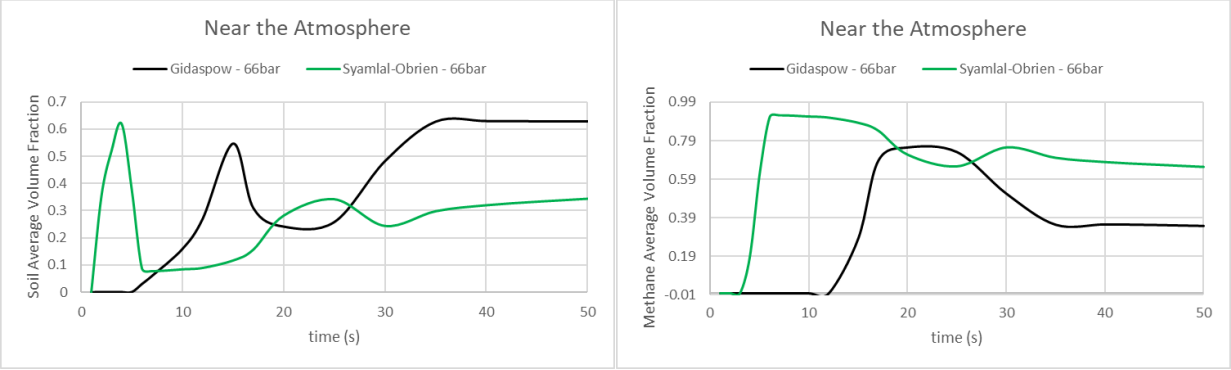

(a) (b)

Figure 53: Average volume fraction with time of soil (a) and methane (b) for the different granular viscosity models at 66 bars near the atmosphere

With this choice, the model is completed where the mesh, particle diameter, turbulence model, frictional viscosity and granular viscosity are specified. The chosen parameters are summarized and displaced in Table 7.

Table 7: The chosen models for the five tested parameters

Parameter / Model	**Trials**
Meshing	Refinement #2
Particle diameter	0.01 cm
Turbulence	Standard k-ω
Frictional Viscosity	Modeled (Shaeffer)
Granular viscosity	Syamlal-Obrien model

6 CASE STUDY

After obtaining the model, a case study is conducted to identify the regimes. The primary aim is to study the effect of the pressure on the regime, and the delineation of the transition regions between the different regimes. These results are aimed to be represented through a nomograph that lumps the significant parameters studied. The pressure is represented by a more representative property that is the force; being the product of the inlet pressure and the area perpendicular to the applied pressure.

Now that the main aim is achieved, various parameters can be varied. Among these, the pipeline burial depth and the release orientation are varied for given pressures, and the result is consulted.

6.1 Pressure

The pressure is varied to validate the result with the experiment[5], and to test new values that help delineate the different regimes. This is why, the pressures tested are: 0.35, 1, 6, 15, 27, 36, 40, 50, 66 and 75bars. The pressures are chosen according to the available information. In the paper, the only tested pressure for migration is around 0.5bars, and the first pressure tested for low uplift is around 8.5bars. Accordingly, 0.35, 1 and 6 bars are tested. This will allow to draw fine boundaries for the transition regime between migration and uplift (or diffusion and fluidization). The transition from low to strong uplift is not clear: the last tested pressure of low uplift is around 20bars and the first pressure tested for strong uplift is 36bars, this is why a pressure of 27 bars is tested. The strong uplift and crater are so close that no clear boundary is set, but 62bar is defined as crater. This is why 50, 66 and 75bars are chosen.

The regimes obtained above ground can be divided into migration, uplift and crater. The corresponding regimes under the ground are diffusion (migration), fluidization and crater. The

uplift is further divided into low and strong according to the uplift height and its capacity to trigger crater with time. A strong uplift occurs when a crater will be observed with time, whereas a low uplift is named when no crater will be seen[5].

A strategy is followed to decide for the migration, low uplift, strong uplift and crater. For each pressure, the volume fraction of methane and soil are plotted at various locations. The ones of interest are the location near the atmosphere and the one between the hole and atmosphere, as shown in Figure 54. A location just near the hole is helpful in case of migration to visualize additional features. The volume fraction near the atmosphere helps evaluating the regime; whereas the volume fraction between the hole and atmosphere and near the hole help visualizing the presence of cracks and openings within ground. The volume fraction between the hole and atmosphere guides for the determination of the regime as well.

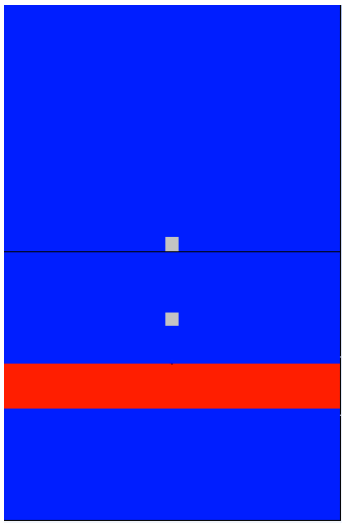

Figure 54: Updated locations of the points between the hole and the atmosphere and near the atmosphere for the computations

The pressure of 1 bar is used as an example to illustrate migration, as this pressure ended up being in the migration regime. Figure 55a shows that the soil volume fraction near the atmosphere is zero, showing that no soil was displaced to the ground, indicating migration. It should be noted that the volume fraction of methane is not helpful here without soil, since methane can be 60% and air 40%, and the regime is migration. Although methane volume fraction surpassed the porosity value, this does not mean the soil was displaced, because originally only air was present at this location. For the location between the hole and the atmosphere, in Figure 55b, the soil is kept at around 63% (packing limit), since methane does not go beyond 37% (porosity), indicating a migration. This is due to the fact that soil is originally there distributed according to the packing limit. Therefore, methane volume fraction needs to at least surpass porosity there in order for displacement to start on the ground.

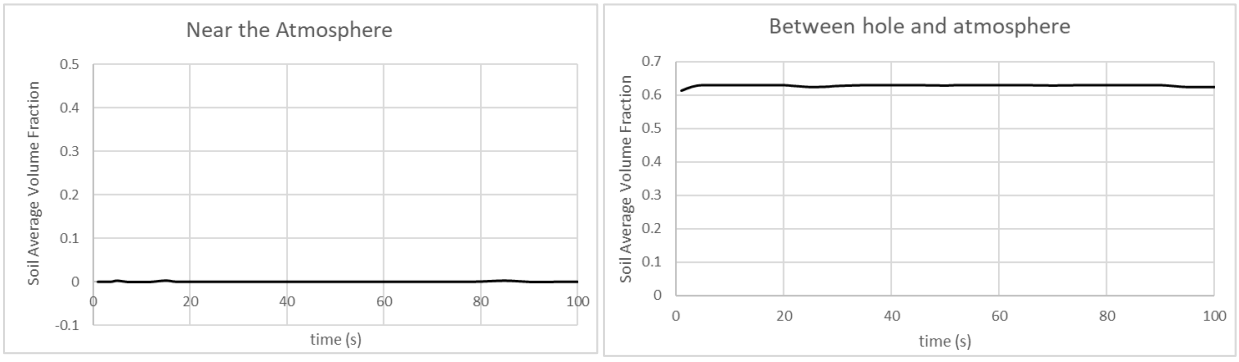

(a) (b)

Figure 55: Soil volume fraction near the atmosphere (a) and between the hole and atmosphere (b) at 1bar

To visualize the small gap created near the hole, methane volume fraction near the hole is plotted. Methane displaces all the soil near the hole and then the value decreases with time while fluctuating around 60% (Figure 56), creating the empty shape available in the experiment[5].

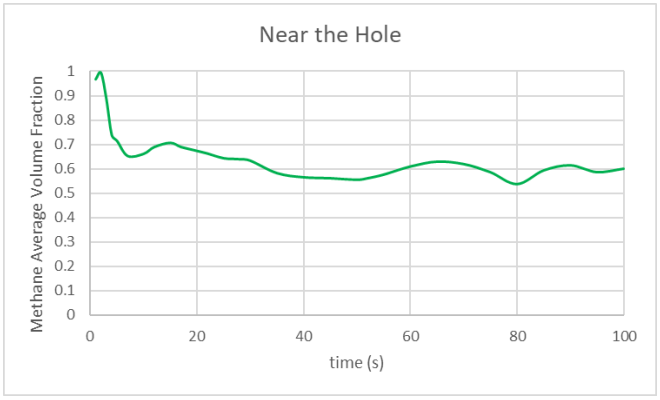

Figure 56: Methane volume fraction near the hole (1bar)

The pressure of 75 bar is used to demonstrate the visualization of a crater through the plots of the soil and methane volume fraction near the atmosphere and between the hole and atmosphere, as presented in Figure 57. Between the hole and atmosphere, methane completely displaces soil, where methane is 100% and soil is 0%. Near the atmosphere, there is an instantaneous crater where the soil is first displaced (going from 0 to 63% that is the packing limit) and then the volume fraction drops to zero because the methane displaces the soil that was uplifted. The volume fraction remains constant (zero) indicating that this is a crater.

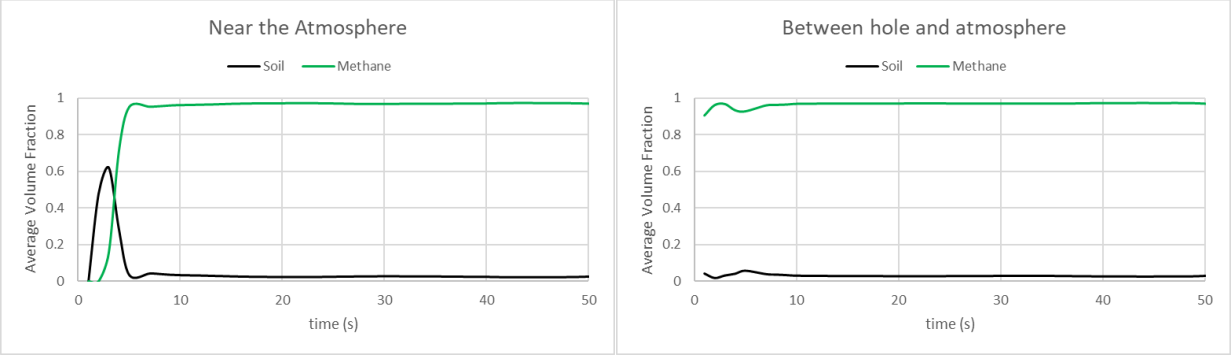

(a) (b)

Figure 57: Soil and methane volume fraction near the atmosphere (a) and between the hole and atmosphere (b) (75bars)

The uplift situation is in between. The case taken here is the case of 15bar, a low pressure case in the low uplift regime. The soil and methane volume fraction between the hole and atmosphere and near the atmosphere are shown in Figure 58. Near the atmosphere, the soil volume fraction increases gradually until reaching around 63% (packing limit). The methane volume fraction increases as well in parallel. Note that the low uplift could have been achieved if the increase to 63% happened faster. The rate of increase does not detect the regime; the trend does. From the location between hole and atmosphere, soil volume fraction reveals the presence of cracks as it dropped to around 0. The cracks are typical in this regime, happening after few seconds from the release. The soil volume fraction goes back to a value equal or slightly less than the packing limit (63%) after the drop when cracks are shown.

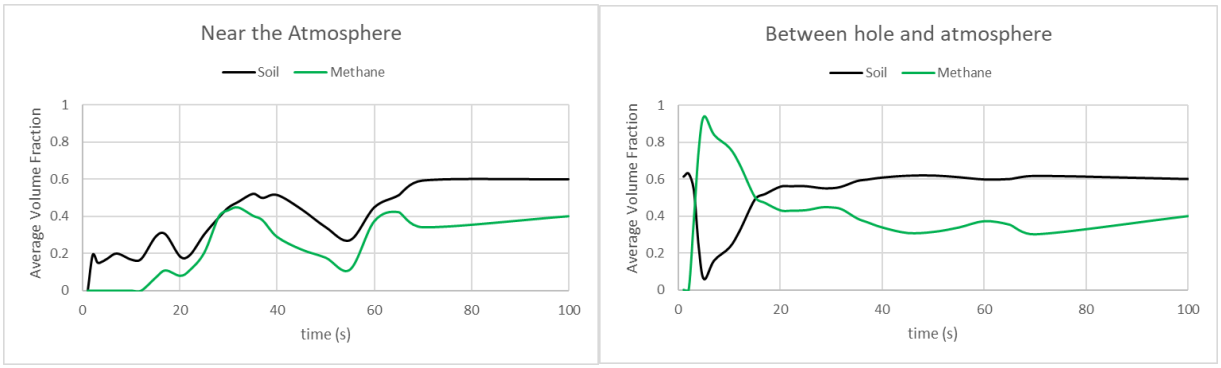

(a) (b)

Figure 58: Soil and methane volume fraction near the atmosphere (a) and between the hole and atmosphere (b) (15bars)

In analogy with the low uplift, the strong uplift has a similar trend but with one difference: the crater generation. From near the atmosphere location, in Figure 59a, it can be shown that there is an instantaneous uplift (soil volume fraction increases to 0.63), followed by a crater, where the soil volume fraction drops again to almost zero (5%) since it was fully displaced by the methane that is almost 100% at this stage. After this, the soil volume fraction increases again to 63% and stabilizes there as is the case of low uplift, but with higher uplift height since the uplift is stronger. The difference between a strong and low uplift is the presence of crater (through the drop of soil volume fraction), and the difference between a strong uplift and a crater is the fact that the crater is stable in the crater regime (soil volume fraction does not go back to packing limit), whereas an uplift (increase of soil volume fraction to packing limit) follows the crater in the strong uplift regime. For the location between the hole and atmosphere, in Figure 59b, there is a drop of the soil volume fraction to almost zero, after which it gradually increases to a value much less than the packing limit, and less than the ones achieved in the low uplift. Whereas during a migration the soil volume fraction goes back (or stays) to the packing limit, in the low uplift it goes back to a value less than or equal to the packing limit, in the strong uplift it goes back to a value less than

the one corresponding to the low uplift, and in the crater regime, the soil volume fraction stays almost zero all the time.

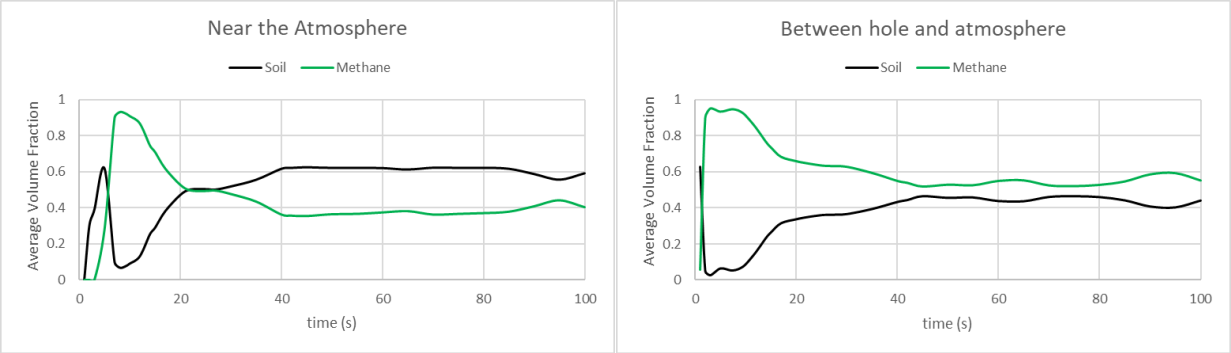

(a) (b)

Figure 59: Soil and methane volume fraction near the atmosphere (a) and between the hole and atmosphere (b) (50bars)

This analysis is used to test the regime of all the pressures. Gathering the plots obtained for all 10 pressures, the soil volume fraction variation with time near the atmosphere is shown in Figure 60. Pressures of 0.35, 1 and 6bars are examples of migration where the volume fraction remains almost zero all the time. For the pressure of 6bars, a very slight movement is detected but it can not be considered as a low uplift, since it did not show any uplift visually, and in this plot, it shows a very big difference from the pressures of 15 and 27 bars triggering a low uplift. For these two pressures (15 and 27bars), the volume fraction increases until reaching around 63% (packing limit) since there, the whole soil is uplifted and so the sphere along which the measurements are taken becomes completely inside the packed soil. For the pressures of 36, 40 and 50 bars, the soil volume fraction increases the same way to the packing limit, but this is followed by a decrease and then an increase

back to 63%. For the pressures of 66 and 75 bars, the soil volume fraction increases and then decreases to zero, and becomes stable there instead of increasing back to 63%.

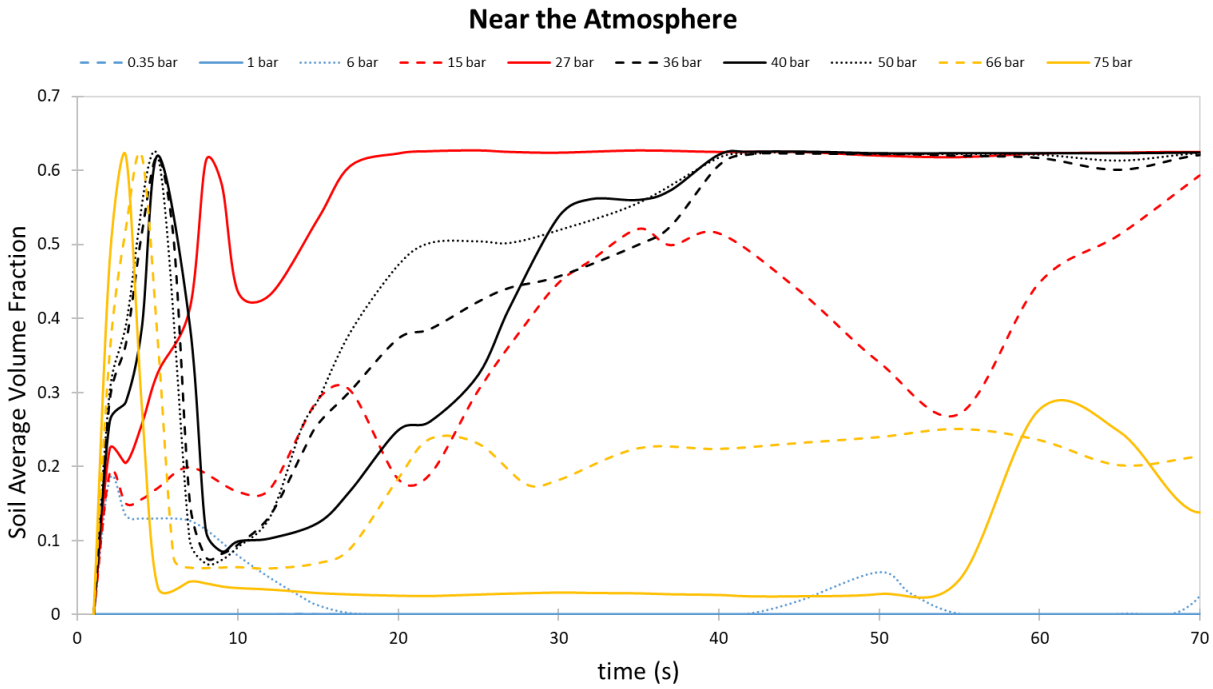

Figure 60: Soil volume fraction distribution near the atmosphere for the different studied pressures

The regimes can also be summarized by the soil volume fraction between the hole and atmosphere, as shown in Figure 61. Pressures of 0.35, 1 and 6bars are examples of migration where the volume fraction remains 63% (packing limit) all the time because no displacement happened. For the pressure of 6bars, there is a decrease in the volume fraction that indicates cracks. This does not make the regime an uplift because the regime is dictated from the volume fraction near the atmosphere, and because they are small cracks when compared to the low uplift. Small cracks are available in migration at the extreme pressures that are near the low uplift as is the case with 6bars.

For the two pressures of 15 and 27bars, the volume fraction decreases due to the available cracks at all pressures and then increases until reaching volume fraction slightly less than 63% since the cracks are continuously available, unlike migration, even if in small degree. The same applies for the pressures of 36, 40 and 50 bars, the only change is that the decrease in the soil volume fraction is bigger as the pressure is bigger, and the increase is lower because methane continuously displaces the soil in the case of strong uplift. For the pressures of 66 and 75 bars, the soil volume fraction is zero at almost all times since the soil is fully displaced.

The pressures are accordingly distributed between the four regimes, as shown in Figure 61. The regimes corresponding to the pressures from the experiment[5] and from the model are joint to delineate the boundaries.

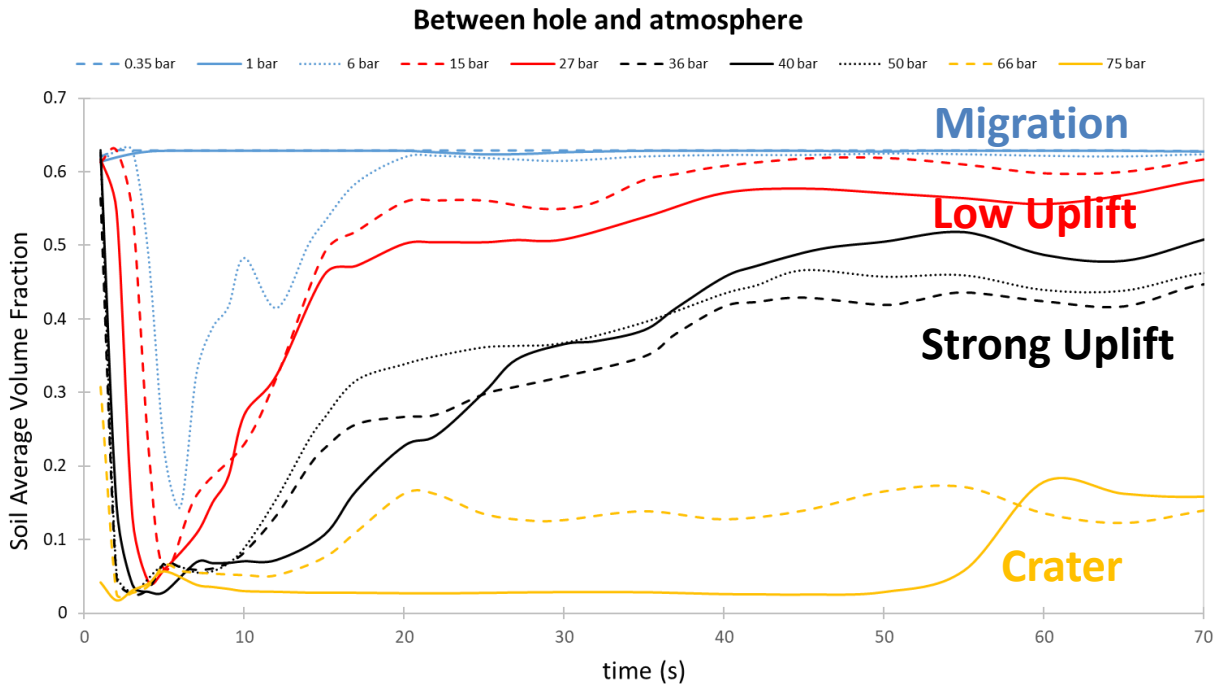

Figure 61: Soil volume fraction distribution between the hole and atmosphere for the different studied pressures

The different pressures used in the experiment and in the model along with the corresponding regimes are all summarized in Table 8. The additional pressures used in the model are helpful in refining the delineation of boundaries between the different regimes.

Table 8: Regimes associated with all tested inlet pressures for a height of 100cm

Pressure (bar)	Regime	Experiment and/or model
0.35	Migration	Model
0.5	Migration	**Experiment**
1	Migration	Model
6	Migration	Model
8.5	Low Uplift	**Experiment**
12	Low Uplift	**Experiment**
15	Low Uplift	**Both**
20	Low Uplift	**Experiment**
27	Low Uplift	Model
36	Strong Uplift	**Both**
40	Strong Uplift	Model
47	Strong Uplift	**Experiment**
50	Strong Uplift	Model
54	Strong Uplift	**Experiment**
57	Crater	**Experiment**
66	Crater	**Both**

Table 8: Continued

70	Crater	**Experiment**
75	Crater	Model

To represent the data, a nomograph is used by plotting the height versus the release force, that is the ratio of the inlet pressure to the cross sectional area of the hole of 1.2cm in this work. This nomograph is represented in Figure 62. The pressures of 15, 36 and 66bar are used for validation, while the others are used to complete the graph. The graph allows the categorization of the regimes according to a given release force and height scenario. To distinguish between the different regimes, a dimensionless coefficient represented as a fraction (or percentage), is assigned according to the outcome generated from the release. This outcome is the result observed within the regimes of migration, low uplift, strong uplift and crater. The regime is dictated by a range for this coefficient, within which various outcomes can be observed under the big title of the regime. This coefficient is between 0 and 100% with 0% dictating migration and 100% dictating crater. Taking the example of gas migration regime, a coefficient of zero means complete gas migration with no cracks at all. A coefficient of 16.66% means that small cracks are expected. The whole range of 0-17 dictates the regime of migration. Between 0 and 17, there will be various observations, all ranging from no observation (migration with no cracks) until small cracks. The low uplift is mostly dictated by cracks. The strong uplift is dictated by a bigger uplift than the low, and accompanied with a crater. A complete crater is assigned a value of 100%. The description of the coefficients is summarized in Table 9.

Table 9: Coefficient definition according to the release outcome[5]

Release outcome in sand	**Coefficient (%)**
Migration – Migration with small cracks	0-17
Cracks with Uplift	17-50
Cracks with Uplift accompanied with a Crater	50-85
Stable Crater after uplift – instantaneous Crater	85-100

Having this coefficient is helpful, however it is not of great interest to know the exact value rather than the regime. This is why, the four different categories (regimes) are matched with four different coefficient intervals as follows: [0-17] as migration, [17-50] as low uplift, [50-85] as strong uplift and [85-100] as crater. Whereas the lowest forces generate migration, the middle forces generate low and then strong uplift and the highest forces generate crater. Accordingly, the different coefficient ranges are used to delineate the boundaries between these regimes associated with the various inlet forces for a height of 100cm and an upward release orientation.

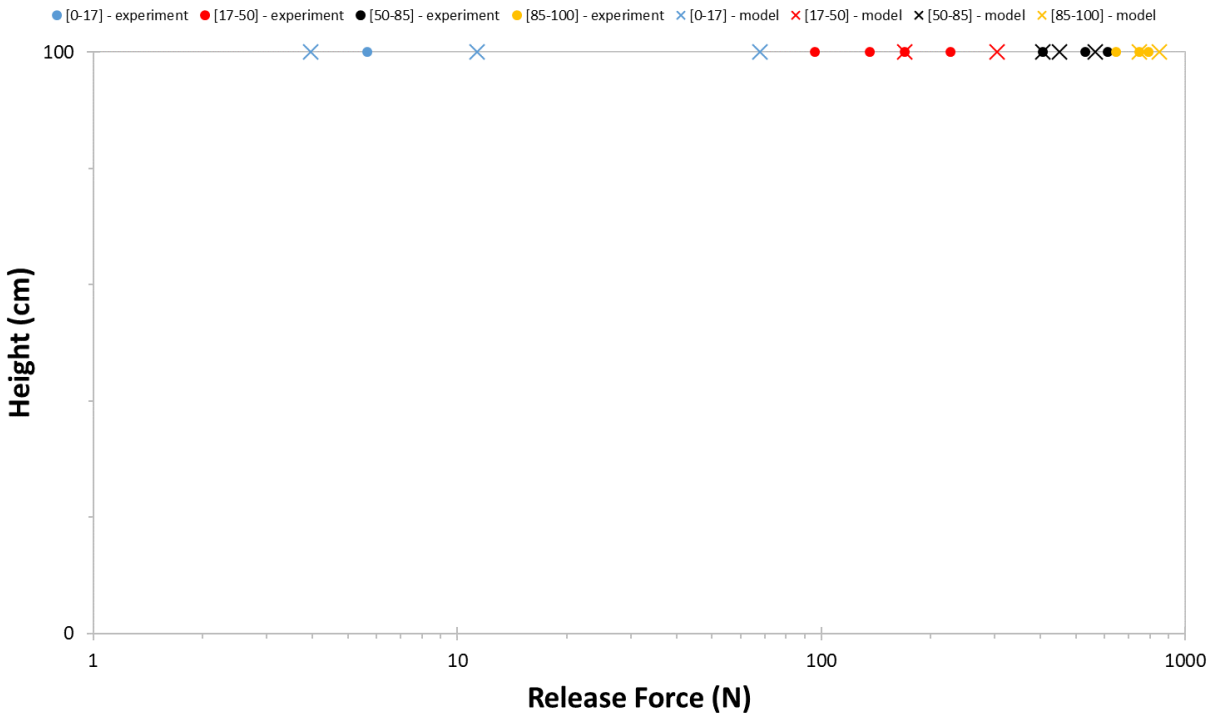

Figure 62: Nomograph showing the different regimes associated with the inlet forces at 100cm burial depth and upward release orientation

Another outcome of the pressure study is a significant property that is of big interest: the mass flow rate released. Therefore, a plot allowing to obtain the release mass rate as function of the release force is drawn and shown in Figure 63. The higher the release force, the higher the release mass flow rate. The best fit of around 99.38% is second order polynomial formula that can be used to obtain the mass flow rate as function of the release force.

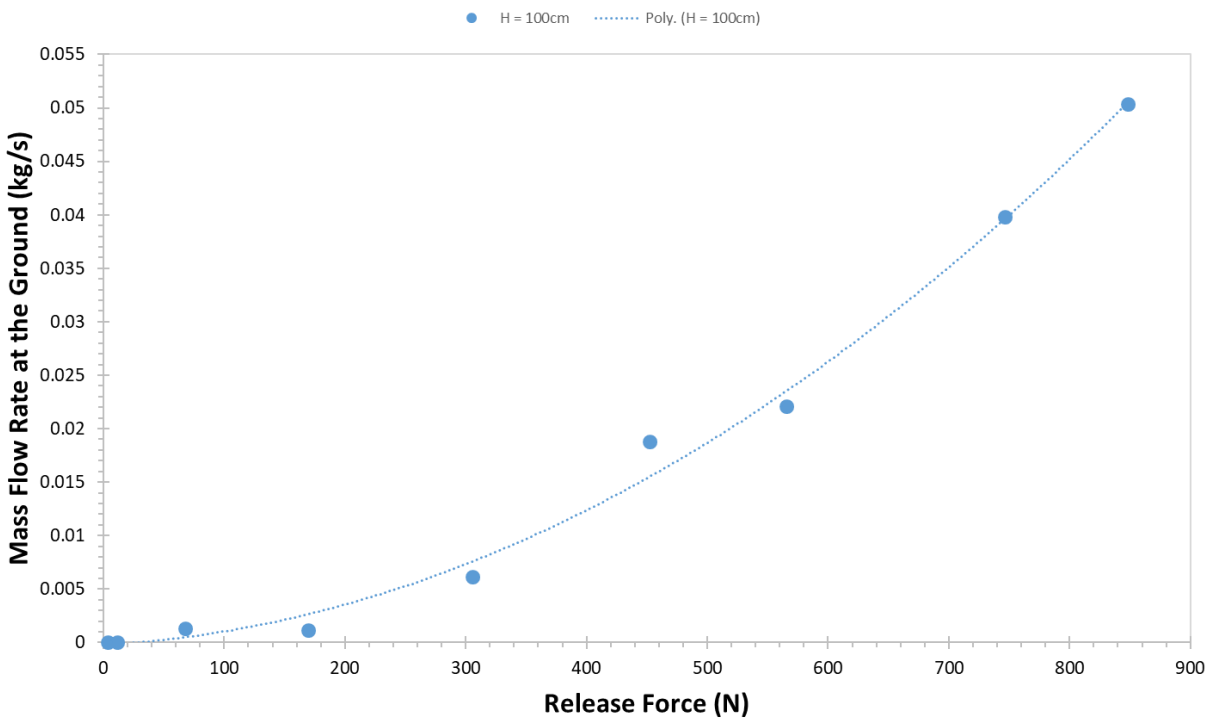

Figure 63: Release rate as function of the release force for burial depth of 100cm and an upward release orientation

6.2 Pipeline burial depth

The main intended parameter of this study is the pressure (or force). However, to illustrate the applicability of this model, another input that is varied is the pipeline burial depth. Two depths are tested aside the initial one (100cm) used throughout the project. The tested heights are 30 and 60cm, at three different pressures of 6, 15 and 50bars. These values are tested because the nomograph obtained by Bonnaud et al.[5] tested low heights (up to 17cm) and Agbomson et al.[4] tested the height of 100cm. Using 30 and 60cm allows to fill some of the gap in their generated nomograph, after placing the points on the nomograph presented in Figure 62.

The first tested pressure is 6bar. The outcome at the original height of 100cm was a migration. For the height of 60cm, the outcome is a low uplift while for 30cm, it is a strong uplift. The obtained

regimes can be visualized in Figure 64. The lower the burial height is, the stronger the regime is for the same release force. This is expected as the methane has to go through less resistance.

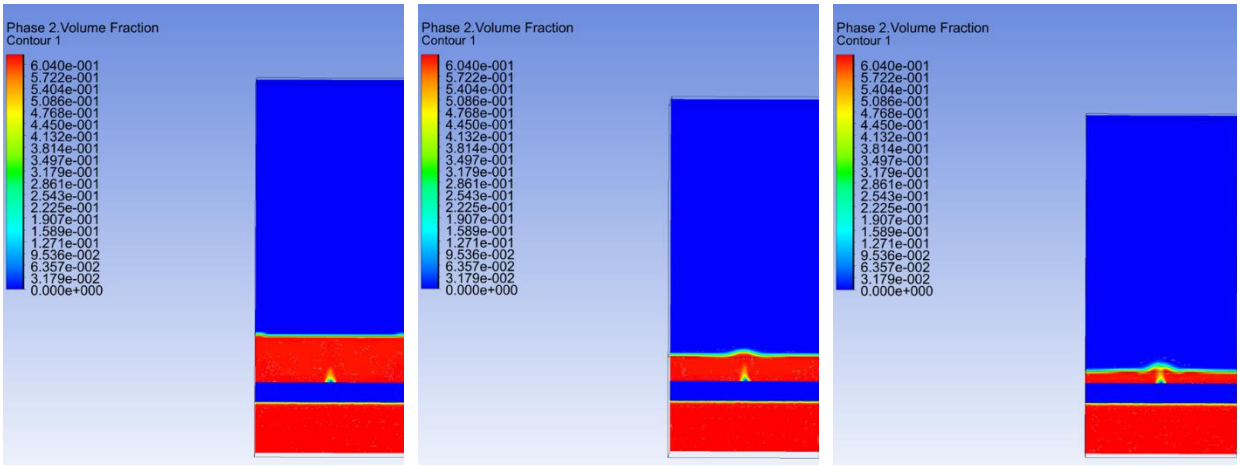

(a) (b) (c)

Figure 64: Soil volume fraction contour for pressure of 6bars at 100cm (a) 60cm (b) 30cm (c)

For the pressure of 15 bar, the same trend can be visualized in Figure 65; whereas the height of 100cm generates a low uplift, the height of 60cm generates a strong uplift and the height of 30cm generates a crater.

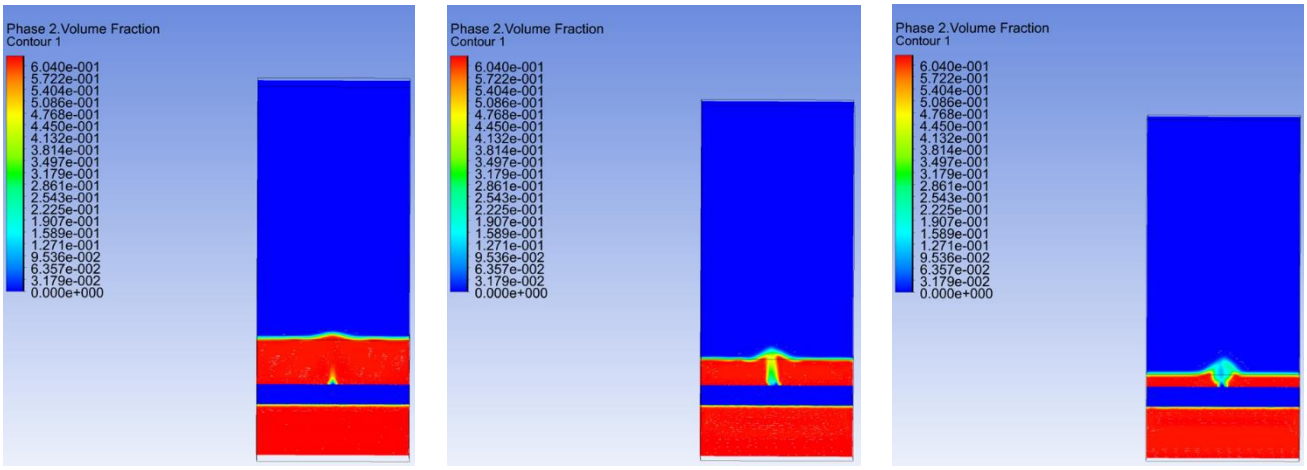

(a) (b) (c)

Figure 65: Soil volume fraction contour for pressure of 15bars at 100cm (a) 60cm (b) 30cm (c)

For the pressure of 50 bar, the height of 100cm generates a strong uplift while both other cases of 60 and 30cm generate a crater, as shown in Figure 66.

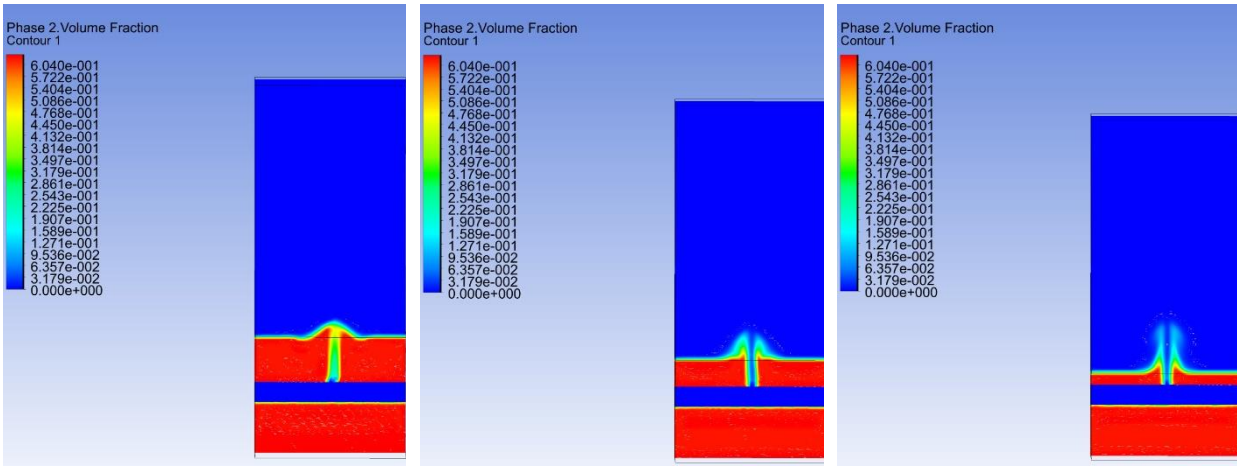

(a) (b) (c)

Figure 66: Soil volume fraction contour for pressure of 50bars at 100cm (a) 60cm (b) 30cm (c)

These outcomes can be represented as points on the nomograph, in addition to the experimental values at low heights. The resulting graph in Figure 67 allows the determination of the regime corresponding to a certain force and height. The end of the various regimes is delineated, dividing the different regimes into categories. The first category includes the migration. The second category contains low uplift points. The third category encloses strong uplift, and the last category is shown to complete the plot. However, the crater does not need to be categorized, because it has no ends. Anything to the right of the crater line is also a crater. It is therefore not an ending line delineated; rather it shows that there is concentrated the region of crater according to the values used so far.

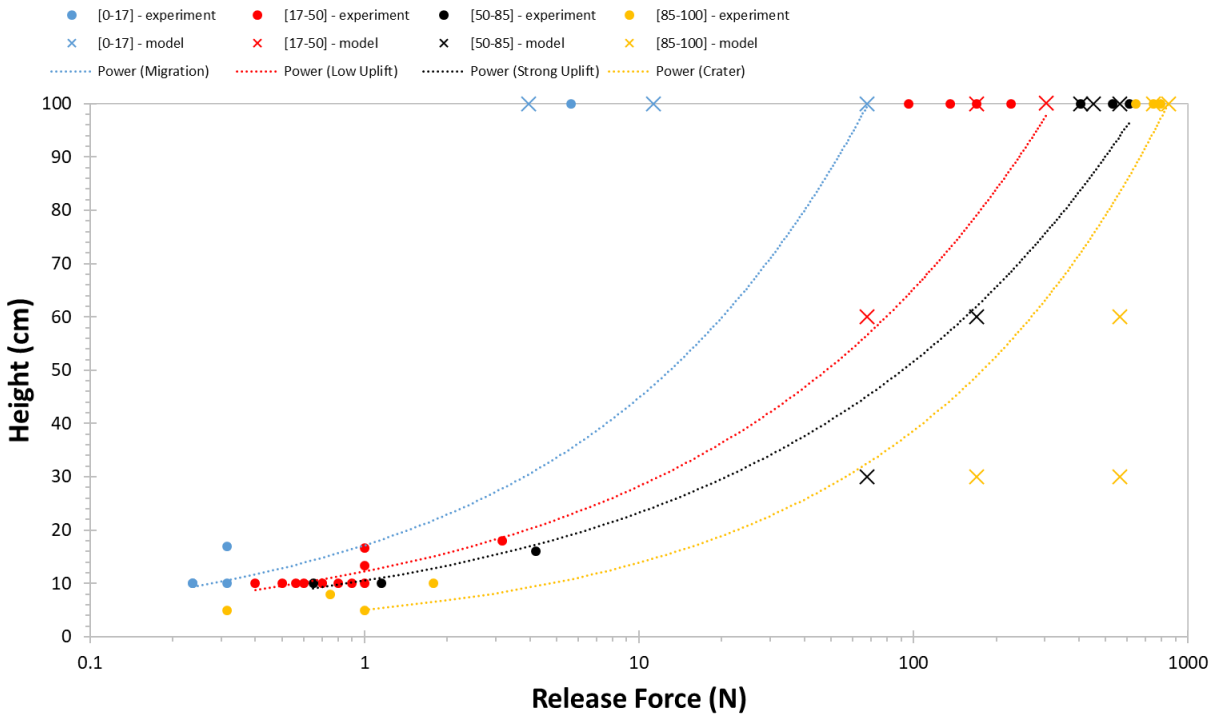

Figure 67: Nomograph showing the different regimes associated with a scenario of given inlet release force and burial depth at an upward release orientation

6.3 Release orientation

The performed analysis was done using an upward release orientation. It is shown that the release orientation affects methane concentration distribution[4,5]. Accordingly, it can affect the regime. To verify this, the pressure of 66bars is tested at four different release orientations: vertical (upward, downward) and horizontal (left and right) as shown in Figure 68. The orientation is drawn in the middle of each of the quadrants, making a 90^{o} with the horizontal in case of vertical orientation and vice versa.

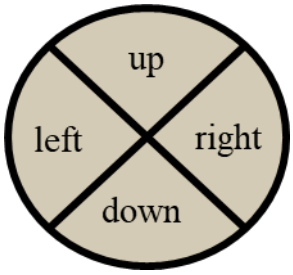

Figure 68: Different quadrants for release orientation

The outcomes obtained from the various release orientations at 66bars are shown in Figure 69. The upward release orientation triggered a crater whereas none of the other orientations did. For the downward release orientation, the outcome was the least: migration. For the left and right orientations, the outcome was an uplift, more serious than the downward orientation but slighter than the upward one.

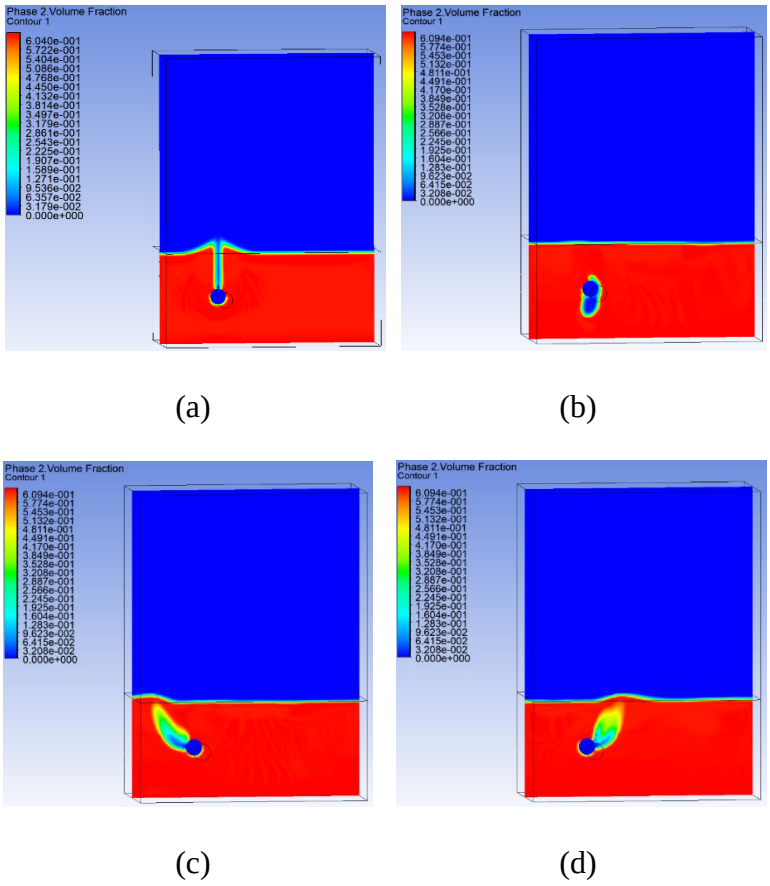

Figure 69: Soil volume fraction contours for different release orientations: upward (a) downward (b) left (c) right (d) at 66bars

This proves that the release orientation has an effect and the upward release orientation triggers the biggest damage. As the downward release orientation triggered migration at 66bars, it is tested at a higher pressure of 75bars, to see if it will cause any further damage. The soil volume fraction contours at 66 and 75bars for the downward release orientation are shown in Figure 70. They reveal that 75bars will trigger an uplift rather than a migration. Accordingly, since higher pressure has the capacity to produce more damage, the downward release orientation of methane leakage can be also dangerous.

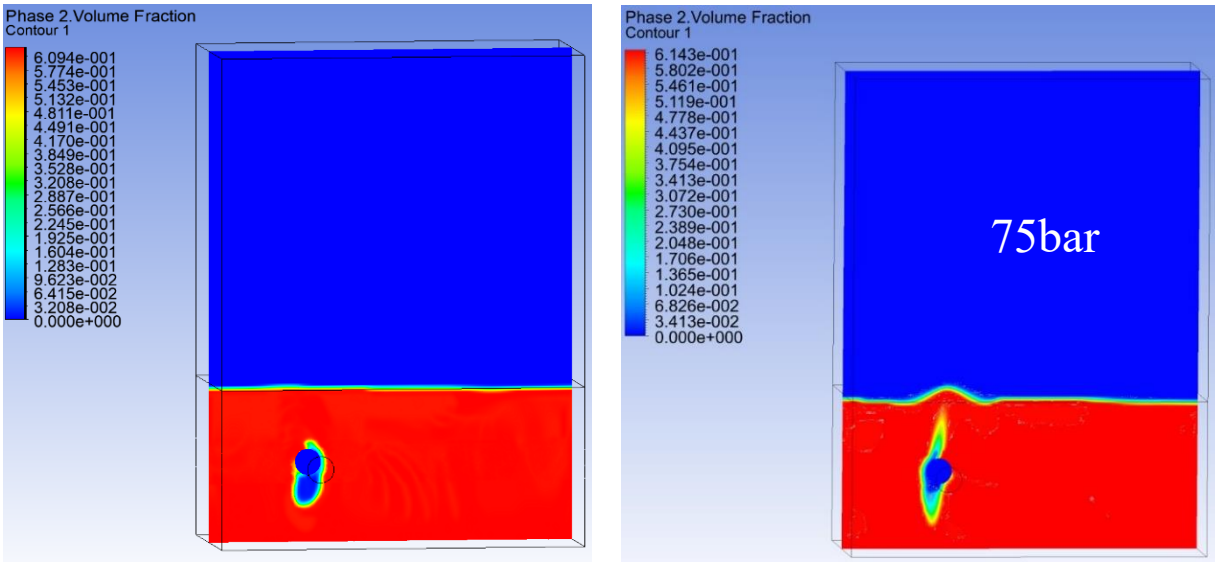

(a) (b)

Figure 70: Soil volume fraction contours for the downward release orientation at 66 bars (a) and 75bars (b)

Further study can be conducted to generate a nomograph for each of the release orientations. However, for this work, the applicability of the model to various release orientations has been proven.

7 CONCLUSIONS AND RECOMMENDATIONS

A CFD model to simulate the underground gas release from buried pipeline is produced after performing a sensitivity analysis to find the optimum parameters for meshing, particle diameter of the soil, turbulence model, granular and frictional viscosity models. The optimum parameters are found to be: meshing of 2.3 million elements, particle diameter of 0.01cm, the standard k-ω turbulence model, the Shaeffer frictional viscosity model and the Syamlal-O'Brien granular viscosity model.

The model can take a variety of inlet conditions: inlet pressure, burial depth, release orientation, soil density, pipeline diameter, hole diameter and others; which are specifications that can be input into the model to obtain the desired result describing the outcome regime, mass flow rate released, etc. For this work, the variables that are changed are the inlet pressure, burial depth and release orientation.

The outcome regime (migration, low uplift, strong uplift, crater) and the release rate associated with various inlet pressure were evaluated for a height of 100cm and an upward release orientation. The effect of three different heights and four various release orientations on the outcome regime was studied for given pressures.

The outcome of the study was presented on a nomograph that allows the determination of the corresponding regime resulting from a certain input pipeline burial depth and release pressure for an upward release orientation.

The existing model can be enhanced by a more advanced representation of the soil. Although diffusion was identified, the flow through the porous zone was not properly represented due to the soil representation as a quasi-fluid. This might have misestimated the concentration of methane in

the bed. The modelling of the interaction between the flowing gaseous phase and the packed solid phase can be enhanced through characterization of the interaction term in the Eulerian-Eulerian model or through the use of the DEM (Discrete Element Method) to model the soil as a discrete phase. Additionally, as the experimental work covered a range of particle diameter for the soil, the population balance model is recommended to be used as it allows testing a range of particle diameter instead of a constant value.

It is also recommended to add a water phase in order to account for the water saturation potentially existing in the soils. This can affect the resulting behavior as the residing water might affect the gaseous flow since it affects the soil cohesion. In addition, it is recommended to consider the temperature variations; which may allow the study of the Joule-Thomson effect.

Moreover, the effect of additional parameters on the regimes such as the type of soil (sand, clay), hole diameter and pipeline diameter can be investigated. Note that this model was established and validated according to the soil in the experimental work. However, in case one aims to test a soil of different nature (sand, clay), various compaction layers, and properties, the model might need to be modified to account for these changes. Hence, it is recommended to update the model according to the desired soil. Examples are the phyllosilicate minerals (especially clays) that exhibit very different mechanical behaviors than classic unconsolidated granular media (sands) due to strong electrostatic forces between platelets. There are other substrates that have a high degree of cohesivity (i.e. soils containing metastable minerals, such as calcite / aragonite [available in Qatar], organic rich substrates such as peat). Another suggestion would be to look at the effects of surface topography above the pipeline on the rupture behavior.

As for the obtained nomographs, it is recommended to test additional pressures to narrow down the transition regions, and additional heights to fill the nomograph. The recommended burial depths are usually higher than 50cm[5] as this is the typical range for urban pipelines.

REFERENCES

1. Energy Information Administration (US), Office GP. Natural Gas. In: *International Energy Outlook 2016, with Projections to 2040.* ; 2016.

2. Amaya-Gómez R, Ramírez-Camacho JG, Pastor E, Casal J, Muñoz F. Crater formation by the rupture of underground natural gas pipelines: A probabilistic-based model. *J Nat Gas Sci Eng*. 2018;54(December 2017):224-239. doi:10.1016/j.jngse.2018.03.011

3. *Rupture and Ignition of a Gas Pipeline Ghislenghien*., 1-6 (2009). https://www.aria.developpement-durable.gouv.fr/wp-content/files_mf/FD_27681_Ghislengheinv_2004ang.pdf

4. Houssin-agbomson D, Blanchetière G, Mccollum D, et al. Consequences of a 12-mm diameter high pressure gas release on a buried pipeline . Experimental setup and results. *J Loss Prev Process Ind*. 2018;54(April):183-189. doi:10.1016/j.jlp.2018.03.016

5. Bonnaud C, Cluzel V, Corcoles P, et al. Experimental study and modelling of the consequences of small leaks on buried transmission gas pipeline. *J Loss Prev Process Ind*. 2018;55(July 2017):303-312. doi:10.1016/j.jlp.2018.06.010

6. Farlow SJ. Partial Differential Equations for Scientists and Engineers. Published 1993. https://app.knovel.com/hotlink/toc/id:kpPDESE002/partial-differential/partial-differential

7. Hibi Y, Fujinawa K, Nishizaki S, Okamura K, Tasaki M. MULTI-COMPONENT MIGRATION IN THE GAS PHASE OF SOIL : COMPARISON BETWEEN RESULTS OF EXPERIMENTS AND SIMULATION BY DUSTY GAS MODEL. *Japanese Geotech Soc*. 2009;49(4):569-581.

8. Okamoto H, Gomi Y, Akagi H. Movement Characteristics of Hydrogen Gas Within the Ground and Its Detection at Ground Surface. 2014;3:49-66.

9. Wakoh H, Hirano T. Diffusion of leaked flammable. 1997;4:260-264.

10. Lu L, Zhang X, Yan Y, Li J-M, Zhao X. Theoretical Analysis of Natural-Gas Leakage in Urban Medium-pressure Pipelines. *J Environ Hum*. 2014;1(2). doi:10.15764/EH.2014.02009

11. Moloudi R, Abolfazli Esfahani J. Modeling of gas release following pipeline rupture: Proposing non-dimensional correlation. *J Loss Prev Process Ind*. 2014;32:207-217. doi:10.1016/j.jlp.2014.09.003

12. Wilkening H, Baraldi D. CFD modelling of accidental hydrogen release from pipelines. 2007;32:2206-2215. doi:10.1016/j.ijhydene.2007.04.022

13. Nouri-Borujerdi A, Ziaei-Rad M. Simulation of compressible flow in high pressure buried gas pipelines. *Int J Heat Mass Transf*. 2009;52(25-26):5751-5758. doi:10.1016/j.ijheatmasstransfer.2009.07.026

14. Ebrahimi-Moghadam A, Farzaneh-Gord M, Arabkoohsar A, Moghadam AJ. CFD analysis

of natural gas emission from damaged pipelines: Correlation development for leakage estimation. *J Clean Prod*. 2018;199:257-271. doi:10.1016/j.jclepro.2018.07.127

15. Ebrahimi-moghadam A, Farzaneh-gord M, Deymi-dashtebayaz M. Correlations for estimating natural gas leakage from above-ground and buried urban distribution pipelines. *J Nat Gas Sci Eng*. 2016;34:185-196. doi:10.1016/j.jngse.2016.06.062

16. Parvini M, Gharagouzlou E. Gas leakage consequence modeling for buried gas pipelines. *J Loss Prev Process Ind*. 2015;37:110-118. doi:10.1016/j.jlp.2015.07.002

17. Mason EA, Malinauskas AP, Evans RB. Flow and Diffusion of Gases in Porous Media. *J Chem Phys*. 1967;46:3199-3216. doi:10.1063/1.1841191

18. Mason EA, Malinauskas AP. *Gas Transport in Porous Media: The Dusty-Gas Model*. Elsevier Science Ltd; 1983.

19. Sleep BE, Sykes JF. Modeling the Transport of Volatile Organics in Variably Saturated Media. *WATER Resour Res*. 1989;25:81-92.

20. Kneafsey TJ, Hunt JR. Non-aqueous phase liquid spreading during soil vapor extraction. 2004;68:143-164. doi:10.1016/S0169-7722(03)00147-5

21. Hoeg S, Schöler HF, Warnatz J. Assessment of interfacial mass transfer in water-unsaturated soils during vapor extraction. 2004;74:163-195. doi:10.1016/j.jconhyd.2004.02.010

22. Poling BE, Prausnitz JM. *THE PROPERTIES OF GASES AND LIQUIDS*.

23. Curtiss CF, Hirschfelder JO. Transport Properties of Multicomponent Gas Mixtures. 1972;550(1949). doi:10.1063/1.1747319

24. Alsaydalani MOA, Asce AM, Clayton CRI. Internal Fluidization in Granular Soils. 2014;140(3):1-10. doi:10.1061/(ASCE)GT.1943-5606.0001039.

25. Zoueshtiagh F, Merlen A. Effect of a vertically flowing water jet underneath a granular bed. *Phys Rev E - Stat Nonlinear, Soft Matter Phys*. 2007;75(5):1-12. doi:10.1103/PhysRevE.75.056313

26. Niven RK, Khalili N. *In Situ Fluidisation by a Single Internal Vertical Jet*. Vol 36.; 1998. doi:10.1080/00221689809498633

27. MacDonald JF, Bridgwater J. Void formation in stationary and moving beds. *Chem Eng Sci*. 1997;52(5):677-691. doi:10.1016/S0009-2509(96)00453-8

28. Massimilla L, Volpicelli G. Flow of fluid-particle suspensions from liquid-fluidized beds. *Ind Eng Chem Fundam*. 1963;2(3):194-199. doi:10.1021/i160007a006

29. Niven RK. Physical insight into the Ergun and Wen and Yu equations for fluid flow in packed and fluidised beds. *Chem Eng Sci*. 2002;57(3):527-534. doi:10.1016/S0009-2509(01)00371-2

30. Peng Y, Fan LT. Hydrodynamic characteristics of fluidization in liquid-solid tapered beds. *Chem Eng Sci*. 1997;52(14):2277-2290. doi:10.1016/S0009-2509(97)00061-4

31. van Zyl JE, Alsaydalani MOA, Clayton CRI, Bird T, Dennis A. Soil fluidisation outside leaks in water distribution pipes – preliminary observations. *Proc Inst Civ Eng - Water Manag*. 2013;166(10):546-555. doi:10.1680/wama.11.00119

32. Luo JH, Zheng M, Zhao XW, Huo CY, Yang L. Simplified expression for estimating release rate of hazardous gas from a hole on high-pressure pipelines. *J Loss Prev Process Ind*. 2006;19(4):362-366. doi:10.1016/j.jlp.2005.06.029

33. Silva EP, Nele M, Frutuoso e Melo PF, Könözsy L. Underground parallel pipelines domino effect: An analysis based on pipeline crater models and historical accidents. *J Loss Prev Process Ind*. 2016;43:315-331. doi:10.1016/j.jlp.2016.05.031

34. Leis BN, Pimputkar SM, Ghadiali ND. Line rupture and the spacing of parallel lines. *Battelle Meml Inst*. Published online 2002.

35. Acton MR, Jackson NW. DEVELOPMENT OF GUIDELINES FOR PARALLEL PIPELINES. In: ; 2010:1-11.

36. COMITÉ DENDEPM. Y ORGANISMOS SUBSIDIARIOS Diseño, construcción, inspección y mantenimiento de ductos terrestres para transporte y recolección de hidrocarburos No. *Doc NRF-030-PEMEX-2009*.

37. Ramírez-Camacho JG, Pastor E, Casal J, Amaya-Gómez R, Muñoz-Giraldo F. Analysis of domino effect in pipelines. *J Hazard Mater*. 2015;298:210-220. doi:10.1016/j.jhazmat.2015.05.033

38. Yan Y, Dong X, Li J. Experimental study of methane diffusion in soil for an underground gas pipe leak. *J Nat Gas Sci Eng*. 2015;27:82-89. doi:10.1016/j.jngse.2015.08.039

39. Vianello C, Maschio G. Quantitative risk assessment of the Italian gas distribution network. *J Loss Prev Process Ind*. 2014;32:5-17. doi:10.1016/j.jlp.2014.07.004

40. Ai G, Liu Y. Effect of the Joule-Thomson cooling on the leak-before-break approach. *Int J Press Vessel Pip*. 2015;130:1343-1358. doi:10.1016/j.ijpvp.2016.03.008

41. Markatos NC. Dynamic computer modeling of environmental systems for decision making, risk assessment and design. *Asia-Pacific J Chem Eng*. Published online 2012:182-205. doi:10.1002/apj

42. Blazek J. *Computational Fluid Dynamics: Principles and Applications*. Butterworth-Heinemann; 2015.

43. Argyropoulos CD, Markatos NC. Recent advances on the numerical modelling of turbulent flows. *Appl Math Model*. Published online 2015:693-732. doi:10.1016/j.apm.2014.07.001

44. Kolev NI. 2 Introduction to turbulence of multi-phase flows. In: *Multiphase Flow Dynamics*. 3rd ed. Springer; 2007:29-54.

45. Liu D, Bu C, Chen X. Development and test of CFD-DEM model for complex geometry: A coupling algorithm for Fluent and DEM. *Comput Chem Eng*. 2013;58:260-268. doi:10.1016/j.compchemeng.2013.07.006

46. Wu Y, Liu D, Ma J, Chen X. Effects of gas-solid drag model on Eulerian-Eulerian CFD simulation of coal combustion in a circulating fluidized bed. *Powder Technol*. 2018;324:48-61. doi:10.1016/j.powtec.2017.10.013

47. ANSYS Fluent Theory Guide. 2013;15317(November):724-746.

48. Dartevelle S. Numerical and Granulometric Approaches to Geophysical Granular Flows. Published online 2003.

49. Passalacqua A, Marmo L. A critical comparison of frictional stress models applied to the simulation of bubbling fluidized beds. 2009;160:2795-2806. doi:10.1016/j.ces.2009.03.005

50. Gyo-soon K. Eulerian – Granular Model. In: *Star Korean Conference 2012*. ; 2012. http://mdx2.plm.automation.siemens.com/sites/default/files/Presentation/04 Korea2012_Eulerian Multiphase Flow_Kim Gyo-soon.pdf

51. *ESTABLISHING THEORETICAL AND TARGET VALUES FOR DENSITY AND MOISTURE CONTENT*.; 2016.

52. ASTM International. Standard Practice for Classification of Soils for Engineering Purposes (Unified Soil Classification System). Published online 2019:1-10. doi:10.1520/D2487-17.